Molecular mechanisms of malignant ascites-induced immunosuppression and options for nanoparticle-based therapeutic interventions

Dissertation
for
the doctoral degree of
Dr. rer. nat.

from the Faculty of Biology
University of Duisburg-Essen
Germany

Submitted by

Antonio Hrvat, mag. mol. biol.
Born in Zagreb, Croatia

Date of submission – 30. November, 2023.

The experiments underlying the present work were conducted in the Research Division of the Department of Otorhinolaryngology, part of University Hospital Essen and University of Duisburg-Essen.

1.　　Examiner: Prof. Dr. rer. nat. Sven Brandau
2.　　Examiner: Prof. Dr. med. Jürgen Becker
3.　　Examiner: Prof. Dr. rer. nat. Markus Kleinewietfeld

Chair of the Board of Examiners: Prof. Dr. rer. nat. Ralf Küppers

Date of the oral examination: 07.06.2024

Table of Contents

Summary

Ovarian cancer is the 5th most common cause of cancer death in women and remains one of the deadliest female malignancies. Due to the vague symptoms, it is often detected after peritoneal carcinomatosis and after ascites has developed. Malignant ascites is a fluidic immunosuppressive microenvironment that promotes disease progression. However, the exact mechanisms remain poorly understood. To explore the immunosuppressive mechanisms operative in malignant ascites, in manuscript 1, we developed an *in vitro* model of NK and T cell interaction with ovarian cancer cells in the presence of patient-derived ascites. We found that ascites inhibited various effector functions such as NK cell degranulation, tumor lysis, cytokine secretion, and calcium signaling. Using potentiometry, we identified imbalanced electrolytes as potential candidates causing immunosuppression. In mechanistic studies high sodium content significantly suppressed NK and T cell signaling and activation. Excess sodium also caused changes in electrolyte channels' protein transcription and expression. Selected sodium ion channel inhibitors restored calcium flux, conjugation to target cells, degranulation, and phosphorylation of signaling molecules in NK cells. These data suggest a novel electrolyte-based immunosuppression mechanism in malignant peritoneal ascites. Therapeutic inhibition of sodium channels could restore effector functions in ascites and other similarly imbalanced environments. Functionalized nanoparticles are versatile tools that can be used to therapeutically target such immunosuppressive cancer environments. Calcium phosphate nanoparticles (CaP-NPs) are biodegradable and biomimicking vehicles that can be functionalized with different moieties for imaging, targeting, and therapy. However, a prerequisite for such nanotherapy is that the therapeutic particles do not impair intrinsic or induced anti-tumor effector functions of immune cells. To test this, in manuscript 2, we utilized an *in vitro* system of NK and ovarian cancer cells. In this coculture system, CaP-NP addition did not impair conjugation or degranulation. Properly sonicated CaP-NPs did not induce unspecific degranulation or cytokine production. These properties indicate that our nanoparticle preparation is safe for biomedical applications. Furthermore, Cetuximab coupled to CaP-NP surface retained its ADCC-inducing properties and enabled EGFR targeting. Successful tumor cell transfection was detected via nanoparticle-coupled FITC. Considering the CaP-NPs biocompatibility and ease of uptake, they could be used for targeted delivery of therapeutics designed to counter imbalanced electrolytes of TME.

Zusammenfassung

Das Ovarialkarzinom ist die fünfthäufigste Krebstodesursache bei Frauen und stellt immer noch eine der tödlichsten Krebserkrankungen bei Frauen dar. Aufgrund der unspezifischen Symptome wird das Ovarialkarzinom häufig erst nach Ausbildung einer Peritonealkarzinose und Aszites entdeckt. Maligner Aszites stellt eine flüssige, immunsuppressive Mikroumgebung dar, die die Krankheitsprogression fördert. Die genauen zugrunde liegenden Mechanismen sind jedoch noch wenig bekannt. Um die im malignen Aszites wirksamen immunsuppressiven Mechanismen zu untersuchen, etablierten wir im ersten Manuskript ein *in vitro* Modell bestehend aus NK- und T-Zellen, die mit Ovarialkarzinomzellen in Anwesenheit von malignem Aszites von Ovarialkarzinompatientinnen interagieren. Wir konnten zeigen, dass Aszites verschiedene NK-Zell-Effektorfunktionen wir Degranulation, Tumorlyse, Zytokinsekretion und Calcium-abhängige Signalübertragung hemmte. Nach potentiometrischer Analyse der Aszitesproben identifizierten wir ein Ungleichgewicht der enthaltenen Elektrolyte als mögliche Ursache für die Immunsuppression. Weiteren mechanistischen Untersuchungen zufolge war ein hoher Natriumgehalt für die signifikante Inhibition der Signalübertragung und Aktivierung von NK- und T-Zellen verantwortlich. Überschüssiges Natrium im Aszites veränderte sowohl die Protein-Transkription als auch Protein-Expression von Elektrolytkanälen. Durch den Einsatz spezifischer Natriumkanalblocker konnte der Calciumeinstrom in die Zelle, die Konjugation zu Zielzellen, die Degranulation sowie die Phosphorylierung von Signalmolekülen in NK-Zellen wiederhergestellt werden. Zusammenfassend stellen diese Daten einen neuartigen, Elektrolyt-basierten immunsuppressiven Mechanismus im malignen peritonealen Aszites vor. Eine therapeutische Hemmung von Natriumkanälen könnte Effektorfunktionen im Aszites und in anderen ähnlich unausgewogenen Mikroumgebungen wiederherstellen.

Funktionelle Nanopartikel sind vielseitige Vehikel, die therapeutisch in solchen immunsuppressiven Mikroumgebungen eingesetzt werden können. Calciumphophat-Nanopartikel (CaP-NP) sind biologisch abbaubare und biokompatible Vehikel, die auf unterschiedliche Weise für ihren Einsatz im Rahmen der Bildgebung, zum zielgerichteten Transport von Substanzen und zu therapeutischen Zwecken funktionalisiert werden können. Voraussetzung für eine solche Nanopartikel-basierte Therapie ist allerdings, dass die eingesetzten Partikel weder intrinsische noch induzierte antitumorale

Effektorfunktionen von Immunzellen inhibieren. Um dies zu überprüfen, wurde im Rahmen des zweiten Manuskripts das *in vitro* Modell aus NK- und Ovarialkarzinomzellen verwendet. In dieser Kokultur führte die Zugabe von Calciumphosphat-Nanopartikel weder zu einer Beeinträchtigung der Konjugation noch Degranulation. Sie lösten auch weder eine unspezifische Degranulation noch Zytokinproduktion aus, wenn die Partikel vor ihrem unmittelbaren Einsatz mittels Ultraschall separiert wurden. Diese Eigenschaften sprechen dafür, dass unsere Nanopräparationen sich für biomedizinische Anwendungen eignen. Weitere Untersuchungen mit Cetuximab-funktionalisierten Nanopartikeln (CaP-NP-Cet) ergaben, dass auch gebundenes Cetuximab seine ADCC-induzierende Wirkung behielt und eine spezifische Bindung an EGFR ermöglichte. Die erfolgreiche Transfektion von Ovarialkarzinomzellen wurde durch den Einsatz FITC-gekoppelter Nanopartikel nachgewiesen. In Anbetracht der Biokompatibilität von CaP-NPs und der einfachen Aufnahme in die Zielzellen könnten sie für die gezielte Verabreichung von Therapeutika eingesetzt werden, die konzipiert sind, ein Ungleichgewicht der Elektrolyte in der Tumormikroumgebung auszugleichen.

List of abbreviations

ADCC	Antibody-dependent cell-mediated cytotoxicity
AML	Acute myeloid leukemia
APC	Antigen-Presenting Cell
ATP	Adenosine triphosphate
BiKE/BiTe	Bi-specific killer cell engagers/Bi-specific T-cell engager
BRCA1/2	BReast CAncer gene ½
CA	Cancer antigen
CaP-NP	Calcium phosphate nanoparticles
CAR-T	Chimeric antigen receptor T cell
CNT	Carbon nanotubes
CTLA4	Cytotoxic T lymphocyte antigen 4
DC	Dendritic cells
DNA	Deoxyribonucleic acid
DNAM1	DNAX Accessory Molecule-1
EGFR	Epidermal growth factor receptor
EMT	Epithelial-mesenchymal transition
FASL/R	FS-7-associated surface antigen
FITC	Fluorescein-isothiocyanate
HLA	Human leukocyte antigens
IDO	Indoleamine-pyrrole 2,3-dioxygenase
IFNγ	Interferon gamma
IgG	Immunoglobulin G
IL	Interleukin
KIR	Killer Cell Inhibitory Receptor
LAMP-1	Lysosomal-associated membrane protein 1
mAb	Monoclonal antibodies
MAC	Membrane attack complex
MHCI	Major histocompatibility complex class I
MICA/B	Major histocompatibility complex class I-related chain A or B
MUC	Mucin
NCR	Natural cytotoxicity receptor
NHE-1	Na^+/H^+ exchanger isoform 1
NK	Natural killer

NKG2D	Natural killer group 2 member D
NP	Nanoparticle
PD-L1	Programmed death-ligand 1
PEI	Polyethylenimine
PFN1	Profilin
PI3K	Phosphoinositide 3-kinases
PTT	Photothermal therapy
PVR	Poliovirus receptor
RNS	Reactive nitrogen species
ROS	Reactive oxygen species
siRNA	Small interfering RNA
TAM	Tumor associated macropages
TCR	T cell receptor
TGF	Transforming growth factor
TIGIT	T cell immunoreceptor with Ig and ITIM domains
TIM3	T cell immunoglobulin mucin-3
TME	Tumor microenvironment
TNF	Tumor necrosis factor
Treg	Regulatory T cell
ULBP	UL16 binding protein
VEGF	Vascular endothelial growth factor
VGSC	Voltage-gated sodium channel

1. Introduction

1.1. Ovarian cancer

Ovarian carcinoma has the worst prognosis of all gynecological malignancies. This is due to its vague and unspecific symptoms (loss of appetite, heartburn, constipation, cramps, etc.), which results in late diagnosis (Dilley et al., 2020). In advanced stages, ovarian cancer usually develops peritoneal metastasis and malignant ascites which is associated with unfavorable outcome.
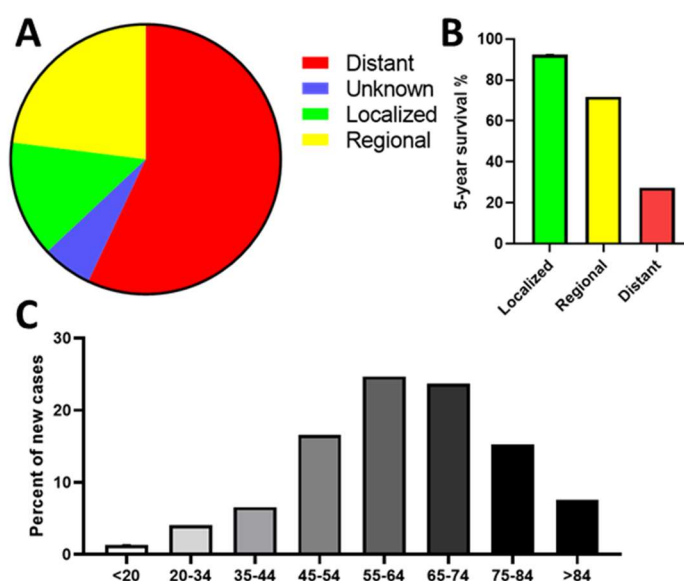

Fig. 1. Ovarian cancer develops and metastasizes silently which causes poor survival prognosis. (A) Pie chart represents distribution of ovarian cancer spread in patients upon diagnosis. **(B)** Average 5-year survival depending on the stage of ovarian cancer spread. **(C)** The risk of ovarian cancer increases with age. Depicted is the new cases percentage in regards to patient age group. Adapted from Nomura et al., 2017

The strongest risk factor is advancing age, reaching the peak at 65 years, but recently incidence rates for women in their thirties are rising (White et al., 2014). Other risks include obesity, postmenopausal hormone therapy and inherited mutations of BRCA-1/2 (Song et al., 2014). While there is no screening method, CA125 (MUC-16 or ovarian cancer-related tumor marker) is found elevated in blood of ovarian cancer patients, which makes it a useful monitoring parameter. Currently, the standard therapy consists of resection surgery, followed by combined cisplatin and taxan chemotherapy. Even in cases of initial response, more than 80% of the patients develop chemo-resistant recurrences (Dasari & Bernard Tchounwou, 2014). Recent implementation of anti-VEGF antibody, Bevacizumab and PARP-inhibitors into standard of care shows promise, but further innovations are needed urgently to improve the therapeutic efficacy. Since ovarian cancer can be considered an

"immunogenic tumor", immunotherapy could be the necessary improvement (L. Zhang et al., 2003).

Among potential targets, EGFR (Epithelial growth factor receptor) is of great interest as it is overexpressed in ovarian cancer and correlates with poor patient survival (Mehner et al., 2017). *In vitro* experiments have shown that anti-EGFR antibody Cetuximab inhibits ovarian cancer growth and could be combined with chemotherapy (Mendelsohn & Baselga, 2003). It was also shown that Cetuximab could enhance natural killer (NK) cell mediated lysis against otherwise highly NK-resistant ovarian cancer cells (Gottschalk et al., 2012). This is because Cetuximab belongs to the IgG class of antibodies, which means it is also capable of activating ADCC immune response (antibody-dependent cell-mediated cytotoxicity) (Roda et al., 2007).

1.2. Microenvironment of ovarian cancer ascites

Inflammation and tissue damage can alter local microenvironment, which is especially true for cancer (Coussens & Werb, 2002). In some cancers, such as ovarian cancer, this process can manifest dramatically as an abnormal fluid buildup in the peritoneal cavity (Ford et al., 2020). Mechanistically, ascites develops due to the lymphatic vessel obstructions and cytokine-induced effects (Chung & Iwakiri, 2013). Here IL-6 and VEGF are especially important since they increase vascular permeability, which causes accumulation of fluid and proteins (Catar et al., 2017). This also increases intraperitoneal pressure, which as a consequence impairs the drug delivery and promotes epithelial-mesenchymal transition (EMT) changes (Asem et al., 2020). Furthermore, patients often develop hypoalbuminia, hypercalcemia and other dangerous homeostatic disorders (Kelly et al., 2015). Because of this, ascites is usually removed by paracentesis or "tapping" (Thomsen et al., 2006). The anti-VEGF-antibody, Bevacizumab, is also used to slow ascites formation and disease progression due to its ability to inhibit neoangiogenesis (REIN et al., 2012).

Ascites composition is heterogeneous and different from healthy peritoneal fluid environment. For example, the fluid contains associated fibroblasts, endothelial cells, and recruited immune cells. Among them, tumor-associated macrophages (TAMs) especially support angiogenesis and inflammation. Ascites associated NK cells are severely impaired compared to peripheral blood NK cells from healthy donors or patients. (Maas et al., 2020; Mantovani et al., 1980). Furthermore, ascites is also heavily infiltrated by activated regulatory (Tregs) and killer T cells,

expressing high PD-1 and CTLA4 which contribute to immunosuppression (Landskron et al., 2015).

Besides the cellular fraction of ascites, the microenvironment is also rich with soluble immunosuppressive pro-tumor factors. Some of these classical suppressive factors are cytokines, shed tumor ligands, and metabolites. Cytokines and chemokines play an important role in cell signaling and recruitment. For example, IL-6 was reported to impair NK cell effector function and support ovarian tumor growth *in vivo* (Wu et al., 2019). Growth factors such as EGF, VEGF, and TGF-β support the neoangiogenesis, and invasivity (Lugano et al., 2020). Among them, TGF-β is of special interest due to its strong immunosuppressive effects (Dahmani & Delisle, 2018).

Other components are shed tumor ligands, which are extracellular protein fragments cleaved away by sheddases. Numerous sources report that released ligands, such as MICA, MICB, or ULBP-2 can block NKG2D receptors on NK cells and CD8+ T cells and impair antitumoral function (Raffaghello et al., 2004; Y. Zhang et al., 2023). Another well-known factor is soluble PD-L1 fragment, which induces CD8+ T cells apoptosis and suppression (Orme et al., 2020). Furthermore, fragments of classical HLA class I were found to induce similar effect on NK cells by binding to the killer-cell immunoglobulin-like receptors (KIRs) (Park et al., 2004).

Metabolites such as extracellular ATP, when converted into adenosine can cause suppression and apoptosis by binding to A2A/A2B receptors on immune cells (Allard et al., 2017). Another often elevated metabolite is kynurenine, which has been shown to inhibit NK cell activity (Chiesa et al., 2006). It is usually produced by tryptophan catabolism via Indoleamine 2,3-dioxygenase (IDO). The increased IDO activity also depletes tryptophan, which dampens the T cell proliferation (Eleftheriadis et al., 2015). Lipids, especially prostaglandins, are of special note since they can suppress T cell receptor signaling and proliferation (Wiemer et al., 2011). All of these listed metabolites and factors were often found elevated in ascites omics data (Shender et al., 2014; Vecchio et al., 2021).

There are many factors with largely unknown role, whose concentration is increased substantially in tumor-bearing patients due to the tissue remodeling and osmotic pressure changes. The ascites fluid can contain up to 100-1000 times higher concentration of cytokines and tumor markers compared to patient serum. Such transition from healthy peritoneal fluid to ascites leaves a molecular signature that could assist in early diagnosis. Studies using proteomic mass spectrometry, multiplex cytokine array, and metabolomics have shown that

such fluid serves as an excellent source for biomarker discovery (Apiz Saab et al., 2023; Terkelsen et al., 2021). Over 450 unique ascites proteins have been described as potential biomarkers, some of them being Cofilin-1, apolipoprotein-E and PFN1(Gortzak-Uzan et al., 2008; Kuk et al., 2009). Metabolomic studies have shown increased presence of glucose-1-phosphate, glycerol-3-phosphate and cholesterol in malignant ascites compared to benign cirrhosis ascites (Shender et al., 2014). Unfortunately, only a few of these markers were investigated for their effect on immune effector function.

Besides these classical factors, the electrolytes have been disregarded in the past as immunoregulators because of their tight homeostatic regulation. The most important ions in cell physiology are sodium (Na^+), potassium (K^+), calcium (Ca^{2+}), chloride (Cl^-) and hydrogen carbonate (HCO_3^-) (Alfarouk et al., 2020). Osmotic gradient, cell signaling and pH are all regulated by ionic gradients, which can be compromised by tumor lysis, necrosis and neoangiogenesis of abnormal vessels (Coiffier et al., 2008). Some studies have demonstrated that pathological ion imbalance can further enhance inflammation and angiogenesis, by upregulating the Tonicity-responsive Enhancer Binding protein (NFAT5/TonEBP) (Borrelli et al., 2021).

Currently, the exact immunosuppressive mechanisms of ascites are unknown. Given that ascites is a source of many immunosuppressive factors and biomarkers, it is important to further explore these possible therapeutic targets.
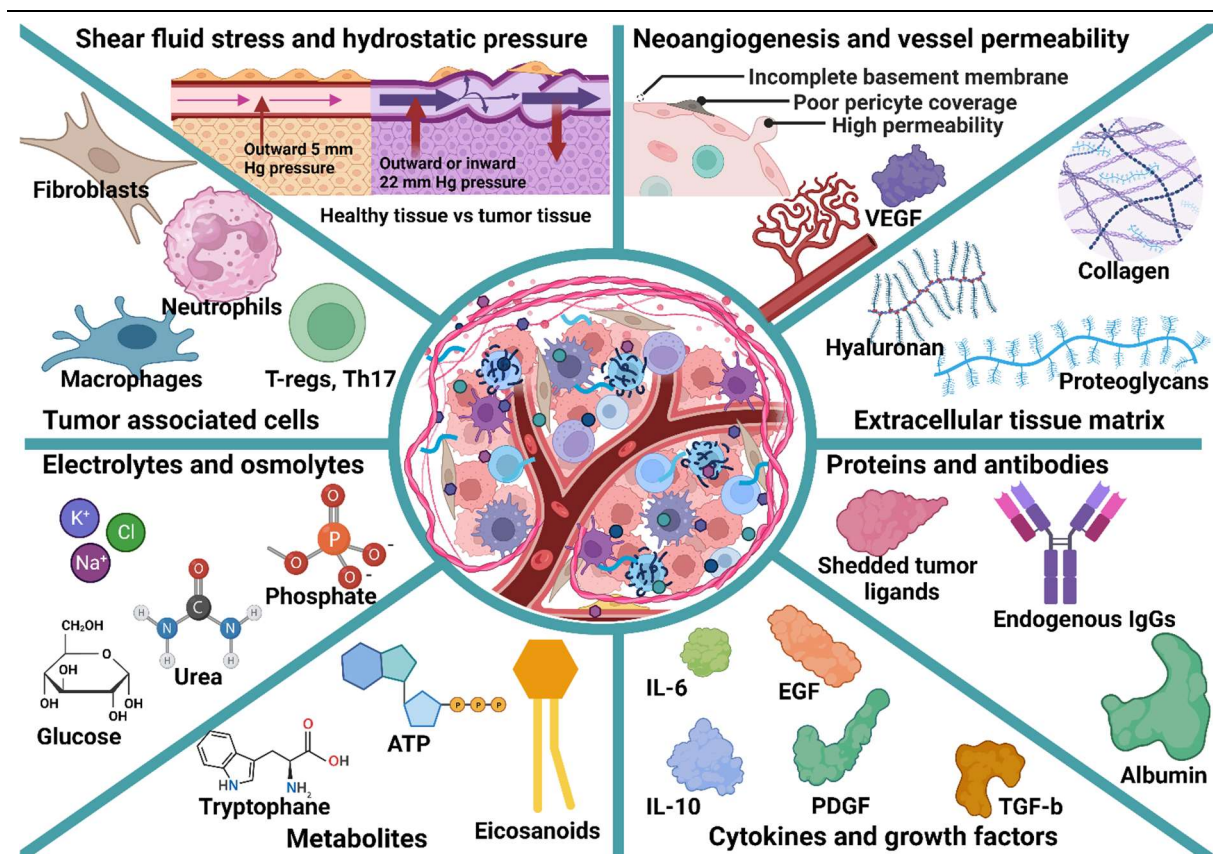
Fig. 2. The ascites microenvironment regulates the tumor growth and metastasis through many different biophysical and biochemical stimuli. This figure serves as a graphical overview of various factors, components and physical changes that are present in ascites or ovarian cancer microenvironment. The figure was constructed using BioRender.

1.3. Natural killer cells and T cells

The primary purpose of NK cells is the elimination of virus infected or transformed cells (Paul & Lal, 2017). As a part of the innate immune system, NK cell function is mediated via germline encoded receptors or effector molecules and does not depend on previous antigen exposure. The main trigger for NK cell activation is the loss of self-antigen, MHC class-I molecules, which are monitored by KIRs (Killer inhibitory receptors) (Moretta & Moretta, 2004).

Other membrane and soluble factors also affect the delicate balance of positive and negative signals determining the NK cell response. For example, Natural cytotoxicity receptors (NCR) such as NKp30, NKp44, NKp46 are triggered by viral particles and tumor markers (Barrow et al., 2019). NKG2D responds to upregulation of stress-induced ligands MICA/B (MHC class I polypeptide-related sequence A/B) and ULBP 1-6 (UL16 binding proteins) (Zingoni et al., 2018). The nectin-like-binding receptors include DNAM-1 (CD226) and TIGIT. Activating receptor DNAM-1 binds to PVR (CD155) or Nectin-2 (CD112), both of which are linked with tumor progression. TIGIT also binds to same ligands, but works antagonistically to the DNAM-1 activation (Pende et al., 2005). Besides these encoded receptors, NK cells can recognize antibody-coated cells via CD16 binding to Fc antibody fragment. This induces the antibody-

dependent cellular cytotoxicity (ADCC), which causes more potent effector response (Wang, 2015). The ADCC response is also one of the reasons why NK cells are considered at the interface of innate and adaptive immune system.

After the NK cell had the initial contact with the target cell and became activated, an NK-target cell conjugate is formed, which assists in delivery of cytotoxic granules containing perforin and granzyme. Perforin molecules oligomerize to form a pore-like structure called membrane attack complex (MAC) on the target cell surface, which enables the entry of pro-apoptotic proteases called granzymes (Dustin & Long, 2010; Lord et al., 2003). The NK cells which undergo degranulation can be detected by the expression of CD107a (LAMP-1, lysosomal-associated membrane protein-1), which protects them against autolysis (Cohnen et al., 2013). Besides directed release of lytic granules, death receptor-mediated apoptosis can be induced by NK cell expressed Fas ligand (CD178) binding to Fas receptor (CD95) on the target cells (Tummers & Green, 2017). Another important NK cell function is the regulation of nearby immune activity, primarily by secreting IFNγ and TNFa. Depending if they are more cytotoxic (CD56$_{dim}$) or cytokine secreting (CD56$_{bright}$), NK cells are functionally divided into these two subtypes.
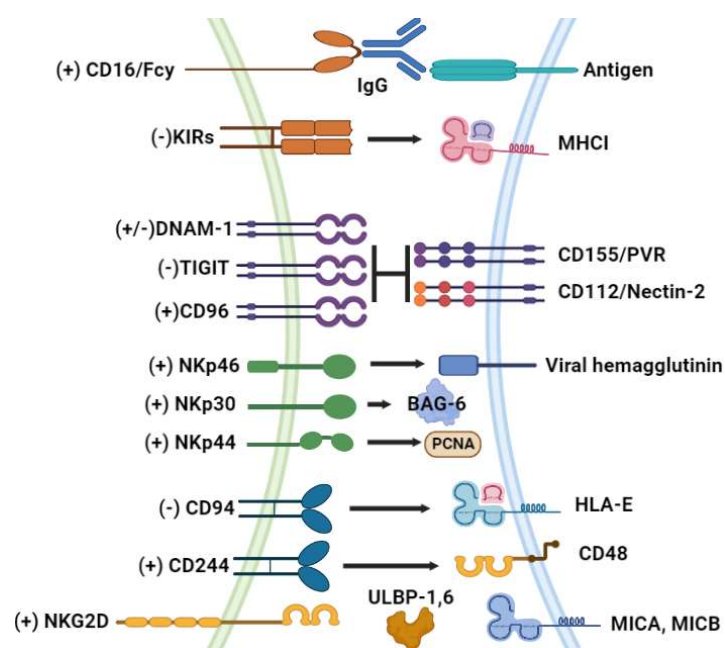

Fig. 3. Overview of activating and inhibitory NK cell receptors and their respective ligands. NK cell receptors (left) are marked depending on their effect to the signal balance (activating + or inhibitory -). The respective ligands (right) are expressed on APC or tumor cell membrane, or secreted in some cases. The figure was constructed using BioRender.

On the other hand, T cells play a central role in the adaptive immune system (Chaplin, 2010). The main T cell receptor (TCR) complex is made from two peptides generated from TCRα and

TCRβ genes. It also includes other TCR associated proteins such as CD3εγ, CD3εδ heterodimers and a CD3ζ homodimer (Ngoenkam et al., 2018). The activation of T cells has two requirements that need to be fulfilled. The first step is TCR recognition of foreign or neoantigen peptide presented by major histocompatibility complex (MHCI or II) on APC dendritic cells, B cells or macrophages. This needs to be followed by antigen-independent co-stimulation, which happens due to interaction between stress induced co-signaling molecules (CD80 and CD86, which comprise B7 protein) on APCs and T cell co-stimulation receptor (CD28) (L. Chen & Flies, 2013). In the absence of co-stimulation, T cells undergo apoptosis or anergy. Similar to NK cell, T cell activation is also regulated by other ligands which can be expressed on APCs or target cells. After T cell stimulation, activation markers such as CD69, CD71 and CD25 are upregulated. Similarly, the expressions of PD-1, TIGIT, TIM3 and CTLA-4 inhibitory receptors are upregulated as well. PD-1 and TIM3 impair T cell activity by interacting with PD-L1 or Galectin-9, respectively. While CTLA-4 competes with CD28 for binding to the CD80/CD86 (Sanchez-Correa et al., 2019).

Since their discovery in 1970s, it was found early on that two major T cell subtypes exist. These subtypes were named depending on their surface expression of CD8 and CD4. CD8+ T cells, also known as "cytotoxic killer T cells", are responsible for elimination of virus-infected and cancerous cells. Unlike CD8+ killer T cells, CD4+ helper T cells are more focused on modulating the ongoing immune reactions. The exact type and mechanism of modulation induced by helper T cells depends on their subtype (Th1, Th2, Th17, Treg, etc.) which is distinguished by different cytokine, protein and gene expressions (Wan, 2010).

1.4. NK and T cell immunotherapy

During carcinogenesis, transformed cells undergo many changes that affect the interactions with immune cells. To escape detection and elimination, cancer cells often alter their expression of surface markers, produce immunosuppressive cytokines and even polarize immune cells into pro-tumor phenotype (Labani-Motlagh et al., 2020). Therefore, there is a strong need for immunotherapies which can restore suppressed effector function of infiltrating immune cells. Currently, the following immunotherapies are being evaluated within clinical studies: cytokine therapies, monoclonal antibodies, and adoptive transfer of primary or modified immune cells like CAR-T/NK cells (Gupta et al., 2022).

Proinflammatory cytokines such as IL-2, IL-12, IL-15, IL-18 and IL-21 can be used to

revert immunosuppressive tumor microenvironment and help stimulate NK and T cells. Th2 T cells can be polarized into more cellular immunity focused Th1 cells with IL-12 and IFN-y (Atallah-Yunes & Robertson, 2022). To induce expansion and activation of existing CD8+ T cells, IL-2 can be used. The main drawback of cytokine therapy is that strong activation also upregulates checkpoint receptors and supports Treg proliferation, which limits the therapeutic effect.

On the other hand, monoclonal antibody (mAb) therapy uses specific antibodies which can activate or block the targeted receptor or secreted factor. For example, humanized antibody Bevacizumab is approved for the treatment of breast, ovarian and colorectal cancer where it binds VEGF and prevents neoangiogenesis (Kurkjian & Kim, 2012). An additional benefit to therapeutic IgG antibodies is the induction of NK-mediated ADCC killing mechanism, which has been shown to have significant impact on clinical response. Previously discussed Cetuximab is a chimeric (mouse/human) antibody which binds to EGFR and is approved for the treatment of metastatic colorectal or head and neck cancer (Seo et al., 2014). Another example of ADCC-inducing antibody is rituximab, which binds to CD20 expressed on the B-cells and can be used to treat autoimmune chronic lymphocytic leukemia and non-Hodgkin lymphoma (Randall, 2016). Monoclonal antibodies have also been used to block inhibitory checkpoint molecules in approach called checkpoint therapy. In 2011, the first anti-cancer CTLA4 checkpoint inhibitor Ipilimumab was approved.

Both cytokine and antibody therapies can be combined with adoptive cell therapy, which is based on immune cells transfer into the patient, either from the patient (autologous) or from another individual (allogenic). The isolated cells can originate from peripheral blood, bone marrow or even from patient tumor tissue. Of special interest in adoptive therapy is the transfer of allogenic or haploidentical NK cells since their KIR receptors cannot be inhibited by tumor cell MHC-I molecules (M. Cheng et al., 2013).

For some of the patients, peripheral blood T cells can be isolated and engineered to express a different TCR variant for specific cancer antigen in procedure called TCR therapy. This personalized treatment ensures that T cells can precisely eliminate cells which present specific antigen in the MHC complex. The approach was refined when it became possible to modify T cells with a synthetic or chimeric antigen receptor, which can interact with antigens even if not presented via MHC complex (CD19, BCMA and MUC1) (X. Chen et al., 2009; MacLeod et

al., 2017; Wachsmann et al., 2023). The promise of this technology can be seen from the fact that in October 2017, FDA has approved the first CAR T cell therapy for large B-cell lymphoma (Papadouli et al., 2020). Still, further improvements are needed to resolve CAR-T therapy side-effects (neurotoxicity, cytokine release syndrom).

1.5.   Application of novel technologies in cancer therapy

The unmet demand for innovative and safe treatments has rallied the efforts to modernize existing conventional approaches. In the last 50 years, there have been many advancements in the fields of immunology, pharmacology and material sciences, however, only a smaller number could be translated into clinical settings.

One such example are bispecific monoclonal antibodies and T/NK engagers (BiKE/BiTe peptides), which are artificial proteins that can simultaneously bind two different antigens (Allen et al., 2021). For instance, Blinatumomab is a clinically used BiTe, which was developed to target CD19 expressed on leukemic B-cells and CD3 on T cells (Burt et al., 2019). Such an engager induces T cell effector function independent of the MHC I or co-stimulatory molecules. Another emerging cancer treatment option is plasma medicine, which is based on application of cold ionized gas. The gas molecules generate ROS, RNS and other free radicals within the TME, which damage and kill cancer cells (Harley et al., 2020). An example of combined therapy consisting of cold plasma and iron nanoparticles was studied *in vitro* on breast cancer cell lines (Irani et al., 2016). Similar iron oxide nanoparticles are also applied for magnetic hyperthermal therapy and targeting (Hilger, 2013). A different innovative approach is photothermal therapy (PTT), which refers to the use of specific wavelength light that induces excited state, vibration and strong heat in gold or graphene nanoparticles. The generated temperatures can range from 40-45 °C and up to 70°C, which causes cell necrosis (Xu et al., 2022). Nanoprobes with dual-modal imaging capabilities used for visualization and photothermal therapy demonstrate the promise of a theranostic approach in clinical setting (Hu et al., 2018). As described here, these innovative treatments often include specifically engineered nanomaterials to mediate their therapeutic effect. Due to the customizability of their properties, new possibilities are available for diagnostic and therapeutic application.
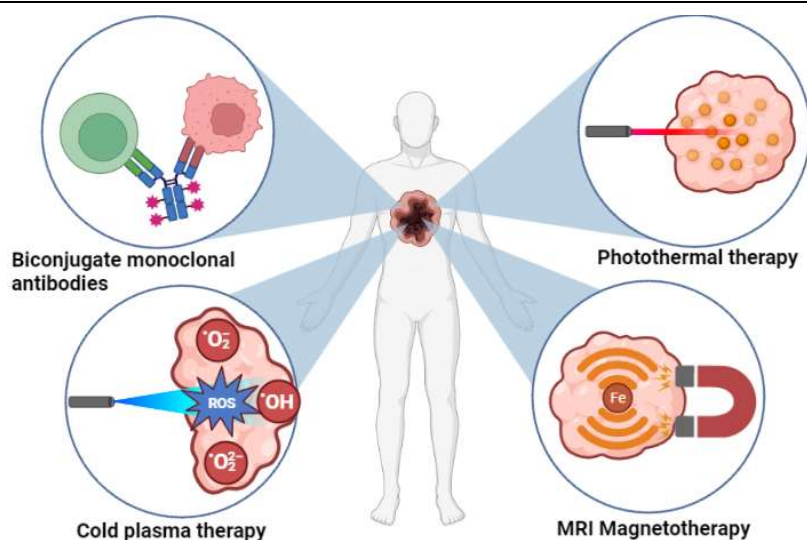
Fig. 4. Overview of emerging technologies applied for cancer treatment. These novel therapies relay on recently developed technologies such as synthetic biology, plasma gas generation and laser beams. They are often combined with nanomaterial constructs either as carrier or as part of the treatment. The figure was constructed using BioRender.

1.6.   Nanoparticles and their biomedical application

By definition, nanomaterials are described to have a unit size of 1 to 1000 nm. Depending on their origin, composition and structure, they can be divided in several groups. Nanoparticles (NPs) can have a natural (naturally occurring or biological) or synthetic (incidental or engineered) origin (Jeevanandam et al., 2018). Synthetic production can start with large bulk materials which are then processed into nanoparticles, for example, by mechanical milling or thermal degradation. This destructive approach is known as top-down synthesis. A bottom-up synthesis inversely uses smaller molecules to form nanomaterial. Examples are chemical vapor deposition or self-assembly (Khan et al., 2019).
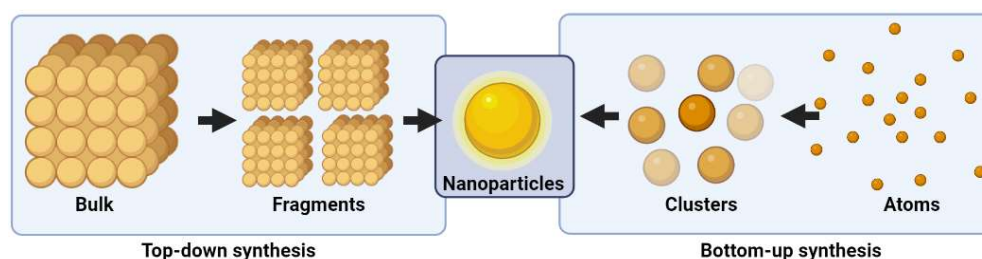

Fig. 5. Top-down and Bottom-up are two main nanoparticle preparation approaches. Graphical illustration of two main processes used in synthetic production of nanoparticles. This figure was constructed using BioRender and is adapted from Rawat, 2015.

Many nanomaterials that originated as curiosities in physics or chemistry have started to gain prominence in other fields due to tunability of physicochemical characteristics (size, controlled disassembly or chemical composition) or surface functionalization (Jeevanandam et al., 2018).

18

The latter being more important for biological applications since coating nanoparticles with organic molecules or polymers improves their solubility, bioavailability and prevents aggregation (Jokerst et al., 2011). Conjugation of different moieties such as drugs, radionuclides or antibodies can limit non-specific cell interactions and toxicity, while improving therapeutic function (Sperling & Parak, 2010).
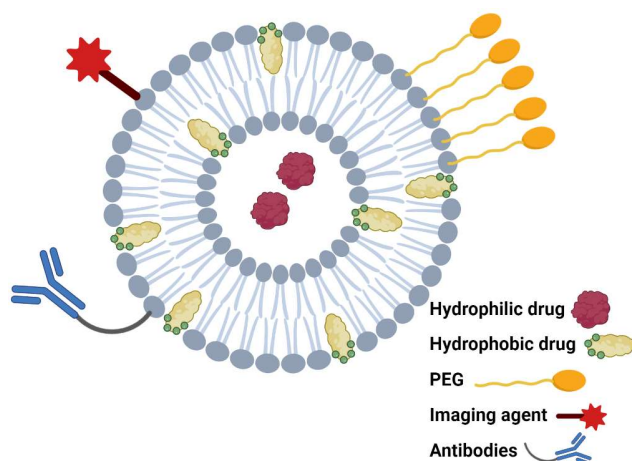

Fig. 6. Nanoparticles can be enhanced for biomedical application through surface functionalization. These enhancements can be therapeutics, targeting antibodies, imaging agents and surface stabilization. The figure was constructed using BioRender.

Most of the nanomaterials can be classified as carbon, organic or inorganic based. Carbon-based nanomaterials refer to single or multiple wall carbon nanotubes (CNTs) and fullerenes (Narendra Kumar & Sunita Kumbhat, 2016). The well-known property of these materials is thermal and electrical conductivity, which makes them promising for photodynamic therapy (Z. Yang et al., 2019). Organic-based nanomaterials are made from biomolecules such as micelle, liposomes, polymers and dendrimers. Some of them, like LipoDox liposomes have excellent biocompatibility, which enables their clinical usage (Sen & Mandal, 2013). Other examples are polymeric nanoparticles made from biocompatible polymers PLGA, PEG (polyethylene glycol) or PEI (polyethylenimine), which makes them good drug delivery systems with reduced cytotoxicity for healthy tissues (Chan et al., 2010). Inorganic-based nanomaterials usually consist of metal atoms or metal oxides. Most of the described examples from literature are based on Au, Ag and TiO_2, ZnO and Fe_3O_4. Due to the inherit properties of these materials, they are used for magnetic- or photo-induced hyperthermia (Liang et al., 2014). Finally, the biomimicking calcium phosphate nanoparticles also belong to inorganic-based group (Sokolova & Epple, 2021).
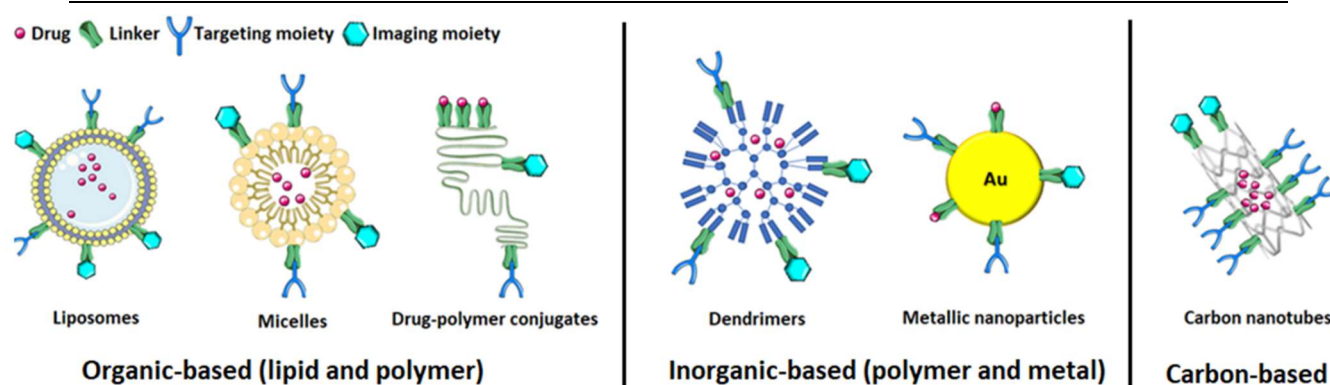
Fig. 7. Different types of nanomaterials used in nanomedicine depending on their structure and composition. These examples can roughly be divided into organic, inorganic and carbon-based nanoparticles. The figure was assembled using material from Servier Medical Art and is adapted from Narendra Kumar & Sunita Kumbhat, 2016.

1.7.   Calcium phosphate nanoparticles

The mentioned biomimicking properties make calcium phosphate nanoparticles (CaP-NP) especially suitable for biomedical application. Since calcium phosphate is an endogenous biomineral present in bones and teeth, CaP-NPs are well-tolerated and can be considered non-toxic (Khalifehzadeh & Arami, 2020). They also show good chemical stability and do not dissolve at physiological pH. Furthermore, their bottom-up synthesis relies on cheap reagents which quickly precipitate into calcium phosphate particles when mixed together (manuscript 2., Supplementary figure S1. A). Due to these favorable properties, they are already clinically applied for treating bone defects, tissue regeneration and implant installation (Jeong et al., 2019). Recent efforts have been made to develop the CaP-NPs as vehicles for various therapeutical molecules, such as antibiotics or cancer vaccines. Furthermore, CaP-NPs are also explored for gene therapy, where packed DNA and siRNA are delivered by the nanoparticle mediated transfections (Dristant et al., 2023). The contained nucleic acids remain safe from nucleases until cell entry. Due to the cationic polymer PEI, nanoparticles promote endosome swelling by neutralizing H+ ions pumped by ATPase. As a consequence, imported chloride ions generate osmotic pressure that leads to endosome rupture and release of nucleic acids (Vermeulen et al., 2018).

To further enhance applicability of these nanoparticles for theranostics, the surface of CaP-NPs needs be functionalized. Imaging moieties that provide diagnostic capabilities or therapeutic antibodies that induce ADCC or targeting, can be conjugated to their surface (Degli Esposti et al., 2018). However, before widespread application, it should be thoroughly tested whether CaP-NPs impair immune effector functions.
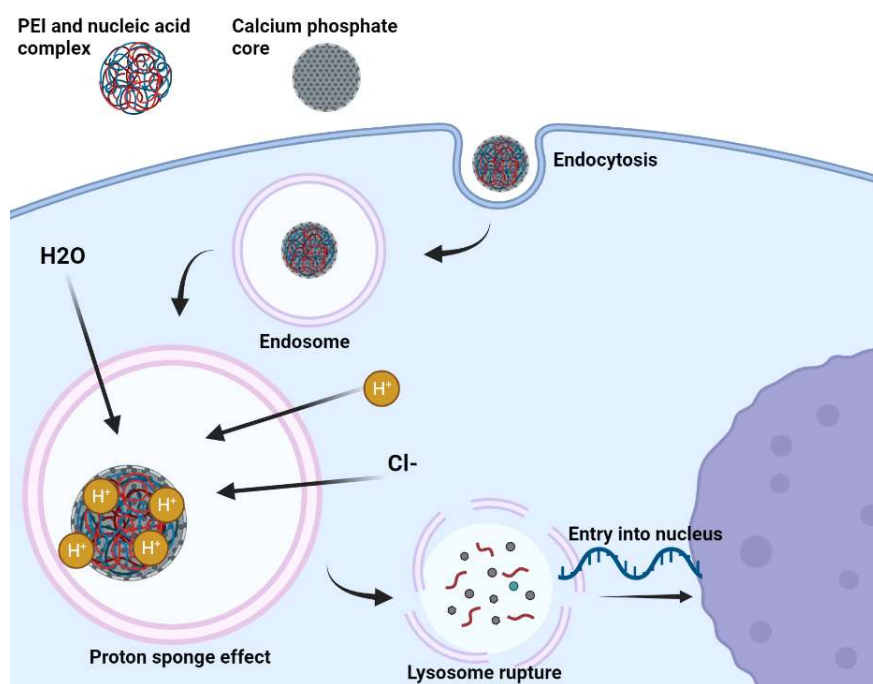
Fig. 8. Illustration of proton sponge effect which leads to endosomal escape and release of CaP-NP payload. Negatively charged PEI polymer causes endosomal swelling by binding protons and increased chloride diffusion. This enables release of payload from endosome and entry into nucleus. The figure was constructed using BioRender and cited sources describing the phenomenon.

2.   Aims and scope of the work

Ovarian cancer cells are highly resistant to NK cell mediated lysis, which impairs efficacy of NK cell adoptive therapy. Furthermore, upon diagnosis most patients have already developed immunosuppressive peritoneal ascites. The current thesis investigates molecular mechanisms of ascites-induced immunosuppression and explores principal aspects of CaP-NP-NK interaction that are important for a potential future therapeutic application.

This thesis has the following specific aims:

I)   A) Describe the immunosuppressive effects of malignant ascites derived from ovarian and other cancer patients on NK and T cell functions

B) Identify acellular components of malignant ascites which potentially mediate this immunosuppression

C) Identify molecular mechanisms of NK and T cell suppression in human malignant ascites

II)   Investigate whether calcium phosphate nanoparticles influence antitumoral and effector functions of NK cells directed against ovarian cancer cells

For this, we established an *in vitro* coculture system that mimicked the interactions of ovarian cancer cells and healthy donor NK or T cells. Comprehensively, we studied antitumoral NK cell effector functions as well as T cell activity considering different components and conditions (ADCC antibodies, inhibitory ascites, calcium phosphate nanoparticles). Here we focused on the analysis of the degranulation, cytotoxicity, and conjugation between NK and tumor cells. Additionally, we examined the gene- and protein expression of crucial signaling molecules in NK and T cells. Finally, we correlated the results of our *in vitro* experiments with patients' clinical data.

The detailed description of materials, methods and results of our studies are presented in this thesis in the format of two peer-reviewed and published publications.

3. Results

3.1. Publications

Electrolyte imbalance causes suppression of NK and T cell effector function in malignant ascites.

Antonio Hrvat, Mathias Schmidt, Bernd Wagner, Denise Zwanziger, Rainer Kimmig, Lothar Volbracht, Sven Brandau, Nina Mallmann-Gottschalk

Reactivity of NK Cells Against Ovarian Cancer Cells Is Maintained in the Presence of Calcium Phosphate Nanoparticles.

Antonio Hrvat, Mathias Schmidt, Martin Obholzer, Sonja Benders, Sebastian Kollenda, Peter A. Horn, Matthias Epple, Sven Brandau, and Nina Mallmann-Gottschalk

3.2.   Cumulative Thesis/Extent of Contribution

Cumulative thesis of Mr. Antonio Hrvat

3.2.1.   Electrolyte imbalance causes suppression of NK and T cell effector function in malignant ascites

<u>Antonio Hrvat</u>, Mathias Schmidt, Bernd Wagner, Denise Zwanziger, Rainer Kimmig, Lothar Volbracht, Sven Brandau, Nina Mallmann-Gottschalk

Contributions:

- Conception – 50%

- Conduction of experimental work – 95% : All experiments excluding IFNy ELISA and clinical chemistry analysis of ascites

- Data analysis – 95%: All data analysis in the study except clinical chemistry analysis of ascites

- Statistical analysis – 100%

- Writing the manuscript – 70%: Contributed to all parts of the manuscript

- Revision of the manuscript – 80%: Revisiting the manuscript, performing additional experiments and responding to reviewer comments

_____   _____
Signature of the Doctoral Candidate   Signature of the Doctoral Supervisor

Check for
updates

Electrolyte imbalance causes suppression of NK and T cell effector function in malignant ascites

Antonio Hrvat[1] , Mathias Schmidt[1] , Bernd Wagner[2] , Denise Zwanziger[2,3] , Rainer Kimmig[4], Lothar Volbracht[2], Sven Brandau[1,5]* and Nina Mallmann-Gottschalk[1,6]

Abstract

Background Malignant ascites commonly occurs in advanced or recurrent stages of epithelial ovarian cancer during peritoneal carcinomatosis and is correlated with poor prognosis. Due to its complex composition of cellular and acellular components malignant ascites creates a unique tumor microenvironment, which mediates immunosuppression and promotes progression of disease. However, the immunosuppressive mechanisms remain poorly understood.

Methods In the present study, we explored the antitumor activity of healthy donor NK and T cells directed against ovarian cancer cells in presence of malignant ascites derived from patients with advanced or recurrent peritoneal carcinomatosis. A wide range of methods was used to study the effect of ascites on NK and T cells (FACS, ELISA, EliSpot, qPCR, Live-cell and confocal microscopy, Western blot and electrolyte flux assays). The ascites components were assessed using quantitative analysis (nephelometry, potentiometry and clinical chemistry) and separation methods (dialysis, ultracentrifugal filtration and lipid depletion).

Results Ascites rapidly inhibited NK cell degranulation, tumor lysis, cytokine secretion and calcium signaling. Similarly, target independent NK and T cell activation was impaired in ascites environment. We identified imbalanced electrolytes in ascites as crucial factors causing extensive immunosuppression of NK and T cells. Specifically, high sodium, low chloride and low potassium content significantly suppressed NK-mediated cytotoxicity. Electrolyte imbalance led to changes in transcription and protein expression of electrolyte channels and impaired NK and T cell activation. Selected inhibitors of sodium electrolyte channels restored intracellular calcium flux, conjugation, degranulation and transcript expression of signaling molecules. The levels of ascites-mediated immunosuppression and sodium/chloride/potassium imbalance correlated with poor patient outcome and selected molecular alterations were confirmed in immune cells from ovarian cancer patients.

Conclusion Our data suggest a novel electrolyte-based mechanism of immunosuppression in malignant ascites of patients with peritoneal carcinomatosis. We show for the first time that the immunosuppression of NK cytotoxicity

*Correspondence:
Sven Brandau
sven.brandau@uk-essen.de

Full list of author information is available at the end of the article

in coculture assays is correlated to patient poor survival. Therapeutic application of sodium channel inhibitors may provide new means for restoring immune cell activity in ascites or similar electrolyte imbalanced environments.

Keywords NK cell, Ascites, Immunosuppression, Sodium, Ovarian cancer, T cell, Channel blocker, Amiloride, Chloride, Electrolyte

Background

Advanced epithelial ovarian cancer is still the gynecological malignancy with worst prognosis [1]. Due to limited efficacy of standard chemotherapies in advanced stages, novel approaches are urgently needed. Because ovarian cancer is considered to be an "immunogenic tumor" promising immunotherapeutic approaches have been conceptualized [2, 3]. Since advanced ovarian cancer usually spreads locally with formation of peritoneal carcinomatosis, intraperitoneal application of cellular and antibody-based immunotherapies is of specific interest [4]. However, until now, such approaches often showed only moderate clinical benefit [5]. Off all epithelial cancers that cause peritoneal carcinomatosis, advanced ovarian cancer is most commonly associated with the formation of malignant ascites, which limits patients´ quality of life and correlates with poor survival [6, 7]. Ascites composition is heterogenous consisting of cancer cells, associated fibroblasts, immune cells and various acellular components that create a proinflammatory environment [8]. Natural killer (NK) cells, innate immune cells and key effectors in antitumor defense, can be isolated in a high proportion in malignant ascites [9]. NK induce natural or antibody-dependent cytotoxicity (ADCC) and secrete antitumoral cytokines like IFNγ or TNFα. However, their functionality in malignant ascites seems to be substantially impaired [10]. Particularly, their cytolytic activity is decreased due to downregulation of Fcγ-receptor CD16 and activating receptor DNAM-1 [11]. Similarly, NK cell-tumor cell-interaction is disturbed since expression of NKG2D is downregulated by soluble MICA and MICB released from adjacent tumor cells [12]. It has been hypothesized that acellular components of malignant ascites contribute to ascites-mediated immunosuppression. Cytokines, proteins, lipids, metabolites and nucleic acids dynamically interact with cellular components of ascites leading to progressive disease [13]. While many studies focused on factors like VEGF and IL6 promoting tumor growth and metastasis [14, 15], only limited data is available about factors which potentially suppress the function of NK cells and other immune effector cells. Among these, IL18 and TGFβ could be identified to suppress NK-mediated ADCC by downregulating CD16 [16]. TGFβ also decreased expression of NK activating receptors NKp30 and NKG2D, whose expression was additionally inhibited by macrophage migration inhibitory factor (MIF) [17, 18]. Among non-cytokine factors MUC16 (CA125) was shown to impair NK cell-mediated

ADCC and conjugation [19]. In other studies low molecular proteins were considered to be inhibitory [20].

This study aimed to identify novel acellular factors and mechanisms of NK suppression in malignant ascites. To this end, we studied structural and functional changes of NK cells directed against ovarian cancer cells in presence of malignant ascites after depletion of cellular components. In order to uncover potential candidates, we correlated the content of different electrolytes and proteins in the acellular ascitic fluid to cytotoxic and secretory NK functions and to the functionality of activated T cells. With this approach, we identified a sodium-chloride-potassium imbalance in ascites as a major immune suppressive mechanism that impairs effector functions of NK cells and T cells.

Methods

Patient ascites and healthy donor serum sample preparation

Ascites samples from 28 adult patients were collected at the Departments of gynecology and obstetrics at the University Hospital Cologne, Cologne and the University Hospital Essen, Essen, Germany. The statistical analysis of reported survival showed a median survival of 12.13 months (range from 5 days to 74 months) (Supplementary table S1, Additional File 1.). The conduction of the study has been approved by the local Ethics Committee of the medical faculties of Duisburg-Essen and Cologne. The ascites samples were collected during clinically indicated cytoreductive surgery or palliative surgery after written information and consent. The isolated ascites was transferred to Falcon 50 tubes and centrifuged at 2000 g for 10 min. After centrifugation only acellular supernatant was collected. T cells from two patient ascites samples were isolated. The collected fraction was sterile filtered using bottle top filters (Sarstedt, 0.2 μm), aliquoted and frozen at -80 °C for long-term storage. Healthy donor serum was obtained using clotting activator serum collection tubes (Sarstedt). Samples were centrifuged 2000 g for 10 min.

Human cancer cell lines and in vitro cell culture

For in vitro killing and activation assays, several EGFR-positive cell line models were used:

The human ovarian cancer cell line IGROV1 was kindly provided by LIMES Institute, University of Bonn, Bonn, Germany. The lung cancer cell line A549 (adenocarcinoma) cell line was obtained from Westdeutsches

Tumorzentrum, University Hospital Essen, Essen, Germany. The colorectal cancer cell line A431 was obtained from DSMZ, Braunschweig, Germany and FaDu head and neck cancer cell line from LGC Standards, Wesel Germany. All used cancer cell lines showed positive expression for EGFR (epidermal-growth-factor-receptor). IGROV1, A549, A431 and FaDu cell lines were cultured in Roswell Park Memorial Institute (RPMI Gibco) supplemented with 10% (v/v) heat-inactivated fetal calf serum (FCS Gibco), 100 U/mL penicillin, and 100 mg/mL streptomycin (PenStrep, Gibco by Life Technologies) (supplemented complete media). Cells were cultivated in plastic flask (Sarstedt) at 37 °C and 5% CO_2 and continuously passaged by treatment with Accutase (Gibco) for 5 min at 37 °C. Cells are regularly tested for mycoplasma and STR Typing was performed by the Leibniz-Institute DSMZ Molecular Biology Group.

NK and T cell isolation from peripheral blood

Healthy donor blood collected in trisodium citrate blood collection tubes (Sarstedt) diluted with Dulbecco's Phosphate Buffered Saline (DPBS, Gibco, Life Technologies Limited) in a 1:1 ratio and overlayed on a 1.077 g/mL separation medium (Biocoll, Merck Millipore). Density centrifugation was performed at room temperature (400 g for 30 min) without acceleration and brake. Same methodology was used during the isolation of T cells from patient ascites samples. PBMCs were collected and plastic adherence was performed to deplete monocytes by incubating them in a T175 flask (Sarstedt) at 37 °C and 5% CO_2 for 1 h. For NK isolation, NK MACS Isolation Kit (Miltenyi Biotec) was used according to the manufacturer's instructions. After isolation 5 U/ml recombinant human IL-15 (50 μg, Immuno Tools) was added to NK cells that were used for functional experiments after incubation overnight. For T cell isolation, CD3 human microbeads (Miltenyi Biotec) were used according to the manufacturer's instructions. Purity of isolated T cells was routinely tested. In case of overnight resting 5–10 U/ml of recombinant human IL-2 (50 μg, Immuno Tools) was added to T cells.

NK degranulation assay

NK cells express CD107a during degranulation, which also correlates to NK cell-mediated tumor cell lysis. To evaluate natural and antibody-dependent NK cell cytotoxicity purified NK cells and target cells were coincubated (1:1 ratio) in a flat-bottom 96-well plate with or without different ascites samples. For ADCC-experiments the human anti-EGFR-antibody Cetuximab 1 μg/ml (Erbitux, 5 mg/mL, Merck (Serono)) was added. NK cells were labeled with anti-CD107a-FITC (25 μg/mL, clone H4A3, Mouse IgG1, k, BD Biosciences) and isotype control, respectively. After incubation for 1 h at 37 °C

and 5% CO_2, Golgistop Monensin (BD Biosciences) was added (1:600). After a further incubation of 5 h NK cells were stained with CD56-BV421 (12 μg/mL, NCAM 16.2, IgG2b,k, BD Biosciences) and isotype control. CD107 expression was analyzed by flow cytometry. In case of sodium channel blocker experiment, NK cells were pretreated for one hour with 15 μM of Amiloride after Cell Tracker Red staining.

NK cell tumor killing assay

NK cells and target cells were coincubated (1:1 ratio) with or without Cetuximab (1 μg/ml) and different ascites samples in resulting ratio 1:4 for 24 h at 37 °C and 5% CO_2. Adherent and suspended cells were harvested with Stem Pro Accutase (Gibco by Life Technologies). After washing cells were stained using PE Annexin V Apoptosis Detection Kit I (BD Biosciences) according to the manufacturer's protocol and analyzed by flow cytometry. Alive cells were defined as Annexin V-/7AAD.

Flow cytometric analysis of NK, T cell and tumor cell markers

After coincubation with 25% supplemented ascites media for 24 h, the following antibodies for the flow cytometric analysis of the NK cell marker expression were used: CD56-BV421 (12 μg/mL, clone NCAM 16.2, mIgG2b,k, BD Biosciences), NKp46-PE (CD335, 50 μg/ml, clone 9E2, k, Biolegend), DNAM-1-PerCP-Cy5.5 (CD226, 200 μg/ml, clone 11A8, mIgG1, k, Biolegend), TIGIT-APC (30 μg/mL, A15153A, mouse IgG2b,k, BioLegend), NKG2D-PE-Cy7 (CD314, 200 μg/ml, clone 1D11, mIgG1, k, Biolegend), CD69-FITC (100 μg/ml, clone FN50, mIgG1, k, Biolegend), followed by a live/dead staining using the fixable viability dye eFluor 780 (eBioscience/Thermo Fisher Scientific, Darmstadt, Germany). After coincubation with 25% supplemented ascites media for 48 h, the following antibodies for the flow cytometric analysis of the T cell marker expression were used: CD4-AF647 (100 μg/mL, OKT4, mouse IgG2b,k, BioLegend), CD25-PE (44 μg/mL, 4 E3, mouse IgG2b,k, Miltenyi), CD8-VioBlue (50 μg/mL, LT8, mouse IgG1,k, Miltenyi), Tim-3-PerCP-eFlour710 (12 μg/mL. F38-2E2, mouse IgG1,k, eBioscience). Ovarian cancer cell surface marker expression were detected by staining with the following antibodies: MICA-APC (5 μg/ml, clone 159,227, mIgG2b, k, RD Systems), UBLP-2/5/6-APC (10 μg/ml, clone 165,903, mIgG2a, k, RD Systems), CD54-PE (100 μg/ml, clone HA58, mIgG1,k, Biolegend), and MHCI-PE (25 μg/ml, clone W6/32, mIgG2a,k, Biolegend), HLA-E-APC (200 μg/mL, 3D12, mouse IgG1,k, Biolegend), CD112-PerCP-Cy5.5 (Nectin-2, 200 ug/ml, TX31, mouse IgG1,k, BioLegend), CD155-FITC (PVR1, 100 ug/ml, SKII.4, mouse IgG1,k, BioLegend), CD178-PE (Fas-L, 200 μg/mL, NOK-1, mouse IgG1,k, Biolegend), CD48-VioBright

FITC (REA(S)293, mouse IgG1,k, Miltenyi), EGFR-PE (6.3 ug/ml, EGFR.1, mouse IgG2b,k, BD Bioscience). The same fixable viability dye as for NK markers was used. In all flow cytometry measurements appropriate isotype controls were used: mIgG1-BV510 (100 µg/ml, clone MOPC-21, Biolegend), mIgG1-PE (50 µg/ml, clone MOPC-21, BD Bioscience), mIgG1-PE-Cy-7 (200 µg/ml, MOPC-21, Biolegend), mIgG1-FITC (500 µg/ml, clone MOPC-21, Biolegend), mIgG1-PerCP-Cy5.5 (200 µg/ml, clone MOPC-21, Biolegend), mIgG1-APC (200 µg/ml, clone MOPC-21, Biolegend), mIgG2b-APC (200 µg/ml, clone MPC-11, Biolegend), mIgG2a-APC (200 µg/ml, clone MOPC-173, Biolegend), mIgG1-PE-Cy7 (200 µg/mL, MOPC-21, BioLegend), mIgG1-PerCP-eFlour710 (200 µg/mL, P3.6.2.8.1, eBioscience), mIgG2a-PE (50 µg/mL, G155-178, BD Bioscience), mIgG2a-PerCP-Cy5.5 (200 µg/mL, MOPC-173, BioLegend), mIgG2b-AF647 (200 µg/mL, MOPC-173, BioLegend), mIgG2b-Alexa Fluor®405 (50 µg/mL, 133,303, R&D Systems), mIgG2b-PE (200 µg/mL, 27–35, BD Biosience).

Stained cells were analyzed with BD FACS Canto II using DIVA 8.01 software (BD Biosciences) or FlowJo10 (LLC, Ashland, Oregon, USA).

Detection of NK IFNγ secretion by ELISpot

The ELISpot-technique was applied for sensitive detection of IFNγ-secreting NK cells. First, a Multiscreen 96-well filtration plate (Merck Millipore) was activated with 35% ethanol and coated with anti-IFNγ capture antibody (200 µg/ml, clone 1-D1K, mIgG1, k, Mabtech). After incubation at 4 °C overnight, the plates were blocked with 200 µl of supplemented complete RPMI-1640-media for 2 h at 37 °C. After the washing step isolated NK cells were coincubated with IGROV1 cells in 1:1 ratio and either with or without ascites samples (ratio 1:4). For ADCC conditions, Cetuximab 1 µg/ml (Erbitux, 5 mg/mL, Merck (Serono) was added. After incubation for 24 h at 37 °C and 5% CO_2 plates were washed in the ELISA-washer (PBS / 0,05% Tween-20.) Biotinylated anti-IFNγ detection antibody (200 µg/ml, clone 7-B6-1, mIgG1, k, Mabtech) was added in 2 µg/ml PBS and 1% BSA. The plates were incubated for 2 h at 37 °C, washed and incubated with 50 µl ExtraAvidin alkaline phosphatase (1:1000 diluted in PBS / 1% BSA, Sigma-Aldrich) at room temperature for 2 h. After the washing steps, 75 µl of the ELISpot substrate BCIP/NBT (Roche) was added and incubated for 5–10 min. Developed cytokine spots were measured using AID Classic ELISpot Reader and the results were analyzed with AID ELISpot 7.0 software.

Detection of T cell IFNγ secretion in culture supernatant by ELISA

100.000 T cells were stimulated by 2,5 µl (1:40 dilution) of CD2/CD3/CD28 activator complex (StemCell

Technologies) either in media or 25% ascites supplemented media for four days. After incubation period the experiment supernatant was collected and secreted IFNγ quantified using ELISA kits (R&D Systems, Wiesbaden, Germany) according to the manufacturer's instructions. The plate was measured using spectrophotometer Synergy2 (BioTek).

Conjugation assay

The conjugation rate of NK and tumor cells was analyzed in presence of ascites. NK cells were stained with Cell Tracker Red (Thermo Fisher Scientific) and tumor cells with Cell Tracker Green (Thermo Fisher Scientific) according to the manufacturer's instructions. NKs (50.000 cells) and IGROV1 tumor cells (200.000 cells) were coincubated (1:4 ratio) in presence of 1 µg/ml Cetuximab with or without 25%-ascites-supplemented media. After centrifugation (20 g (570 rpm), 1 min) tubes were placed in a water bath at 37 °C for 45 min. Afterward, the samples were retrieved and briefly vortexed. 300 µl of ice-cold 0,5% PFA in PBS was added and samples were analyzed by flow cytometry. Using flow cytometry, events positive for both cell trackers were determined as conjugates. In case of sodium channel blocker experiment, NK cells were pretreated for one hour with different Amiloride concentrations (1.5, 15 and 150 µM) after Cell Tracker Red staining and dose-response was studied.

Live cell imaging of tumor killing kinetics

100.000 IGROV1 cells per well were seeded in the 96-well plate overnight. Cells were stained with 10 ug/ml Hoechst (Thermo Fisher Scientific) at 37 °C in PBS, HS 3%. After 30 min. cells were washed in PBS and stained with 1:250 dilution of CalceinAM-Orange Red (Thermo Fisher Scientific) at 37 °C in serumless RPMI 1640 for 30 min. The staining solution was replaced by phenol-free RPMI1640 supplemented with 10% (v/v) heat-inactivated fetal calf serum (FCS Gibco), 100 U/mL penicillin, and 100 mg/mL streptomycin (PenStrep, Gibco by Life Technologies) (supplemented complete media). Cells were imaged with ImageXpress Pico Automated Cell Imaging System (Molecular Devices) using 4x objective. Images were captured for three hours, once every 15 min. Hoechst and CalceinAM-Orange Red were visualized at Ex370/Em450 nm for 40 ms (DAPI) and Ex530/Em594 nm for 90 ms (TRITC), respectively. Cells were cultured in the incubating unit at 37.5 °C and 5% of CO_2.

Confocal imaging of PI3K membrane recruitment

50.000 healthy donor T-cells were seeded per well in a 96-well plate. Cells were cocultured either complete media or 25% ascites-supplemented media. T cells were stimulated for 5 min with CD2/CD3/CD28 activator

complex (StemCell Technologies) diluted at 1:20 at 37 °C. In the case of sodium blocker experiments, 150 μM of Amiloride (Sigma-Aldrich) was added to the coculture. After stimulation cells were fixed and permeabilized using Cytofix/Cytoperm (BD Biosciences). Following permeabilization, cells were stained with PIK3R1/p85 antibody and corresponding secondary. T cells were stained by following antibodies in confocal microscopy experiments: PIK3R1/p85 (500 μg/ml, Rat IgG2a, k, W16101a, Biolegend), rat-IgG2a (KLH/G2a-1-1, Dianova), donkey anti-rat AF555 (H+L, 2 mg/ml, polyclonal, Invitrogen) The staining and imaging were performed in Permawash (BD Biosciences). Cells were imaged with confocal microscope Zeiss Elyra PS. (Zeiss) using 1.4 NA 60x oil immersion objective. Alexa Fluor 555 was visualized at Ex561/Em579 nm for 3.85 s per frame. Stained cells were analyzed with ImageJ.

T cell proliferation assay

Isolated healthy donor T-cells were stained using Cell Proliferation Dye EFluor 450 (Thermo Fisher Scientific, 1:1000) for 10 min at 37 °C. For the assay, 50.000 T cells were seeded per well in a 96-well plate. The assay was performed either in complete media or 25% ascites-supplemented media. T cells were stimulated for four days with CD2/CD3/CD28 activator complex diluted at 1:40 (StemCell Technologies). Stained cells were analyzed with BD FACS Canto II using DIVA 8.01 software (BD Biosciences) and FlowJo10 (LLC, Ashland, Oregon, USA).

Electrolyte flux assay

For assessment of intracellular calcium or sodium flux T-cells were stained using Fluo-4 (Thermo Fisher Scientific) or CoroNa Green (Thermo Fisher Scientific), respectively, according to the manufacturer's specifications. For every experimental condition, 250.000 prestained T-cells from original suspensions were taken and incubated either in phenol-free media or 25% ascites-supplemented media in 96 well plates. This was done to ensure consistent dye loading and allow for comparison between samples. In the case of sodium blocker experiments, 150 μM of Amiloride (Sigma-Aldrich), Lidocaine (Sigma-Aldrich), Cariporide (Sigma-Aldrich) and Digitoxin (Sigma-Aldrich) were added to the media as well. The baseline was recorded for 1 min and then 10% (%v/v) of CD2/CD3/CD28 activator complex was added to induce T-cell activation. Intracellular calcium flux was measured at 37 °C using spectrophotometer Synergy2 (BioTek) for 10–15 min in intervals of every 3 s. Intracellular calcium flux data were normalized according to the average unstimulated baseline of media or ascites. In the case of intracellular sodium flux experiment was measured at 37 °C for 20–25 min in intervals of every

5–7 s depending on the experiment. Absorbance was recorded at 480/25 for both Fluo-4 and CoroNa Green. Data for every experimental condition was normalized to the appropriate blank (ascites fluid only) control and presented as fold change of starting point measurement. In the case of calcium flux, comparison was made between peak values of the flux. For sodium influx, endpoint value was compared between conditions. ROC curve analysis was used to confirm significance between different measured flux curves.

Gene expression analysis by quantitative RT–PCR

For quantitative RT–PCR analysis total RNA was isolated from NK and T cells using the RNeasy Mini kit (Qiagen) and reverse transcribed with random-hexamer primer and Superscript II RT, according to the manufacturer's instructions (Thermo Fisher Scientific). Quantitative real-time PCR was conducted with Luna® Universal qPCR Master Mix (New England Biolabs). Primers are listed in Supplementary Table S2, Additional File 1. Representative signal transduction and ion channel genes from different groups were selected for screening. The selection was done according to their functional importance and expression in NK cells as reported in existing RNAseq databases (Gene Expression Omnibus ID GSE153713, https://www.ncbi.nlm.nih.gov/geo/query/acc.cgi?acc=GSM4650127) [21]. The annealing temperature was 62 °C for all primers. Gene expression was normalized according to the chosen housekeeping gene (NK cells – β2-microglobulin, T cells – β-actin) and referent control sample.

Clinical chemistry analysis of patient ascites

Concentrations of sodium, potassium and chloride were measured potentiometrically using an ion-selective electrode on the Atellica CH Analyzer (Siemens Healthineers). Determinations of magnesium (xylidyl blue method), phosphate (ammonium molybdate method), calcium (o-cresol phthalein complexone method), glucose (hexokinase method), total protein (pyrogallol red method), albumin (bromocresol green method) were performed photometrically on the Atellica CH Analyzer (Siemens Healthineers). Immunoturbidimetric methods were used in the measurements of Lp(a), Apo A1, and Apo B on the Atellica CH Analyzer (Siemens Healthineers). Immunonephelometric concentration determinations of IgG, IgA, IgM, the IgG subclasses, α1-antitrypsin, α2-macroglobulin and transferrin were performed on the BN-II (Siemens Healthineers). Measurements of IgE-activity and concentrations of CA 125, CA 15−3, CA 19−9, and CA 72−4 were performed via chemiluminescent sandwich immunoassays on the Atellica IM (Siemens Healthineers). Ammonia concentrations were determined on Dimension XPand Plus

(Siemens Healthineers) by enzymatic method using glutamate dehydrogenase. Measurements of pH values were performed on the pH meter pH700 (Eutech Instruments). Controls of the instruments were performed according to the manufacturer's instructions. Parameters are accredited according DIN EN ISO 15189:2014.

Ultracentrifugation filtration, dialysis and depletion of lipids from ascites samples

Ultracentrifugation filters (Amicon, 0.5 ml, MCWO 3 kDa) were filled up with ascites and centrifuged at 14.000–15.000 g. The centrifugation was stopped for 15 min, after which the remaining ascites in the insert tube was resuspended and centrifugation was continued for 15 min. Upon completion colorless permeate was collected and used without any volume changes or adjustments. For experiments using heated samples permeate was inactivated by heating to 90 °C for 30 min. The volume of the retentate fraction was measured with the pipette during the collection. Subsequently, the retentate was restored to the original volume using phenol-free RPMI 1640. This washing and resuspension of retentate was repeated three times before using the fraction for in vitro testing. For dialysis of ascites samples, dialysis tubing was filled up with ascites and put in beaker containing 1 L of cell culture medium RPMI 1640 (Pura-lyzer, Sigma-Aldrich, 1 kDa and 25 kDa). Tubing was left to incubate for 24 h, after which dialyzed sample was retrieved. Delipidation of ascites samples was done via activated charcoal (20/40 mesh, Supelco) stripping according to an existing protocol [22].

Migration assay

To study the effects of ascites on NK cell migration, 100.000 NK cells in 200 µl of media were added on top of the transwell insert (Sarstedt, 3 µm) that was put onto a 24well plate (Sarstedt). To induce of NK cells the migration, NK cell chemoattractant SDF-1a (Prepotech) was added to the bottom of the transwell assay at 100 ng/ml concentration. Different ascites samples were added as well to the bottom of the transwell in a 1:4 ratio. One well was prepared without chemoattractant to serve as a control for spontaneous migration and another was with added cells but without insert to simulate maximum migration. The migration experiment was incubated at 37 °C for 3 h. After the insert was removed migrated cells were transferred into a 1.5 ml Eppendorf tube. Cells were washed in PBS and resuspended in 200µL of PBS with 3% human serum addition and 25µL of 123count™ eBeads (Thermo Fisher Scientific). Migration was measured by flow cytometry. A stopping gate was set on counting beads (gated on via 488 nm excitation source) and 5.000 beads were acquired in each sample. The migration was calculated according to the following formula: Absolute count (cells/µl) = $\frac{Cellcount+eBeadsvolume}{Cellvolume+eBeadscount} * eBeadsconcentration$. The absolute count of every condition was normalized to the absolute count of maximum migration control.

Electrophoresis and western blot

For mechanistic experiments, 10^6 of NK cells were stimulated for five minutes with 50 ng/ml of PMA and 1 µg/ml of Ionomycin, and lysed with Urea buffer containing 25 mM HEPES (pH 7.3), 0.1% SDS, 1% Triton X-100, 10 mM EDTA, 10 mM sodium pyrophosphate, 10 mM NaF, 125 mM NaCl, 1% protease inhibitor cocktail I, 1% protease inhibitor cocktail III, and 10% PhosStop. Cell debris was removed by centrifugation, and the lysates were incubated with SDS sample buffer (pH 6.8) 50 mM Tris, 4% glycerine, 0.8% SDS, 1.6% β-mercaptoethanol, and 0.04% bromphenol blue) before boiling them at 95 °C for 10 min. 5 µl Spectra Multicolor broad range protein ladder (Thermo Fisher) was included as a molecular marker. The protein of total lysates (18 µl of each cell line) was separated by SDS-7.5%-polyacrylamide gel and immunoblotted according to the semi-dry-blot-method onto polyvinylidene difluoride membrane (PVDM, Roche Diagnostics). The membrane was incubated with the primary antibody followed by HRP-conjugated secondary goat-anti-rabbit IgG. For immunodetection the following antibodies were used: phospho-PI3K-p85/p55 (Cell Signaling Technology), phospho-PLCγ1 (Cell Signaling Technology), phospho-MAPK-p38 (Cell Signaling Technology), Granzyme B (Cell Signaling Technology), PIK3R1/p85 (Rat IgG2a, Biolegend) (Cell Signaling Technology), CLIC1 (Cell Signaling Technology), SLC24A2 (Cell Signaling Technology), GAPDH (total protein) (Cell Signaling Technology, clone 14C10), goat anti-rabbit IgG HRP (Cell Signaling Technology, No. 7074) and goat anti-rat IgG HRP (Dianova). Bands were visualized after the application of the Clarity and Clarity Max ECL Western Blotting substrates (Bio-Rad) and chemiluminescent transformation. The chemiluminescent signal was recorded with the Amersham Imager 600 (GE Health-Care, Chicago, Illinois, USA). Images were analyzed using ImageJ. Phosphorylation was determined by densitometry and normalized to GAPDH and respective ascites and blocker treated controls.

Statistical analysis

Graph data are shown as single values (either single ascites samples or healthy blood donors), means as center values and error bars for the standard deviation (SD). Data points shown in heatmap represent mean values. Statistical tests are described in details in the respective figure legend. Post hoc tests were used after ANOVA when appropriate. All calculations and statistical tests were performed using GraphPad Prism 8 software.
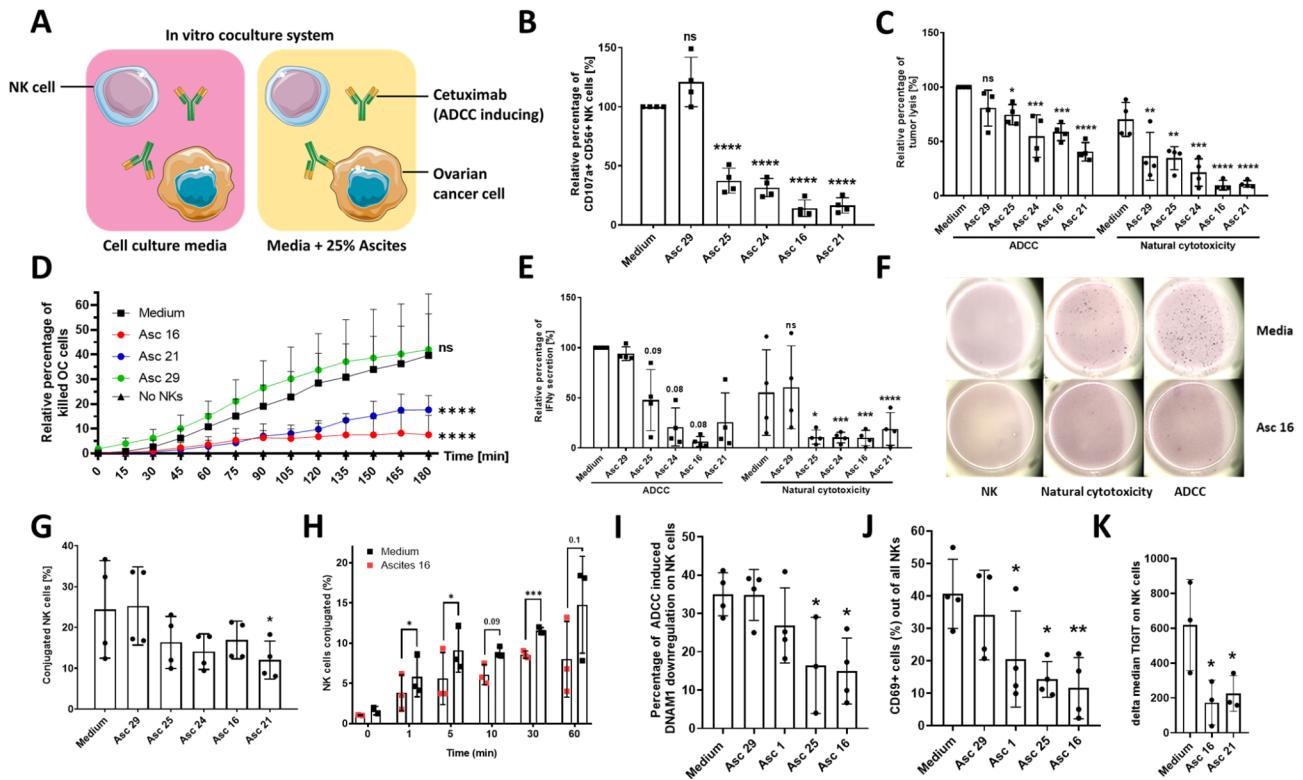
Fig. 1 Malignant ascites impairs different NK cell effector functions. **(A)** Graphical illustration portraying components of performed coculture experiments. **(B)** NK-ADCC in presence of ascites. Resting NK cells from healthy donors were coincubated in 1:1 ratio with IGROV1- cells for six hours with addition of ADCC-inducing anti-EGFR-antibody Cetuximab (1 μg/ml) and malignant ascites (No. 16, 21, 24, 25) and benign ascites (No.29), respectively. **(C)** Tumor cell lysis in presence of ascites. Resting NK cells were directed in 1:1 ratio against IGROV1-cells and coincubated with or without Cetuximab and various ascites samples. After 24 h tumor killing was quantified and relative percentage of lysis is shown. **(D)** Time-dependent tumor cell killing. IGROV1 cells cocultured to resting NK cells and Cetuximab were prestained with CalceinAM-OrangeRed and Hoechst. Dead cells were quantified by loss of CalceinAM dye and normalized to control. **(E+F)** IFNγ secretion of NK cells in presence of ascites. **(E)** Relative percentage of IFNγ secreting NK cells in ELISpot assay **(F)** Representative ELISpot-experiment showing IFNγ secretion spots. **(G and H)** Effect of ascites on NK-tumor cell-conjugation. NK and IGROV1-cells were mixed in 4:1 effector to target ratio in presence of Cetuximab and 25%-ascites-supplemented media. **(G)** Percentage of conjugated NK cells measured by flow cytometry after 45 min of coincubation **(H)** Kinetics of conjugation formation. **(I-K)** Expression of NK markers in presence of ascites. NK cells were cocultured (1:1) with IGROV-1-cells and Cetuximab with or without ascites for 24 h. Surface expression of **(I)** DNAM-1, **(J)** CD69, and **(K)** TIGIT was determined using flow cytometry. Each datapoint represents one healthy donor. The relative percentages are shown after normalization to normal medium control. For significance testing ordinary one-way ANOVA (1.B, C, E, G, I-K) and two-way ANOVA (1.D) were performed, followed by Dunnett's multiple comparison posthoc test between ascites and medium control group where appropriate. Paired t-test was used (1.H). ns (non-significant), * ($p < 0.05$), ** ($p < 0.01$), *** ($p < 0.001$), **** ($p < 0.0001$)

t-SNE analysis was performed using online tool (https://cs.stanford.edu/people/karpathy/tsnejs/csvdemo.html) based on published algorithm [23]. Hierarchical clustering and PCA analysis were performed using online tool ClustVis which was previously published [24].

Results

Malignant ascites strongly inhibits anti-tumor NK cell effector function

For initial experiments NK cells of healthy donors were coincubated with ovarian cancer cells (IGROV1) with or without 25% ascites supplemented media. Natural cytotoxicity (NC) was assessed by determining the expression of CD107a on NK cells. Antibody-dependent cellular cytotoxicity (ADCC) was induced by addition of the specific antibody Cetuximab directed against

EGFR (epidermal growth factor receptor) on target cells (Fig. 1A). Using this setup, we tested the relative inhibitory capacity of ascites samples on NK cell degranulation and killing in both NC and ADCC conditions. Complete characterization of all 28 patient ascites samples regarding their inhibitory potential on NK ADCC degranulation enabled a categorization in very strong, strong, medium, weak inhibitory samples and stimulatory (Table S3, Fig S1A, Additional File 1.). In subsequent functional experiments, we focused on ascites samples which have caused strong or very strong inhibition.

Using this approach, we observed that several malignant ascites samples (no. 25, 24, 21, 16) induced statistically significant inhibition of NK-ADCC after 6 h (Fig. 1B) in a concentration-dependent manner (Fig. S1B). This ascites-mediated immunosuppression of

NK cytotoxicity operated over a wide range of ADCC-inducing Cetuximab antibody concentration (Fig. S1C). Benign ascites (no. 29) derived from a patient with congestive heart failure did not restrict NK-ADCC (Fig. 1B). Healthy donor peripheral blood serum was used as an additional control since it is often compared to ascites fluid in regards to its composition and is much easier to obtain then healthy peritoneal fluid. The addition of the serum only marginally reduced NK function (Fig. S1B). The inhibitory effect of malignant ascites also extended to tumor lysis of ovarian cancer cells in presence (ADCC) or absence of Cetuximab (natural cytotoxicity) after 24 h (Fig. 1C), and was already significant after 2 h (Fig. 1D). In order to exclude that suppression of cytotoxic NK cell function is depending on a specific target cell line, we confirmed our results by using other EGFR-positive cell lines (Fig. S1D, E). Further control showed that ascites did neither directly affect NK cell viability (Fig. S1F) nor tumor cell viability (Fig. S2A, Additional File 1). Accordingly, expression of various surface markers on tumor cells, which are considered to be relevant for the interaction between NK and target cells, remained largely unchanged or did not correlate with ascites-induced inhibitory capacity (Fig. S2B-L, Additional File 1.). Our next experiments evaluated the effect of ascites on cytokine secretion by NK cells. Performing ELISpot assay we could observe that secretion of IFNγ of NK cells cocultured to ovarian cancer cells was substantially reduced in presence of malignant ascites while benign ascites did not affect secretory NK cell function. This impairment was demonstrable for NC- and ADCC-condition (Fig. 1E and F). In further experiments, we examined the impact of ascites on the NK-tumor cell-interaction. It could be demonstrated that the conjugation between NK and cocultured ovarian cancer cells in presence of Cetuximab was substantially reduced by malignant ascites but not by benign sample (Fig. 1G), and this effect could be observed early, already after 5 min (Fig. 1H). Similarly, only the presence of malignant ascites inhibited NK cell migration capabilities (Fig. S3A, Additional File 1.). Corresponding, the expression of regulatory and activation NK cell markers like DNAM-1, CD69 and TIGIT were negatively affected only by malignant ascites (Fig. 1I-K).

In conclusion, in these initial experiments we show that malignant ascites derived from patients with ovarian carcinoma or other adenocarcinoma but not benign ascites causes substantial suppression of major antitumoral NK cell effector functions during interaction with various EGFR-positive target cells.

Malignant ascites interferes with in vitro activation of NK and T cells

After examination of ascites-mediated suppression of NK cells during their interaction with target cells, we next studied ascites-mediated inhibition in a target cell-independent system. To this end, we stimulated NK cells with IL2 in presence of ascites and determined the expression of the regulatory and activation surface markers. As illustrated in Fig. 2A the IL2-mediated upregulation of DNAM-1, CD69 and TIGIT was impaired by malignant ascites but not by benign sample. The expression of NKG2D and NKp46 was similarly affected, although to a lesser extent (data not shown). Comparably, malignant ascites also inhibited target-independent NK degranulation in PMA/Ionomycin-stimulated NK cells (Fig. 2B). To test whether ascites-mediated immunosuppression also affected T cells, we stimulated prestained T cells in the presence of ascites samples. As illustrated in Fig. 2C and D proliferation of T cells was significantly inhibited by malignant ascites. In parallel, IFNγ secretion of activated T cells was reduced (Fig. 2E), along with impaired upregulation of IL2-receptor alpha chain CD25 and activation/exhaustion marker TIM3 (Fig. 2F). Since the calcium influx into the cell is an important prerequisite for the early activation of central effector functions in immune cells, we studied calcium influx in activated T cells in the presence of ascites. We could demonstrate that calcium influx, particularly the peak of calcium influx, was substantially reduced upon addition of malignant suppressive ascites (Fig. 2G). In addition, this inhibition could be detected very early (2–3 min) after addition of the activating complex (Fig. 2H). Interestingly, benign ascites (no. 29) seemed to even support calcium flux into the cell. When assessed via ROC curve analysis, T-cell flux in medium was significantly different when compared to flux in suppressive ascites 16 and 21, while no significance was found for non-suppressive ascites 29 (Fig. 2I). We also tested IL2-stimulated NK cells against additional EGFR-positive cancer cells (A549) in presence of ascites and found that malignant ascites suppressed natural cytotoxicity and ADCC (Fig. S3B, Additional File 1.), tumor lysis (Fig. S3C, Additional File 1.) and conjugation (Fig. S3D, Additional File 1.) of IL2 stimulated NK cells as well.

In summary, here we could show that malignant ascites directly impairs immune cell functions, even in the absence of target cells. This suppression was observed for resting NK cells, stimulated NK cells and T cells.

Electrolyte imbalance in malignant ascites is a major inhibitory mechanism during immunosuppression

In the next series of experiments, we aimed to identify components and molecular determinants which might be responsible for ascites-mediated immunosuppression. In an exploratory approach, we quantified various serum proteins and different electrolytes in ascites samples, corresponding patient serum as well as healthy donor serum and correlated the values to different NK
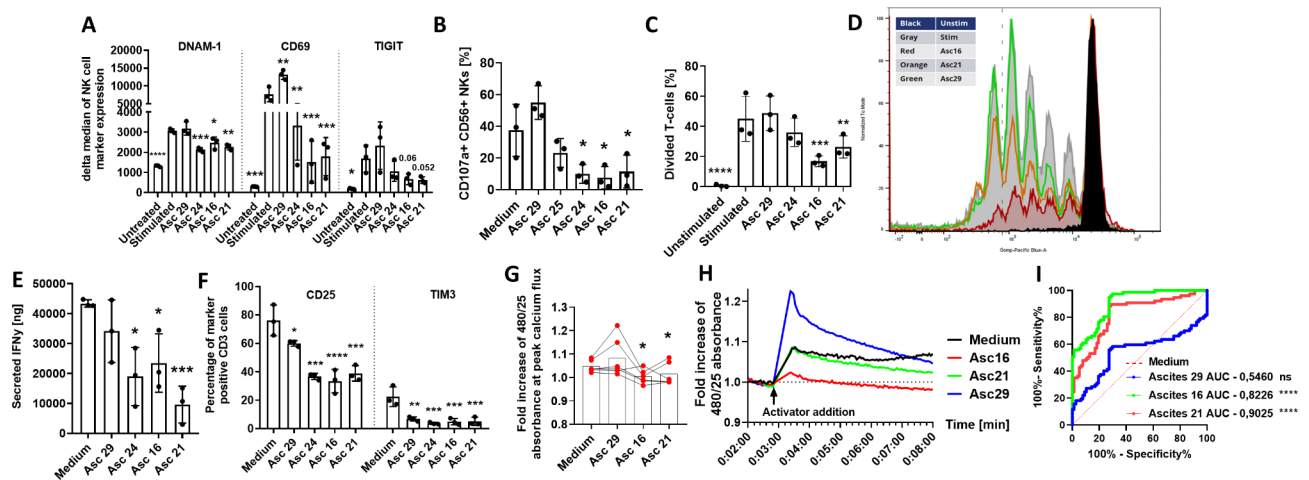
Fig. 2 Malignant ascites causes dysfunction during in vitro activation of NK and T cells. **(A)** Expression of surface markers on stimulated NK cells in presence of ascites. Isolated healthy donor NK cells were coincubated with IL2 (400 U/ml) either in medium or 25%ascites-supplemented media. After 48 h expression of DNAM-1, CD69 and TIGIT was measured by FACS. **(B)** NK cytotoxicity of stimulated NK cells in presence of ascites. Percentage of CD107a-positive NK cells was assessed by FACS after 6-hours of stimulation with PMA (50ng/ml) and Ionomycin (1 µg/ml) either in media or 25% ascites-supplemented media. **(C-F)** Stimulation of T cells in presence of ascites. Isolated healthy donor T-cells were prestained with Cell Proliferation Dye EFluor 450 and stimulated using CD2/CD3/CD28 activator complex (1:40) either in medium or 25%ascites-supplemented media for four days. **(C)** Graph showing T cells proliferation. **(D)** Representative experiment showing T cell proliferation. **(E)** Secreted IFNγ [ng/ml] during T cell proliferation determined by ELISA. **(F)** Percentage of CD25-positive (left column) and TIM3-positive T cells (right column). **(G + H + I)** Intracellular Calcium-flux during T cell stimulation in presence of ascites. T cells were exposed to CD2/CD3/CD28 activator either in presence of ascites or medium. Intracellular Ca2 + flux was monitored via Fluo-4 dye. **(G)** Fold increase of 480/25 absorbance at peak of calcium flux. **(H)** Representative experiment of calcium flux after T cell stimulation in presence of ascites. **(I)** ROC analysis shows significant difference between calcium flux curves in suppressive ascites environment (red and green line) compared to medium (dotted red line). Data are presented as individual values with mean value as center of error bar ± standard deviation. Each datapoint represents one healthy donor. The normalization was done according to normal medium control. For significance testing ordinary one-way (2.A-C, E-F) and paired (2.G) ANOVA or ROC analysis (2.I) were performed, followed by Dunnett's multiple comparison posthoc test between ascites and medium control group where appropriate. * ($p < 0.05$), ** ($p < 0.01$), *** ($p < 0.001$), **** ($p < 0.0001$)

effector functions (Fig. 3A, B). Interestingly, correlative statistical analysis revealed a potential connection between NK cytotoxicity and concentrations of distinct electrolytes (particularly, Na, K, Cl, Fig. 3B) in ascites. In detail, high concentration of sodium in ascites was in fact negatively correlated to NK ADCC while high concentrations of chloride and potassium showed positive correlation to cytotoxic activity of NK cells (Fig. 3B, C). Furthermore, by ROC analysis the electrolyte concentration served as a prognostic factor for a 50% reduction in NK activity (Fig. 3D). Hierarchical clustering (Fig. 3E) was performed using all obtained clinical chemistry data (taken from Fig. 3A). Ascites cluster 1 (AC1) contained samples with high sodium and low chloride content. All cluster 1 samples also had strong or very strong inhibitory activity (categories taken from table S3). In contrast, cluster 3 (AC3) displayed a different clinical chemistry profile and mostly contained ascites samples of medium or weak inhibitory activity. Thus, the three formed sample clusters mirror our ranked list of samples, separating them into strong, medium and weak suppressive clusters (Supplementary Table S3 (Additional File 1.), Fig S1A). To further substantiate the connection between electrolyte content and immunosuppressive activity of ascites we used the t-SNE method with ascites electrolyte data

as dimensions (Fig. 3F). t-SNE plots grouped ascites samples into distinct clusters, which closely resembled the functional subgroups found in NK assays (Fig. 3C, left). Importantly, high chloride content in malignant ascites as well as the capacity of the ascites to reduce NK cytotoxicity were all correlated with poor survival of ascites-donors (Fig. 3G), which underscores a potential clinical relevance of our experimental findings. The investigated electrolyte imbalance was only specific to the ascites, as sodium concentration in matched patient peripheral blood sera did not differ from normal values in healthy donor control serum (Fig. 3H). A strong trend regarding chloride concentration in ascites was noted as well. Except for CA125 concentrations, no correlations could be found between patient serum and patient ascites components. Additionally, the concentration of patient serum components was not correlated to effector function (data not shown). To further assess differences between healthy donor serum, patient serum and ascites we performed PCA analysis using all clinical chemistry data, and found that a considerable number of patient ascites samples segregates from serum samples of patients and healthy donors (Fig. 3I).

Based on these detailed analyses of patient ascites, the consecutive experiments aimed to provide experimental
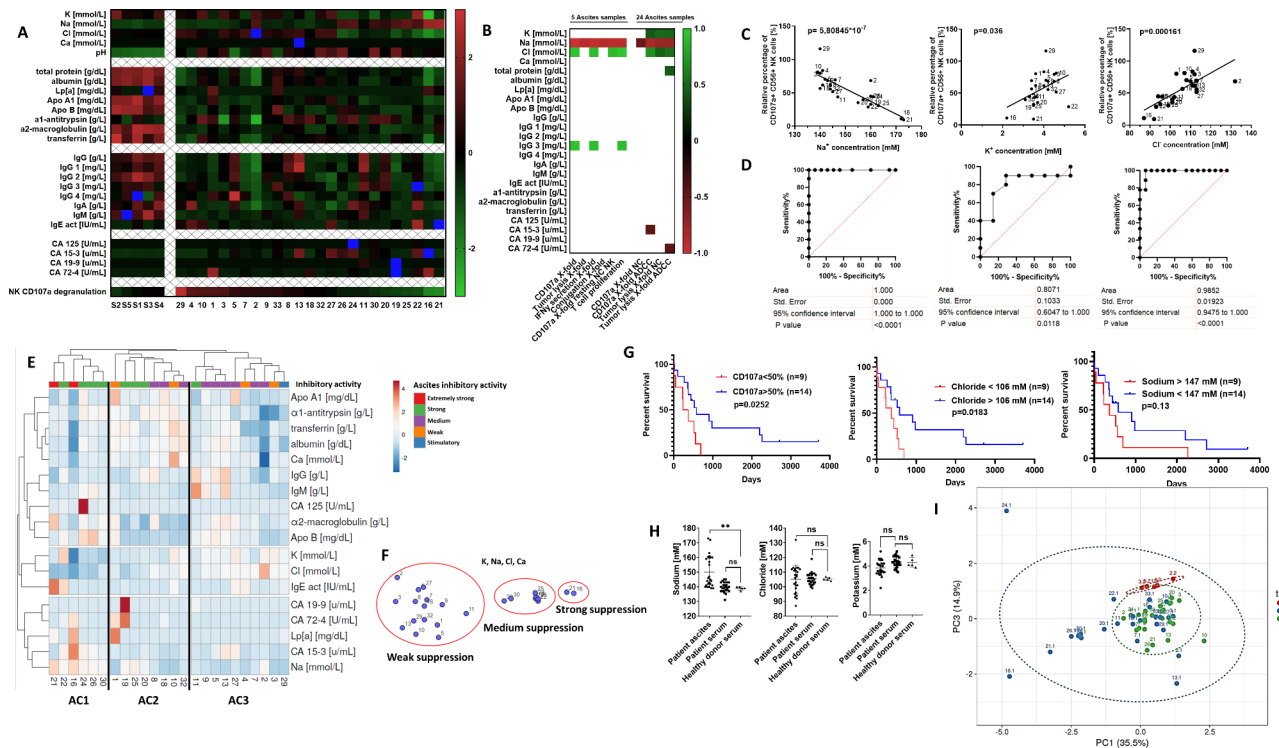
Fig. 3 Aberrant electrolyte concentrations in malignant ascites contribute to suppression of immune cell functions. **(A)** Content of ascites and healthy donor serum. Components of ascites samples and healthy serum samples were determined by clinical chemistry analysis. Presented in the heatmap are calculated z-score values for each component. **(B)** Correlation between quantified ascites components and NK effector function. The matrix depicts significant positive and negative correlations (p < 0,05) between quantified ascites components and different NK effector functions. **(C)** Correlation between NK ADCC and electrolyte content in ascites. Pearson correlation shows negative correlation for sodium (left) and positive correlation for potassium (middle) and chloride (right) with NK ADCC. **(D)** Relationship between electrolytes in ascites and NK cytotoxicity. ROC (Receiver operating characteristic) curve showing the relationship between the concentrations of sodium (left), potassium (middle) and chloride (right) and 50% of NK cell degranulation inhibition. **(E and F)** Clustering of ascites samples. **(E)** Hierarchical clustering of ascites samples according to clinical chemistry data. **(F)** t-SNE plot showing the clustering of ascites samples according to electrolyte content. **(G)** Impact of electrolyte content in ascites on patient survival. Kaplan-Meier curves showing significant negative association of suppressed NK cytotoxicity (left), low chloride (middle) and high sodium content in ascites with patient survival. **(H and I)** Composition comparison of ascites, patient serum and healthy donor serum. **(H)** Comparison of the concentrations of sodium (left), chloride (medium), and potassium (right) between healthy donor and patient serum and ascites. **(I)** PCA plot showing clustering of ascites, patient and healthy donor serum done using clinical chemistry data. Two-tailed Pearson correlation (3.C) and ROC analysis (3.D) were used. Kaplan Meier curves (3.G) for overall survival were used with Mantel-Cox test (log-rank). Each datapoint represents one ascites sample. For significance testing ordinary one-way ANOVA was performed, followed by Dunnett's multiple comparison posthoc test between ascites and healthy or patient serum (3.H). ns (non-significant), ** (p < 0.01)

evidence for an involvement of electrolyte imbalance in suppression of NK cytotoxicity. For this purpose, proteins in ascites samples were depleted using 3 kDa ultracentrifugation filters (Fig. 4A). Electrolyte and protein content was quantified in ascites permeate fraction (contains no proteins > 3 kDa) and ascites retentate fraction (all proteins > 3 kDa) by clinical chemistry analysis (Fig. 4B) and electrophoresis (Fig. 4C). With this approach we demonstrate that the ascites permeate fraction retained its capability to impair T cell proliferation and NK ADCC comparably to unmodified ascites (Fig. 4D and E). Furthermore, the inhibitory effect of the permeate fraction was still present after heat treatment at 90 °C indicating that the inhibitory component is heat-resistant (Fig. 4F). The inhibitory effect persisted even after performing charcoal stripping, which excludes lipids and other

lipid-based molecules as main inhibitory mediators (Fig. S4A and B). To further explore the impact of these small heat resistant non-lipid molecules, we performed dialysis for 24 h on ascites samples using 1 kDa or 25 kDa dialysis columns (Fig. 4G). After the dialysis, electrolyte and protein content were quantified and it was shown that electrolyte concentrations were successfully restored to levels contained in cell culture medium RPMI 1640, in which dialysis was performed (Fig. 4H). Additionally, no substantial loss of proteins or IgG antibodies happened during the dialysis. When dialyzed samples were used in NK degranulation assay, NK cells achieved significantly higher degranulation compared to untreated samples (Fig. 4I). The restorative effect was the strongest in ascites samples with highest electrolyte imbalance.
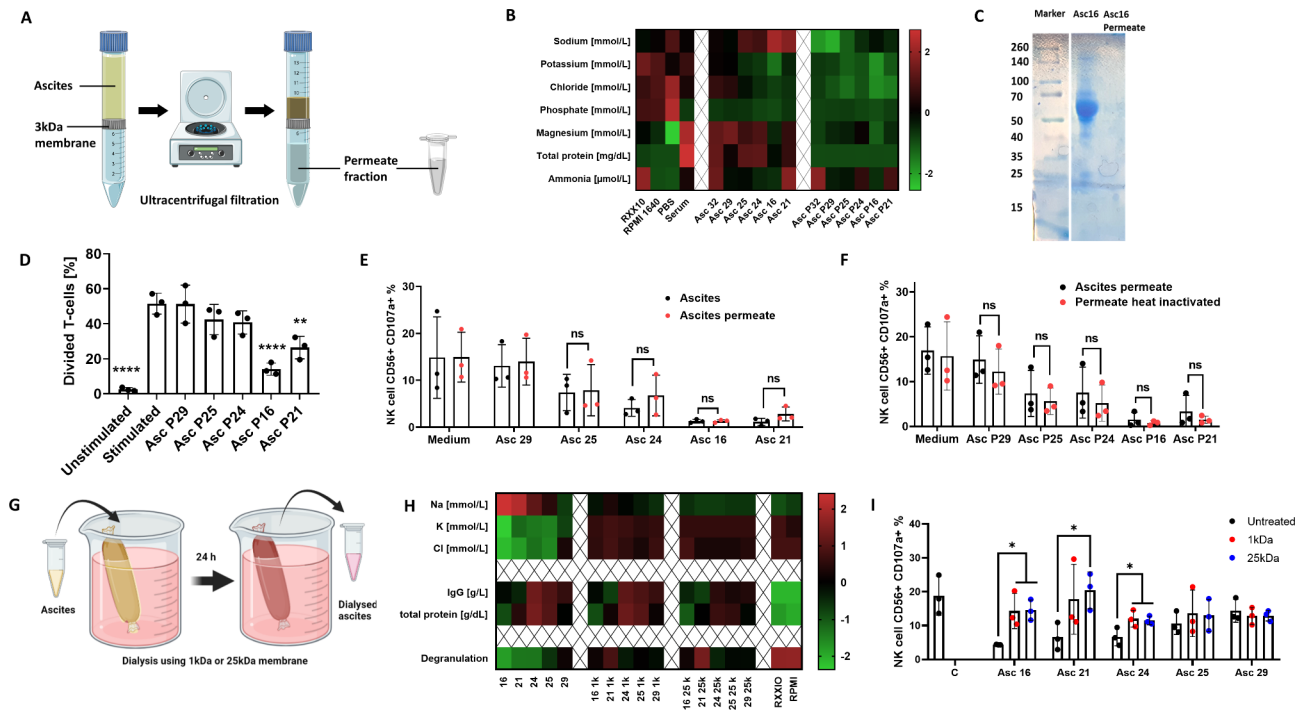
Fig. 4 Ascites dialysis partially reverses inhibitory properties caused by non-protein and heat resistant components. **(A)** Graphical illustration of protein depletion in ascites. Ascites sample was processed via ultracentrifugal filtration and protein-rich retentate and protein-less permeate are collected. **(B)** Composition of ascites before and after protein depletion. Heatmap showing altered composition of protein-depleted ascites samples and protein-rich retentates. **(C)** Electrophoresis of ascites sample. Representative electrophoresis blot of ascites sample 16 and corresponding permeate. **(D)** Proliferation of activated T cells in presence of protein-depleted ascites. Prestained donor T-cells were stimulated using CD2/CD3/CD28 activator complex (1:40) in protein-less ascites permeate. **(E)** NK ADCC in presence of ascites permeate. Resting NK cells were coincubated in 1:1 ratio with IGROV1 cells with addition of ADCC-inducing anti-EGFR antibody Cetuximab in presence of unmodified or protein-less ascites permeate. **(F)** NK ADCC in presence of heat inactivated ascites permeate. Resting NK cells were coincubated in 1:1 ratio with IGROV1-cells and ADCC-inducing anti-EGFR antibody Cetuximab with protein-depleted ascites permeate which was heat inactivated at 90 ℃ for 1 h. **(G)** Graphical illustration of ascites dialysis in cell culture medium. Ascites samples were processed in medium overnight using 1 kDa or 25 kDa cutoff dialysis columns. **(H)** Composition of ascites before and after dialysis. Heatmap showing altered composition of ascites samples processed by dialysis. **(I)** NK ADCC in presence of dialyzed ascites. Resting NK cells were coincubated in 1:1 ratio with IGROV1 cells with addition of ADCC-inducing anti-EGFR antibody Cetuximab in presence of unmodified or dialyzed ascites. After 6 h expression of CD107a on NK cells was determined by flow cytometry. Each datapoint represents one healthy donor. For significance testing ordinary one-way ANOVA followed by Dunnet posthoc test (4.D) and two-way ANOVA followed by Sidak posthoc test was used (4.E, F and I). ns (non-significant), * ($p < 0.05$), ** ($p < 0.01$), **** ($p < 0.0001$)

All presented data support the hypothesis that electrolyte content, and not protein function, inhibits anti-tumoral NK and T cell activity in malignant ascites. Specifically, high concentrations of sodium and low content of chloride and potassium caused reduced effector function.

Malignant ascites alters expression of ion channels, signaling pathways and effector molecules

In the next series of experiments, we wanted to identify ion channels and down-stream signaling pathways that were modulated by our clinical ascites samples. To this end, resting and IL2-stimulated NK cells as well as T cells were exposed to different ascites samples. In an explorative analysis we assessed the mRNA-expression of 18 different highly expressed genes which are known to be crucial [21] for signal transduction during various effector functions of NK and T cells and examined expression

levels of essential electrolyte channels (Fig. 5A). Further statistical analysis revealed significant correlations between immune cell effector function, ascites electrolyte composition and mRNA-expression of selected genes (Fig. 5B). Suppressive ascites samples induced significant downregulation of signaling molecules such as PIK3CD (Fig. S5A, left, Additional File 1.) and PRKCQ (Fig. S5B, left, Additional File 1.). As expected, expression of these signaling molecules correlated with effector functions in NK (Fig. S5A, right, Additional File 1.) and T cells (Fig. S5B, left, Additional File 1.). In the same way, ascites affected transcript levels of various ion channels, for example, SLC24A2 (NCKX4, Sodium/potassium/calcium exchanger 4), which was found to have a strong positive correlation to most effector functions (Fig S5B, right, Additional File 1.). We also observed significantly reduced expression of CLIC1 (chloride intracellular channel protein 1) in presence of malignant ascites (Fig. S5C,
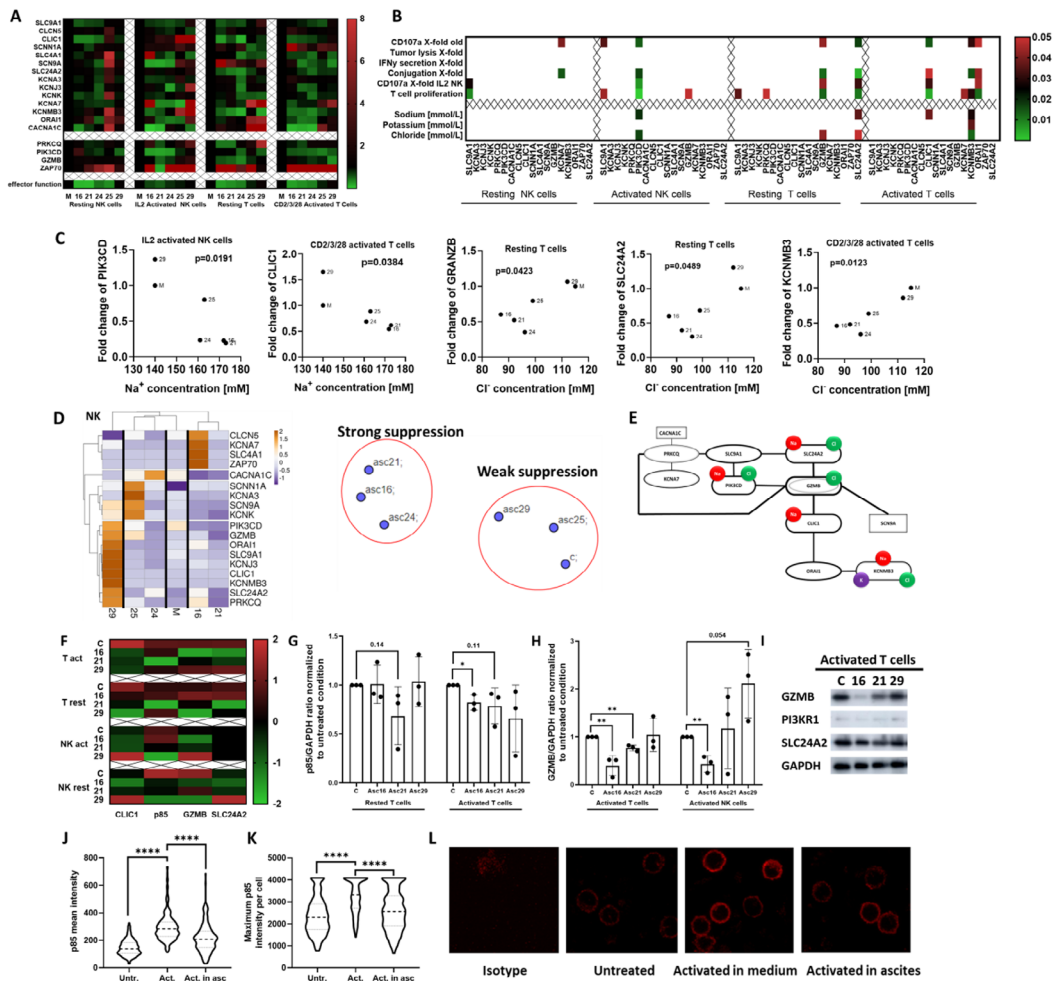
Fig. 5 Malignant ascites causes transcriptional and translational changes of signaling proteins and electrolyte channels in immune cells. **(A)** Heatmap showing altered transcriptional gene expression in immune cells in presence of ascites. Resting NK cells were incubated with ascites for 6 h, and IL2 activated NK cells for 24 h. Resting T cells were incubated with ascites for 24 h and the activation complex was treated for 48 h. Total RNA was isolated from NK and T cells. Quantitative real-time PCR was conducted with annealing temperature of 62 °C for all primers. Primers are listed in Supplementary Table S2 **(B)** Correlation between NK effector function, electrolyte content in ascites and altered mRNA-expression of selected genes. Correlation matrix depicts significant gene expression changes (p < 0,05) in resting and activating NK cells (left) and resting and activated T cells (right). **(C)** Correlation between electrolyte content in ascites and altered mRNA-expressions of selected genes. Significant Pearson correlations of gene expression changes and electrolyte content in ascites. Sodium correlation to PI3K in IL2-activated NK cells (first panel). Chloride correlation to Granzyme B (third panel) and SLC24A2 (fourth panel) in resting T cells. Correlation of CLIC1 to sodium (second panel) and KCNMB3 to chloride (fifth panel) in complex activated T cells. **(D)** Clustering of mRNA-transcripts of stimulated NK cells in presence of ascites. Hierarchical clustering done according to gene expression data from ascites treated activated NK cells (left). t-SNE plot demonstrating unbiased grouping of ascites samples according to most affected genes (right). **(E)** Graphical illustration of crucial transcriptional changes in NK and T cells after ascites exposure. Portrayed genes were affected by ascites exposure significantly as shown by both ANOVA and Pearson correlation. Lines connecting genes show Pearson correlation relationships. Every gene affected by specific electrolyte was marked with appropriate symbol (Na-red, Cl-Green and K-Purple). **(F, G, H and I)** Protein expression of electrolyte channels and immune effector molecules in NK and T cells affected by ascites. Both NK and T cells were incubated in medium or 25% ascites supplemented medium for 24 h (resting cells) or 48 h (activated cells). NK cells were treated with 50 ng/ml of PMA, 1 µg/ml of Ionomycin, while T cells were activated by adding 5 µl of CD2/CD3/CD28 activator. Protein expression was determined by densitometric analysis of western-blots and normalized to GAPDH. **(F)** Heatmap overview showing protein expression comparison between the healthy donor (C), two inhibitory (No.16, 21), and one non-inhibitory (No.29) ascites- treated NK and T cell samples. **(G)** p85 expression in samples from resting and activated T cells as determined by western blot. **(H)** Bar graph depicting different Granzyme B expression in samples from activated T and NK cells. **(I)** Western blot bands from representative experiment. **(J, K and L)** Ascites-mediated inhibition of p85 membrane recruitment in T cells. Isolated T cells were activated for 5 min with CD2/CD3/CD28 activator in either medium or ascites 21 supplemented medium. Surface localization and expression of p85 was determined by confocal microscopy. **(J)** Violin plot depicting p85 mean intensity on T cell surface. **(K)** Violin plot depicting the maximum of p85 intensity of each cell. **(L)** Representative confocal microscopy images showing T cell surface expression of p85 (red) in different conditions. Data are presented as individual values with mean value as center of error bar ± standard deviation. For significance testing two-tailed Pearson correlation were used (5.B, C), paired t-test was used to assess the significance (5. G, H), ordinary one-way ANOVA and Dunnett posthoc (5.J. K). *($p < 0.05$), **($p < 0.01$), ****($p < 0.0001$).

right, Additional File 1.) and CLIC1 expression was connected to NK ADCC degranulation (Fig.S5C, left, Additional File 1.). Finally, we wanted to link those findings to actual electrolyte concentrations in ascites samples. To achieve this, we plotted concentrations of sodium and chloride against expression levels of molecules from our gene expression analysis and found a significant correlation between the content of sodium and chloride and expression level changes of PIK3CD, CLIC1, GRANZB, SLC24A2, and KCNMB3 respectively (Fig. 5C). Considering all significant gene expression changes and correlations, we aimed to see if assessed genes could serve as a specific signature of ascites-induced changes. Using hierarchical clustering on gene expression data of activated NK cells (Fig. 5D, left) we were able to generate heatmaps that successfully clustered treated cells depending on which ascites samples they were exposed to. Similarly, by using gene expression data from IL2-activated NK cell for t-SNE, ascites samples segregated into more and less suppressive groups (Fig. 5D, right). Our data suggest a functional connection between electrolyte imbalance, ion channels and immune effector function, which we have portrayed in a gene network map that summarizes the connections between the individual genes and the impact of different electrolytes on their expression (Fig. 5E).

To confirm the clinical relevance of our data we assessed the expression of investigated genes in T cells isolated from ascites of two ovarian cancer patients. The expressions of PIK3CD, AKT1, SLC9A1, and SCNN1A transcripts were consistently downregulated in both patient ascites-isolated T cells and two ascites-treated healthy donor T cells (Fig. S6A). Additionally, ZAP70, SCN9A, and CLCN5 were upregulated in patient cells similar to one of the ascites treated samples (Fig. S6B). T cells from ascites also showed a unique gene set that was not induced in HD T cells exposed to ascites (e.g. PRKCQ, GZMB, CACNA1C) (Fig. S6A, left). To further demonstrate the similarity between ascites-isolated and ascites-treated T cells we used the t-SNE method with gene expression data as dimensions (Fig. S6C). t-SNE plot grouped untreated healthy donor T cells in distance to ascites-treated and patient-isolated T cells. In addition, we performed a re-analysis of published RNAseq dataset by Fraser et al. [21] and found that GZMB, SLC4A1 and CACNAC1 and KCNA7 were similarly downregulated in both ascites-treated and patient-isolated NK cells (Fraser study, data not shown) and our study (Fig. 5A).

For further confirmation, we also assessed the protein expression of selected important ion channels and effector molecules to show that ascites-induced effects are not limited to the level of transcript. As illustrated in Fig. 5F ascites No.16 and No.21 negatively affected the expression of all investigated proteins in both T and NK cells in either rested or activated state (Fig. 5F). The most pronounced ascites-induced effects were the significant decreases in p85 and Granzyme B protein expressions, especially observed during T and NK cell activation (Fig. 5G - I).

Since PI3K plays a crucial role in T cell signalling and the membrane recruitment of p85 can be used for defining T cell activation state, our next experiments examined the p85 membrane expression in presence of ascites. Our first assessment confirmed that p85 is indeed localized on the membrane and is present to some degree even in resting non-activated T cells. As illustrated in Fig. 5J, K and L (second and third panel) the activation of T cells induced a strong increase of p85 membrane recruitment compared to untreated control cells. However, the presence of ascites during the activation significantly impaired p85 membrane expression (Fig. 5J, K and L (forth panel)). These data support the important role of PI3K in activation and ascites-mediated inhibition of functional T cells.

In summary, our experiments show that malignant ascites substantially downregulated the transcript and protein expression of various signal transduction molecules, notably PI3K, as well as distinct ion channels.

Sodium channel inhibitors prevent ascites-induced sodium influx and immunosuppressive effects

As our current data suggest that high concentrations of sodium in ascites are causally involved in suppression of immune cell function, in our final series of experiments we used selected inhibitors of sodium channels and examined their potential as modulators of ascites-induced immunosuppression. First, we determined the intracellular concentration of sodium in T cells upon coincubation with different ascites samples. As illustrated in Fig. 6A and B high sodium ascites samples (No. 16 and 21) induced a significant influx of sodium during the 25-minute period of incubation, while the low sodium benign ascites sample No. 29 caused a significant efflux of intracellular sodium (Fig. 6A, B and C). Interestingly, PBS control also induced influx of sodium (Fig. 6A) which may be due to the low chloride-high sodium content in PBS solution. Next, we used the sodium channels inhibitors amiloride, lidocaine, cariporide and digitoxin in order to manipulate the sodium flux in T cells in presence of different ascites samples. We found that all used inhibitors (Fig. 6D, left) prevented sodium influx in T cells in presence of high sodium ascites sample (No. 21). In contrast, in presence of benign ascites (No. 29), which has physiological sodium content, the influx of sodium was only minimally altered. On the contrary, particularly amiloride and lidocaine were even able to augment efflux of sodium into extracellular space (Fig. 6D, right).

As we could demonstrate that malignant ascites is able to impair calcium influx into T cells (Fig. 2G and
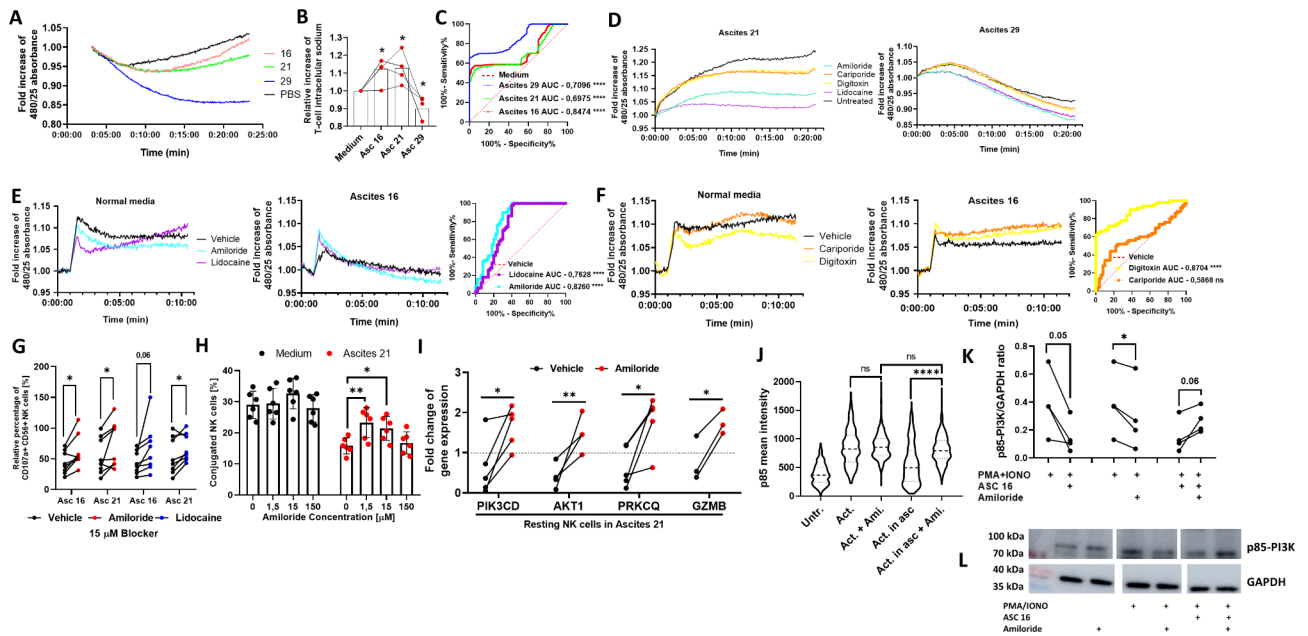
Fig. 6 Malignant ascites-mediated immunosuppression can partially be reversed by inhibitors of sodium channels. **(A, B and C)** Sodium influx in T cells in presence of ascites. T cells were exposed to 25%-ascites supplemented media or PBS and media control, respectively. After 25 min. influx of sodium was measured using fluorescent CoroNa Green dye. **(A)** Representative experiment showing sodium influx in T cells in presence of different malignant ascites samples. **(B)** Relative increase of intracellular sodium in T cells in presence of different ascites samples. Comparison is made between experiment endpoint values. **(C)** ROC curve analysis shows significant difference between measured sodium flux curves in suppressive ascites environment (red and green line) compared to medium (dotted red line). **(D)** Sodium influx in T cells in presence of ascites and inhibitors of sodium channels. CoroNa Green prestained resting T-cells were exposed to different samples of 25%-ascites-supplemented media (left: ascites 21, right: ascites 29) and media control, respectively. Different inhibitors of sodium channels were added (150 μM). Results were normalized to starting fluorescence. Representative experiments are shown. **(E and F)** Calcium influx in activated T cells in presence of ascites and inhibitors of sodium channels Fluo-4 prestained resting T cells were activated using CD2/CD3/CD28 complex either in normal media or high sodium malignant ascites sample No.16. Sodium channel inhibitor were added with activator complex simultaneously. **(E)** Representative experiment of calcium influx in activated T cells in presence of amiloride and lidocaine and ascites 16 (middle panel) and media control (left panel). ROC curve analysis (right panel) shows significant differences between measured calcium flux curves in ascites 16 with addition of amiloride (cyan line) or lidocaine (purple line), compared to vehicle control (dotted red line). **(F)** Representative experiment of calcium influx in activated T cells in presence of cariporide and digitoxin and ascites 16 (middle panel) and media control (left panel). ROC curve analysis (right panel) shows significant difference between measured calcium flux curves in ascites 16 with addition of cariporide (orange line) or digitoxin (yellow line), compared to vehicle control (dotted red line). **(G)** NK cell degranulation in presence of ascites and sodium channel inhibitors. Isolated NK cells were pretreated with water (vehicle control) or 15 μM addition of amiloride or lidocaine for one hour. Washed NK cells were exposed to 25%-ascites supplemented media and media control, respectively. After 6 h NK cell degranulation was measured using FACS. **(H)** NK-TC conjugation in presence of ascites and amiloride. Isolated NK cells were pretreated with water (vehicle control) or 1,5, 15 or 150 μM addition of amiloride for one hour. NK cells and IGROV1-cells were mixed in 4:1 effector to target ratio in presence of 1 μg/ml Cetuximab and in presence or absence of 25%-ascites-supplemented media. **(I)** Expression of NK cell signal transduction and effector molecules in presence of ascites 21 and amiloride. Resting and activated NK cells were incubated with ascites sample No. 21 and water (vehicle control) or 150 μM addition of amiloride for 3 h. Fold change of PIK3CD, AKT1, PRKCQ and GZMB gene expressions. Gene expression was normalized to housekeeping gene and respective ascites treated controls. **(J)** p85 membrane recruitment in activated T cells in presence of ascites 21 and amiloride. Isolated T cells were activated with CD2/CD3/CD28 activator in either medium or ascites 21 supplemented medium with addition of 150 μM of Amiloride for five minutes. Surface localization and expression of p85 was determined by confocal microscopy. Violin plot depicts p85 mean intensity on T cell surface. **(K and L)** Phosphorylation of signal transduction protein p85-PI3K in NK cells in presence of ascites 16 and amiloride. **(K)** Isolated NK cells were exposed to were exposed to 25%-ascites supplemented media and media control. During the incubation, NK cells were treated with 50 ng/ml of PMA, 1 μg/ml of Ionomycin and/or 150 μM of amiloride for five minutes. Phosphorylation was determined by densitometry and normalized to GAPDH and respective ascites treated controls. **(L)** Western blot bands from representative experiment and GAPDH control. Each datapoint represents one healthy donor. For significance testing RM one-way ANOVA followed by Dunnett's multiple comparison posthoc test (6.B and J), two-way ANOVA followed by Dunnett's multiple comparison posthoc test (6.H) and paired t-test were used (6.G, I and K). ns (non-significant), * ($p < 0.05$), ** ($p < 0.01$), ****($p < 0.0001$).

H), which subsequently suppressed immune cell functions, we examined whether sodium channel inhibitors were able to normalize calcium flux in activated T cells. Indeed, most of the tested sodium channel inhibitors restored calcium influx in activated T cells incubated with high sodium ascites No. 16 (Fig. 6E and F,

middle panels). Restorative effects of amiloride, lidocaine and digitoxin on T cell calcium flux in ascites environment were confirmed as significant by ROC curve analysis (Fig. 6E and F, right panels). The preincubation of NK cells with amiloride or lidocaine prior to ADCC assay in ascites environment partially restored NK

degranulation (Fig. 6G). Similarly, preincubating NK cells with amiloride significantly reversed ascites-induced inhibition of NK conjugation (Fig. 6H).

In order to further substantiate these data, we examined the expression of different signaling molecules in NK cells in presence of malignant ascites (no.21) and sodium channel inhibitors. Here we observed that sodium blocker amiloride restored ascites-induced downregulation of PIK3CD, PRKCQ, GZMB and AKT1 in resting NK cells incubated with ascites (Fig. 6I). Lidocaine had a similar, but less pronounced effect in activated cells (data not shown). In line with these data the addition of amiloride during T cell activation also restored membrane recruitment of p85 in ascites treated cells (Fig. 6J). Lastly, western blot was performed to examine the impact of ascites and amiloride on phosphorylation of p85-PI3K regulatory subunit in PMA/Ionomycin activated NK cells. Here we were able to demonstrate that after five minutes PI3K phosphorylation was impaired by presence of ascites. Interestingly, while amiloride caused a moderate inhibition of PI3K phosphorylation in medium conditions, in presence of sodium rich ascites the inhibitor increased phosphorylation and this counteracted ascites-induced suppression in all four independently performed experiments (Fig. 6K and L).

In summary, the presented data show that a sodium imbalance in ascites is mechanistically involved in regulation of calcium flux, downstream signaling, and NK/T effector functions (Fig. 7).
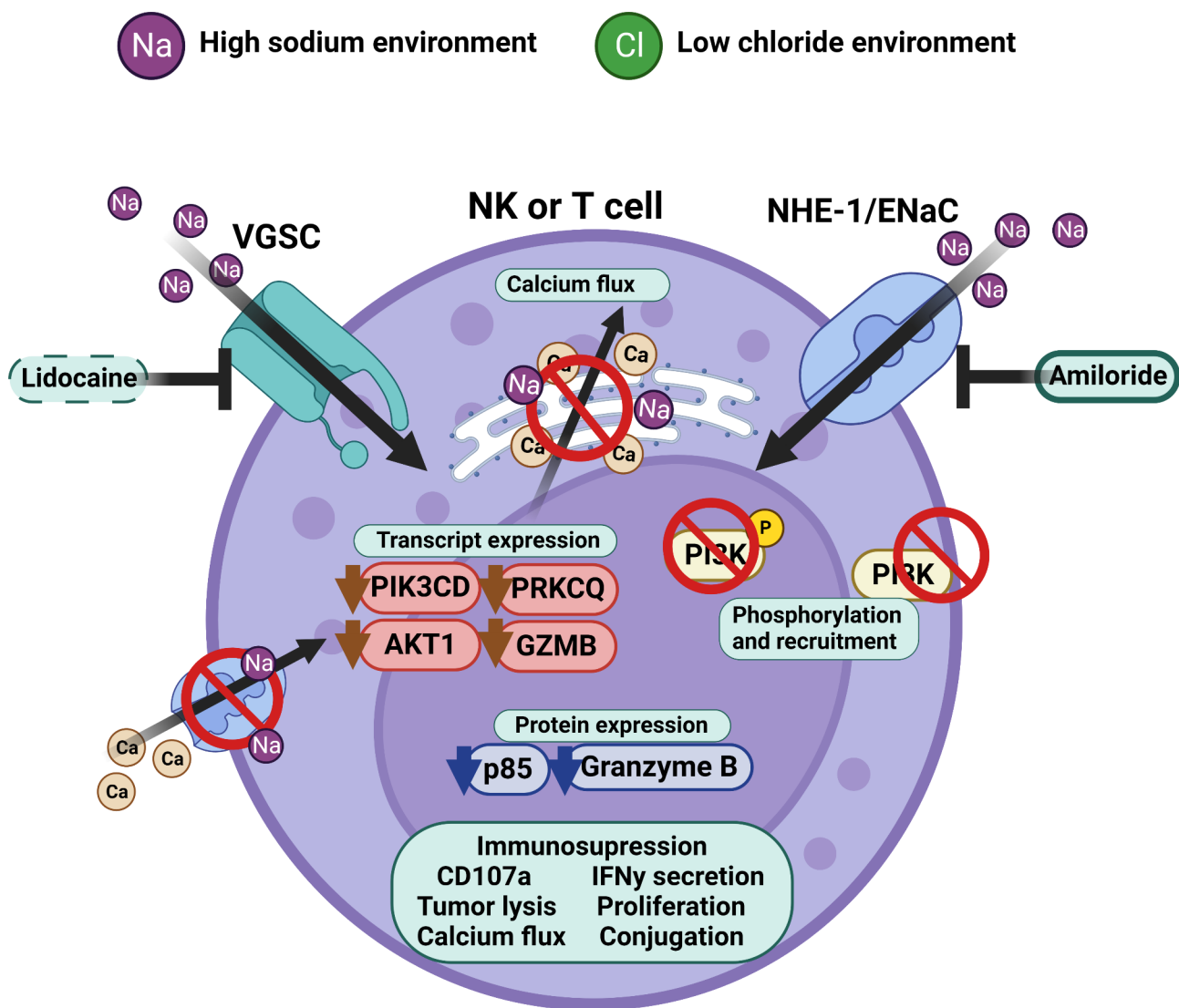

Fig. 7 Illustration of proposed inhibitory molecular mechanism. Malignant peritoneal ascites is characterized by a sodium/chloride imbalance. This imbalance suppresses NK and T cell effector function by interfering with calcium signaling and signal transduction. Sodium channel blockers can prevent inhibitory effects caused by excess of sodium. Illustration was created with BioRender

Discussion

Immunotherapeutic approaches offer great potential for cancer treatment, but success in epithelial ovarian cancer is still limited. Advanced or recurrent ovarian cancer is mostly associated with the presence of malignant ascites, a pathological fluid accumulation in the peritoneal cavity [6]. Its heterogeneous composition generates a unique tumor microenvironment that has long been known to mediate immunosuppression and promote disease progression [8]. Thus, malignant ascites limits response to immunotherapy and results in poor patient survival [7].

At present, the molecular mechanisms that mediate the immunosuppressive effects of malignant ascites are still poorly understood. Previous studies focused on the characterization of cellular components and studied tumor cell-related mechanisms promoting tumor growth and metastasis [15, 25]. Further studies regarding soluble factors mainly concentrated on analyzing cytokines or metabolites and for some of those factors, prognostic relevance or immunosuppressive effects could be demonstrated [17, 18]. Furthermore, ascites protein fraction might contribute to immunosuppression, since even some healthy serum proteins are reported to negatively regulate immune cell activity [26, 27]. Among these, intrinsic serum immunoglobulins are able to compete with therapeutic antibody and impair ADCC [28]. However, existing reports about properties of potential inhibitory factors in malignant ascites are inconsistent regarding their immunosuppressive power, sensitivity to heat, or degradation by proteases [20, 29, 30]. These inconsistencies could be based on methodological challenges as the application of standard biochemical methods, precipitation agents [20, 30, 31], proteases in different vehicle fluids [20, 29, 30] and other chemical additives [29, 32] might result in irreversible alteration of the original ascites. Other studies used methods of chromatographic fractionalization with the potential risk of dilution or loss of proteins and other non-proteinous components [20]. Thus, methodological challenges in biochemically separating ascites components, while retaining full biological activity, could have contributed to the failure of fully identifying immunosuppressive components in ascites so far.

In the first part of our study, we examined the immunosuppressive potential of malignant ascites on antitumoral activity of NK cells. We compared different ascites samples of patients with advanced or recurrent ovarian cancer, gastrointestinal adenocarcinoma and benign diagnosis, respectively. We studied their impact on different effector functions of NK cells directed to ovarian cancer cells. We could demonstrate that cytotoxic and secretory NK cell functions were substantially impaired by malignant ascites which is consistent with other studies [16]. Upregulation of NK activation marker CD69

and TIGIT as well as downregulation of DNAM-1 was inhibited, suggesting that ascites-mediated immunosuppression was mainly due to hindered NK cell activation and not due to NK cell exhaustion [16]. In line with some previously published work, we showed that inhibition was independent from presence of target cells and also affected T cell activity directly [33, 34]. Of note, also downregulation of HLA-E, a molecule implicated in the regulation NK activity under certain conditions, did not affect tumor cell lysis in our systems. Interestingly, studying flux of calcium ions in proliferative T cells in presence of ascites demonstrated that inhibition of effector cell activity was initiated early, after few minutes. Accordingly, NK cell killing and conjugation was already affected shortly after incubation with ascites. Remarkably, all suppressive effects were only mediated by malignant ascites but not by benign sample derived from patient with congestive heart failure.

In the second part of our study, we aimed to identify novel factors and mechanisms which are responsible for immunosuppression in malignant ascites. In contrast to previous qualitative approaches [20, 30], we initially performed a comprehensive quantitative analysis of ascites composition. To this end, we fractionated acellular ascites samples without chemical alteration. With this approach, we found that a small, non-proteinous component was responsible for immunosuppressive activity. Thus, we quantified the concentrations of various electrolytes and serum proteins in ascites samples by clinical chemistry analysis and correlated our results to antitumoral NK cell activity and patient survival. Interestingly, we could identify aberrant electrolyte content in malignant ascites as novel factors suppressing immune cell functions. Specifically, high sodium content as well as low content of chloride and potassium were significantly correlated with reduced NK and T cell effector function. Thereby, ROC curve analysis revealed that all three electrolytes predicted inhibition of immune functions. Furthermore, high sodium was significantly correlated to patient poor survival in our cohort. In contrast, excessive chloride content was significantly associated with favorable patient outcome suggesting an independent protecting role by positive modulation of immune function. In addition, the extent of NK inhibition by malignant ascites was correlated to patient outcome as well. In conclusion, the association between NK inhibition and patient survival also suggests that the degree of NK inhibition corresponds to immunosuppression in the peritoneal cavity of patients. Further reprocessing of ascites samples revealed that after ultracentrifugation protein-depleted permeate fraction still suppressed NK cell cytotoxicity and T cell proliferation. Additionally, by inactivating ascites samples by heating, we confirmed that potential inhibitors are heat resistant. Charcoal stripping excluded lipids as

major mediators of suppression. Correction of the electrolyte imbalance by dialysis abrogated the immunosuppressive effect, especially in ascites samples with strong electrolyte imbalance. The hypothesis of electrolyte-mediated suppression of immune cell functions has been explored in some earlier studies [35–37]. These studies provided initial evidence that sodium and potassium cations may affect NK cell function. It was reported that NK cell function was reduced in environments with unphysiologically low or high concentrations of sodium (75nM – 150 nM) [38]. Similarly, monocyte-mediated ADCC was affected by extracellular Na^+ and K^+ concentrations [35]. However, these studies were mostly observational and often no detailed underlying molecular mechanisms could be identified. More recent studies predominantly focused on the impact of high salt diet on immune cell functions [39, 40] and the relevance of high sodium in the microenvironment of solid tumors [41]. In this context, extracellular potassium originating from necrotic tumor areas could impair T cell effector functions [42]. A possible explanation for suppression in these examples is that ions can bind to protein helices, which changes their conformation and can prevent interaction with ligands or other proteins [43]. Two studies show that chloride binding to specific residues affected the catalytic activity of pancreatic α-amylase [44] and the permeability of the SLC4A1 channel [45]. Beside regulating enzymatic activities in phagocytes [46], in the few existing studies chloride was shown to be essential for regulating immune cell function [47, 48]. In conjunction with our findings, these data from other disease settings underscore the relevance of electrolytes homeostasis and imbalance for proper immune function or dysfunction, respectively.

In the final part of our study, we mechanistically explored a novel immunosuppressive mechanism in the liquid tumor microenvironment of the peritoneal cavity. This mechanism is primarily mediated by defective intracellular calcium signaling as well as modulation of signal transduction pathways and ion channels of NK and T cells. We confirmed that specific ion channels such as SLC9A1 (NHE-1), SLC24A2 (NCKX4), and SCNA9 (Nav1.7, VGSC) were closely linked to other key effector molecules like Granzyme B or signal transducers like PI3K-δ and PKC-θ, which are necessary for proper immune function. Furthermore, malignant ascites induced downregulation of Granzyme B and PI3K-δ not only on transcription level, but also on protein level, which correlated to weaker effector function and ascites sodium content. In addition, the presence of inhibitory ascites impaired the rapid membrane recruitment of p85 (the 85KDa regulatory subunit of PI3Kinase) during the T cell activation, which provides a molecular basis for the early onset of activation failure.

To provide causal evidence for the involvement of ion channels, we used the channel blocker amiloride (ENaC/NHE-1), lidocaine (VGSC), cariporide (NHE-1), and digitoxin (Na+/K+ATPase) to modulate the activity of sodium channels. We observed immunosuppressive effects of sodium excess on T cell activation as sodium channel blockers amiloride, lidocaine and digitoxin restored T cell calcium influx in sodium-rich ascites coculture within first five minutes of exposure. In subsequent experiments preincubation with amiloride or lidocaine blockers had caused a reversal of ascites-mediated inhibition of effector functions. Both NK cell degranulation (six hours) and NK-TC conjugation (45 min) were significantly higher after amiloride or lidocaine pretreatment. Furthermore, using a similar approach we confirmed the mechanism of sodium-induced aberrant gene expression. The direct addition of sodium channel blocker, amiloride, prevented ascites-mediated downregulation of PIK3CD, PRKCQ, AKT1, and GZMB transcripts. After short activation and exposure to ascites environment (five minutes), amiloride was also able to partially restore the phosphorylation of signaling protein p85-PI3K and to completely restore its membrane recruitment in NK and T cells, respectively. These experiments open the possibility to use sodium channel blockers as immunomodulatory agents that may restore immune activity in suppressive microenvironments [36, 49].

Conclusion
In summary, here we report novel factors and mechanisms causing immunosuppression in malignant ascites in peritoneal carcinomatosis. The quantitative analysis of various acellular components in malignant ascites and their correlation to impaired antitumoral NK activity identified imbalanced electrolytes (sodium, potassium and chloride) as the source of inhibition. High sodium content was proven to substantially inhibit all crucial effector functions of NK cells and impair T cell activity as well. Furthermore, we could show for the first time that the extent of immunosuppression on NK cytotoxicity is correlated to patient poor survival. Unexpectedly, the positive correlation of chloride content to patient outcome suggests a protective effect of elevated chloride. Therapeutic application of selected ion channel inhibitors may provide novel means to restore immune effector cell activity in ascites and counteract immunosuppression.

Abbreviations

NC	Natural toxicity
ADCC	Antibody-dependent cellular cytotoxicity
ASC	Ascites
AC	Ascites cluster
P	Permeate
Act.	Activated
Untr.	Untreated
Ami.	Amiloride

Data Availability

The original contributions presented in the study are included in the article/Supplementary Material. Further inquiries about the data access can be directed to the corresponding author.

Declarations

Ethics approval and consent to participate

The studies involving human participants were reviewed and approved by the ethics committees of the medical faculties of the University Duisburg-Essen and of the University of Cologne. The participants provided their written informed consent to participate in this study.

Consent for publication

All authors have contributed and reviewed the final manuscript. All authors agreed with decision to submit with intent to publish.

Competing interests

SB receives research support from Roche/Genentech in the context of the imcore network outside of this work. All other authors declare no potential conflicts of interest.

Author details

[1]Experimental and Translational Research, Department of Otorhinolaryngology, University Hospital Essen, Hufelandstrasse 55, 45147 Essen, Germany
[2]Department of Clinical Chemistry, University Hospital Essen, 45147 Essen, Germany
[3]Department of Endocrinology, Diabetes and Metabolism, University Hospital Essen, 45147 Essen, Germany
[4]Department of Gynecology and Obstetrics, University Hospital Essen, 45147 Essen, Germany
[5]partner site Essen-Düsseldorf, German Cancer Consortium (DKTK), 45147 Essen, Germany
[6]Department of Gynecology and Obstetrics, University Hospital of Cologne, 50931 Cologne, Germany

References

1. Sung H, Ferlay J, Siegel RL, Laversanne M, Soerjomataram I, Jemal A, et al. Global Cancer Statistics 2020: GLOBOCAN estimates of incidence and Mortality Worldwide for 36 cancers in 185 countries. CA Cancer J Clin. 2021;71(3):209–49.
2. Hwang WT, Adams SF, Tahirovic E, Hagemann IS, Coukos G. Prognostic significance of tumor -infiltrating T cells in ovarian cancer: a meta-analysis. Gynecol Oncol. 2012;124(2):192–8.
3. Cibula D, Rob L, Mallmann P, Knapp P, Klat J, Chovanec J, et al. Dendritic cell-based immunotherapy (DCVAC/OvCa) combined with second-line chemotherapy in platinum-sensitive ovarian cancer (SOV02): a randomized, open-label, phase 2 trial. Gynecol Oncol. 2021;162(3):652–60.
4. Hoogstad-van Evert J, Bekkers R, Ottevanger N, Schaap N, Hobo W, Jansen JH, et al. Intraperitoneal infusion of ex vivo-cultured allogeneic NK cells in recurrent ovarian carcinoma patients (a phase I study). Med (Baltim). 2019;98(5):e14290.
5. Steis RG, Urba WJ, VanderMolen LA, Bookman MA, Smith JW 2nd, Clark JW, et al. Intraperitoneal lymphokine-activated killer-cell and interleukin-2 therapy for malignancies limited to the peritoneal cavity. J Clin Oncol. 1990;8(10):1618–29.
6. Ayantunde AA, Parsons SL. Pattern and prognostic factors in patients with malignant ascites: a retrospective study. Ann Oncol. 2007;18(5):945–9.
7. Lane D, Matte I, Rancourt C, Piche A. Prognostic significance of IL-6 and IL-8 ascites levels in ovarian cancer patients. BMC Cancer. 2011;11:210.
8. Ahmed N, Stenvers KL. Getting to know ovarian cancer ascites: opportunities for targeted therapy-based translational research. Front Oncol. 2013;3:256.
9. Vazquez J, Chavarria M, Lopez GE, Felder MA, Kapur A, Romo Chavez A, et al. Identification of unique clusters of T, dendritic, and innate lymphoid cells in the peritoneal fluid of ovarian cancer patients. Am J Reprod Immunol. 2020;84(3):e13284.
10. Lai P, Rabinowich H, Crowley-Nowick PA, Bell MC, Mantovani G, Whiteside TL. Alterations in expression and function of signal-transducing proteins in tumor-associated T and natural killer cells in patients with ovarian carcinoma. Clin Cancer Res. 1996;2(1):161–73.
11. Carlsten M, Norell H, Bryceson YT, Poschke I, Schedvins K, Ljunggren HG, et al. Primary human tumor cells expressing CD155 impair tumor targeting by down-regulating DNAM-1 on NK cells. J Immunol. 2009;183(8):4921–30.
12. Vyas M, Reinartz S, Hoffmann N, Reiners KS, Lieber S, Jansen JM, et al. Soluble NKG2D ligands in the ovarian cancer microenvironment are associated with an adverse clinical outcome and decreased memory effector T cells independent of NKG2D downregulation. Oncoimmunology. 2017;6(9):e1339854.
13. Kim S, Kim B, Song YS. Ascites modulates cancer cell behavior, contributing to tumor heterogeneity in ovarian cancer. Cancer Sci. 2016;107(9):1173–8.
14. Nilsson MB, Langley RR, Fidler IJ. Interleukin-6, secreted by human ovarian carcinoma cells, is a potent proangiogenic cytokine. Cancer Res. 2005;65(23):10794–800.
15. Zhan N, Dong WG, Wang J. The clinical significance of vascular endothelial growth factor in malignant ascites. Tumour Biol. 2016;37(3):3719–25.
16. Greppi M, Tabellini G, Patrizi O, Candiani S, Decensi A, Parolini S et al. Strengthening the AntiTumor NK cell function for the treatment of Ovarian Cancer. Int J Mol Sci. 2019;20(4).
17. Castriconi R, Cantoni C, Della Chiesa M, Vitale M, Marcenaro E, Conte R, et al. Transforming growth factor beta 1 inhibits expression of NKp30 and NKG2D receptors: consequences for the NK-mediated killing of dendritic cells. Proc Natl Acad Sci U S A. 2003;100(7):4120–5.
18. Krockenberger M, Dombrowski Y, Weidler C, Ossadnik M, Honig A, Hausler S, et al. Macrophage migration inhibitory factor contributes to the immune escape of ovarian cancer by down-regulating NKG2D. J Immunol. 2008;180(11):7338–48.

19. Kline JB, Kennedy RP, Albone E, Chao Q, Fernando S, McDonough JM, et al. Tumor antigen CA125 suppresses antibody-dependent cellular cytotoxicity (ADCC) via direct antibody binding and suppressed Fc-gamma receptor engagement. Oncotarget. 2017;8(32):52045–60.
20. Oh SK, Moolten FL. Purification and characterization of an immunosuppressive factor from ovarian cancer ascites fluid. Eur J Immunol. 1981;11(10):780–8.
21. Fraser CC, Jia B, Hu G, Al Johani LI, Fritz-Klaus R, Ham JD, et al. Ovarian Cancer Ascites inhibits transcriptional activation of NK cells partly through CA125. J Immunol. 2022;208(9):2227–38.
22. Chen RF. Removal of fatty acids from serum albumin by charcoal treatment. J Biol Chem. 1967;242(2):173–81.
23. MLVaH GE. Visualizing data using t-SNE. J Mach Learn Res. 2008;9:2579–605.
24. Metsalu T, Vilo J. ClustVis: a web tool for visualizing clustering of multivariate data using principal component analysis and heatmap. Nucleic Acids Res. 2015;43(W1):W566–70.
25. Latifi A, Luwor RB, Bilandzic M, Nazaretian S, Stenvers K, Pyman J, et al. Isolation and characterization of tumor cells from the ascites of ovarian cancer patients: molecular phenotype of chemoresistant ovarian tumors. PLoS ONE. 2012;7(10):e46858.
26. Kragballe K, Ellegaard J, Herlin T. Antibody-dependent monocyte-mediated cytotoxicity. The interference by platelets, immune complexes, and normal serum. Scand J Haematol. 1980;25(1):67–75.
27. Dickinson AM, Shenton BK, Alomran AH, Donnelly PK, Proctor SJ. Inhibition of natural killing and antibody-dependent cell-mediated cytotoxicity by the plasma protease inhibitor alpha 2-macroglobulin (alpha 2 M) and alpha 2 M protease complexes. Clin Immunol Immunopathol. 1985;36(3):259–65.
28. Preithner S, Elm S, Lippold S, Locher M, Wolf A, da Silva AJ, et al. High concentrations of therapeutic IgG1 antibodies are needed to compensate for inhibition of antibody-dependent cellular cytotoxicity by excess endogenous immunoglobulin G. Mol Immunol. 2006;43(8):1183–93.
29. Medoff JR, Clack VD, Roche JK. Characterization of an immunosuppressive factor from malignant ascites that resembles a factor induced in vitro by carcinoembryonic antigen. J Immunol. 1986;137(6):2057–64.
30. Bains SJYS, Landskron J, Bjorge L, Rokkones E, Taskén K. Characterization of Immunosuppressive Properties of Malignant Ascites in Ovarian Carcinoma. Gynecology&Obstetrics (Sunnyvale). 2016;6(8):6.
31. Elg SA, Mayer AR, Carson LF, Twiggs LB, Hill RB, Ramakrishnan S. Alpha-1 acid glycoprotein is an immunosuppressive factor found in ascites from ovaria carcinoma. Cancer. 1997;80(8):1448–56.
32. Hess AD, Gall SA, Dawson JR. Partial purification and characterization of a lymphocyte-inhibitory factor(s) in ascitic fluids from ovarian cancer patients. Cancer Res. 1980;40(6):1842–51.
33. Tran E, Nielsen JS, Wick DA, Ng AV, Johnson LD, Nesslinger NJ, et al. Polyfunctional T-cell responses are disrupted by the ovarian cancer ascites environment and only partially restored by clinically relevant cytokines. PLoS ONE. 2010;5(12):e15625.
34. Simpson-Abelson MR, Loyall JL, Lehman HK, Barnas JL, Minderman H, O'Loughlin KL, et al. Human ovarian tumor ascites fluids rapidly and reversibly inhibit T cell receptor-induced NF-kappaB and NFAT signaling in tumor-associated T cells. Cancer Immun. 2013;13:14.
35. Ladisch S, Ulsh L, Feig SA. Influence of monovalent cation concentrations on monocyte-mediated ADCC. Adv Exp Med Biol. 1982;146:255–64.
36. Huwyler T, Hirt A, Felix D, Morell A. Effect of cations and cation channel blockers on human natural killer cells. Int J Immunopharmacol. 1985;7(4):573–6.
37. Schlichter L, Sidell N, Hagiwara S. Potassium channels mediate killing by human natural killer cells. Proc Natl Acad Sci U S A. 1986;83(2):451–5.
38. Schlichter LC, MacCoubrey IC. Interactive effects of na and K in killing by human natural killer cells. Exp Cell Res. 1989;184(1):99–108.
39. Zielinski CE. Regulation of T cell responses by ionic salt signals. Cells. 2021;10(9).
40. Muller DN, Wilck N, Haase S, Kleinewietfeld M, Linker RA. Sodium in the microenvironment regulates immune responses and tissue homeostasis. Nat Rev Immunol. 2019;19(4):243–54.
41. Leslie TK, James AD, Zaccagna F, Grist JT, Deen S, Kennerley A, et al. Sodium homeostasis in the tumour microenvironment. Biochim Biophys Acta Rev Cancer. 2019;1872(2):188304.
42. Eil R, Vodnala SK, Clever D, Klebanoff CA, Sukumar M, Pan JH, et al. Ionic immune suppression within the tumour microenvironment limits T cell effector function. Nature. 2016;537(7621):539–43.
43. Luscher BP, Vachel L, Ohana E, Muallem S. Cl(-) as a bona fide signaling ion. Am J Physiol Cell Physiol. 2020;318(1):C125–C36.
44. Maurus R, Begum A, Kuo HH, Racaza A, Numao S, Andersen C, et al. Structural and mechanistic studies of chloride induced activation of human pancreatic alpha-amylase. Protein Sci. 2005;14(3):743–55.
45. Salhany JM, Sloan RL, Cordes KS. The carboxyl side chain of glutamate 681 interacts with a chloride binding modifier site that allosterically modulates the dimeric conformational state of band 3 (AE1). Implications for the mechanism of anion/proton cotransport. Biochemistry. 2003;42(6):1589–602.
46. Wang G. Chloride flux in phagocytes. Immunol Rev. 2016;273(1):219–31.
47. Prochazka G, Landon C, Dennert G. Transmembrane chloride flux is required for target cell lysis but not for golgi reorientation in cloned cytolytic effector cells. Golgi reorientation, N alpha-benzyloxycarbonyl-L-lysine thiobenzyl ester serine esterase release, and delivery of the lethal hit are separable events in target cell lysis. J Immunol. 1988;141(4):1288–94.
48. Gray LS, Russell JH. Cytolytic T lymphocyte effector function requires plasma membrane chloride flux. J Immunol. 1986;136(8):3032–7.
49. Roselli F, Livrea P, Jirillo E. Voltage-gated sodium channel blockers as immunomodulators. Recent Pat CNS Drug Discov. 2006;1(1):83–91.

Publisher's Note
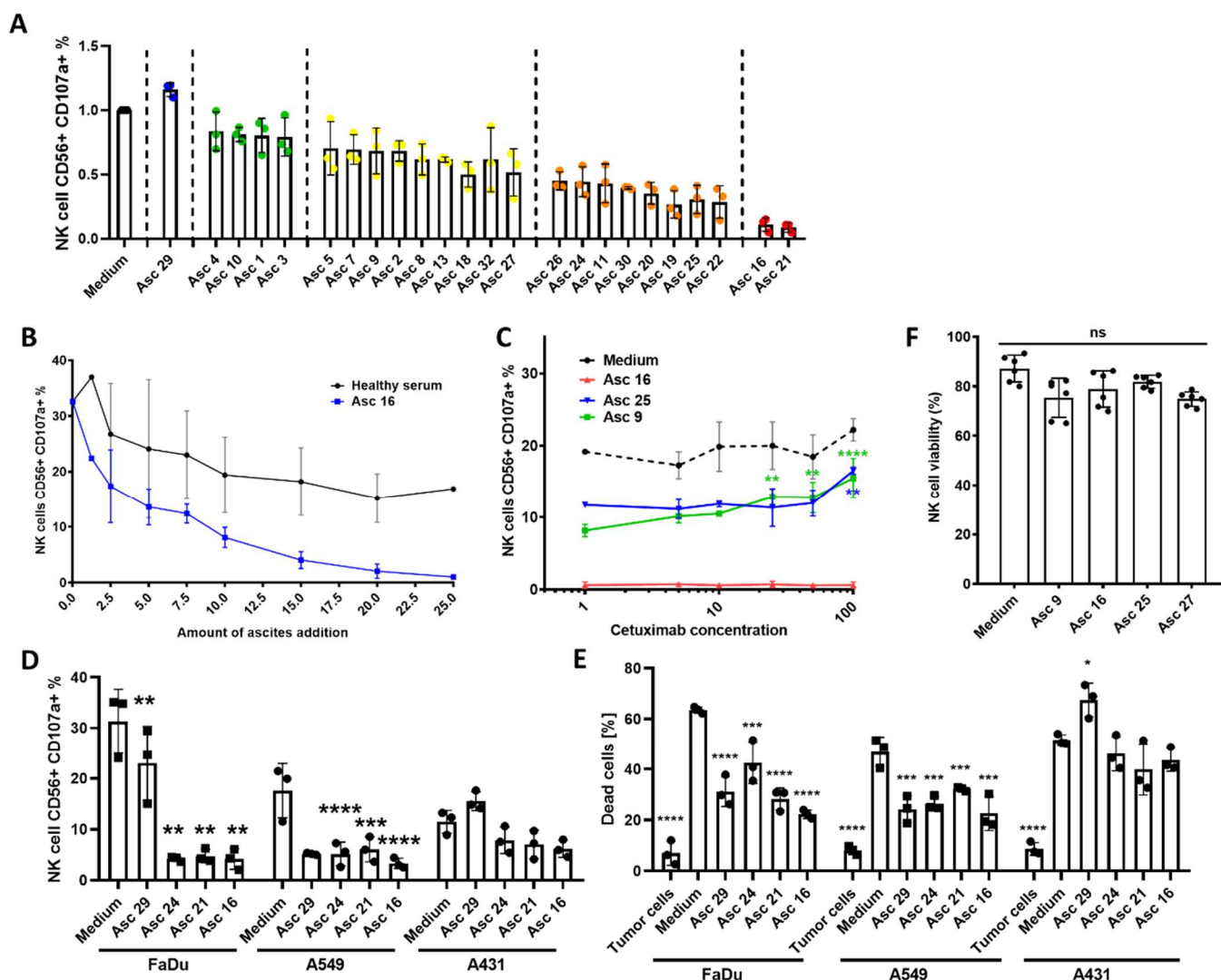
Supplementary Figure 1. – Malignant ascites impairs interaction between NK cells and different types of EGFR-positive cancer cells. (A) Ascites dependent inhibition of NK-ADCC. NK cells were coincubated in 1:1 ratio with EGFR-positive IGROV1 ovarian cancer cells in presence of various ascites samples and ADCC-inducing antibody Cetuximab (1 µg/ml). Percentage of CD107a-positive NK cells was determined after 6 hours by flow cytometry and was normalized to medium control. **(B) Comparison of NK-ADCC inhibition by malignant ascites and healthy donor serum.** NK cells were coincubated in 1:1 ratio with EGFR-positive A549 lung adenocarcinoma cells in increasing concentration of healthy donor serum or ascites 16 added to media and ADCC-inducing antibody Cetuximab (1 µg/ml). Percentage of CD107a-positive NK cells was determined after 6 hours by flow cytometry. **(C) Cetuximab-concentration-independent inhibition of NK-ADCC by malignant ascites.** NK cells were coincubated with A549 lung adenocarcinoma cells in 1:1 ratio either in media or media supplemented with 25% of different malignant ascites samples. ADCC-inducing antibody Cetuximab was added in increasing concentration. Percentage of CD107a-positive NK cells was measured after 6 hours by flow cytometry. **(D and E) NK ADCC and tumor lysis of EGFR-positive cancer cells in presence of ascites.** NK cells were coincubated in 1:1 ratio with head and neck cancer cell line FaDu, lung cancer cell line A549 and epidermoid cancer cells, respectively. Cetuximab (1 µg/ml) was added with or without 25% ascites supplemented media. **(C)** After 6 hours percentage of CD107a-positive NK cells directed against FaDu (left column), A549 (middle column) and A431 (right column) was determined by flow cytometry. **(D)** After 24 hours percentage of lysed FaDu cells (left column), A549 (middle column) and A431 cells (right column) was quantified by Annexin/7AAD-staining in the flow cytometer. **(F) NK cell viability in presence of ascites.** NK cells were coincubated with media or media supplemented with 25% of different ascites samples. Percentage of viable cells was assessed after Annexin/7AAD-staining by flow cytometer. Data are presented as individual values with mean value as center of error bar ± standard deviation. For significance testing ordinary one-way ANOVA (S1.D-F) and two-way ANOVA (S1.B, C) with Dunnet posthoc test was used. NK cells were coincubated in media or media supplemented with 25% of different ascites samples for 24h. Viability of NK cells was quantified by Annexin/7AAD staining by using flow cytometry. ns (non-significant), * ($p<0.05$), ** ($p<0.01$), *** ($p<0.001$), **** ($p<0.0001$).
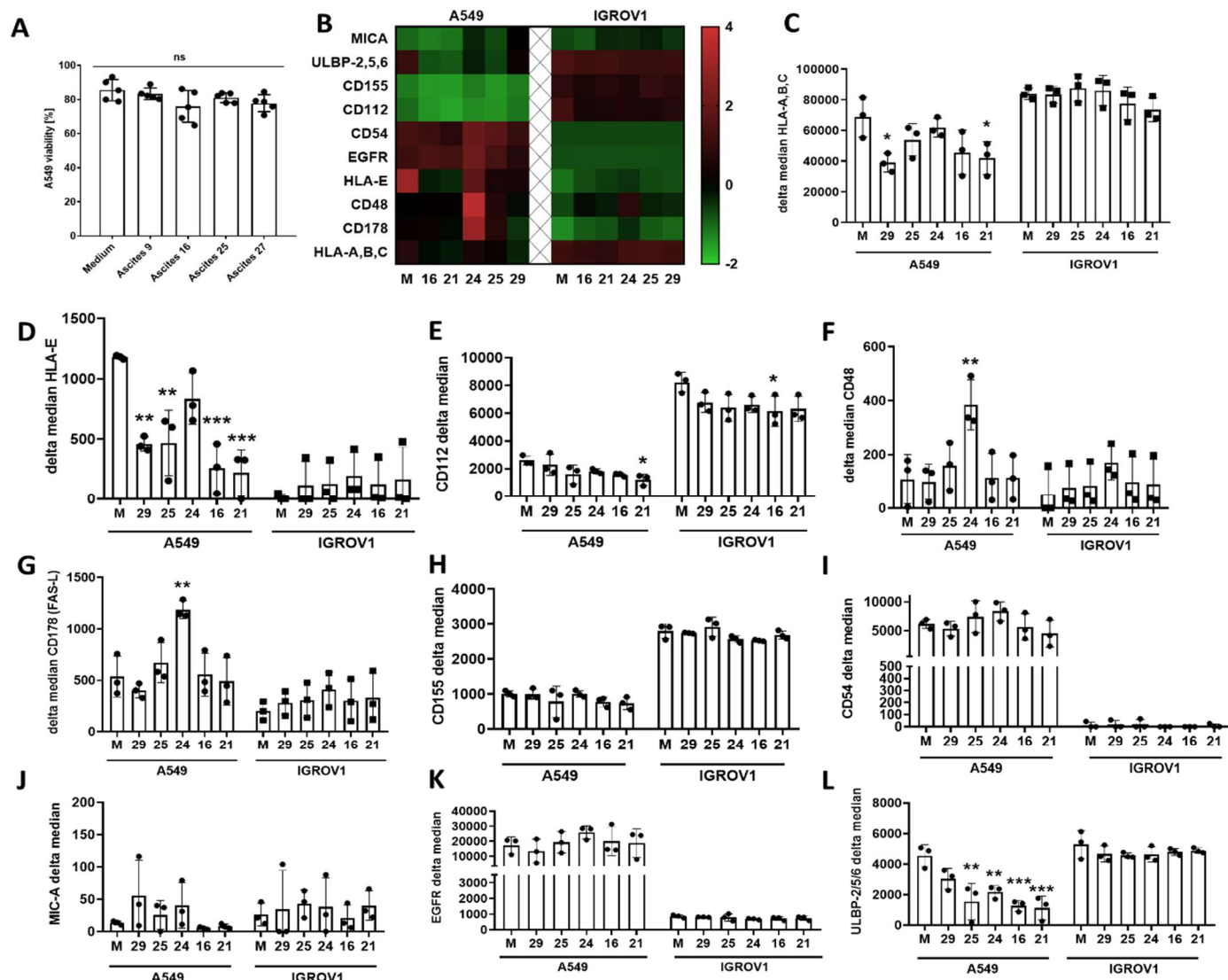
Supplementary Figure 2. – Malignant ascites does not affect viability and surface marker expression of different EGFR-positive cancer cells. Different types of EGFR-positive cancer cells were co-incubated with 25% ascites-supplemented media or media control for 24 hours. **(A) Percentage of viable A459 cells** after Annexin/7AAD-staining by flow cytometer **(B)** Heat map of receptor expression showing a summary of all surface marker expression changes in IGROV1 and A459 cell lines after treatment with different ascites samples after 24 hours. Color intensity of individual fields corresponds to calculated z-score of marker expression. Surface marker expressions portrayed in heat map were shown as individual graphs: **(C)** HLA-A,B,C **(D)** HLA-E **(E)** CD112 **(F)** CD48 **(G)** CD178 **(H)** CD155 **(I)** CD54 **(J)** MICA **(K)** EGFR **(L)** ULBP-2,5,6. Data are presented as individual values with mean value as center of error bar ± standard deviation. For significance testing ordinary one-way ANOVA (S2.A, C-L) with Dunnet posthoc test was used. * ($p<0.05$), ** ($p<0.01$), *** ($p<0.001$).
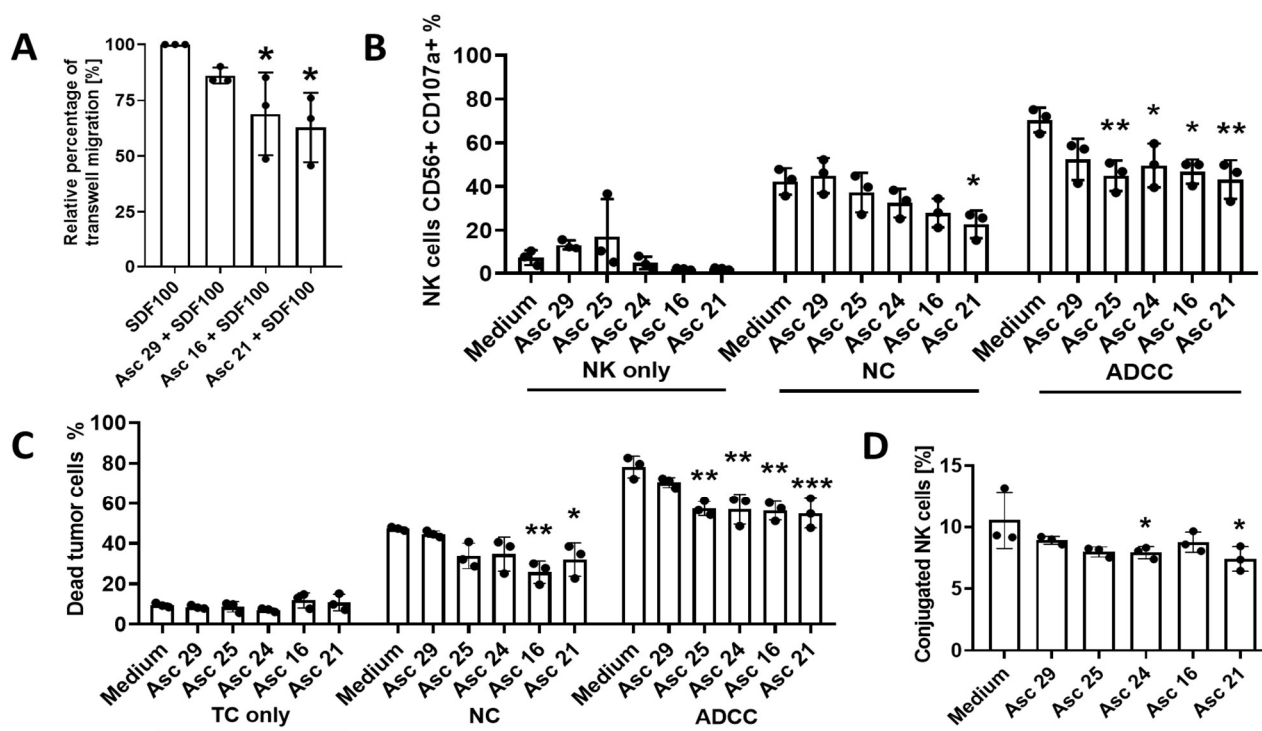
Supplementary Figure 3. – Malignant ascites impairs different effector functions in IL2 stimulated NK cells.
(A) Migration of NK cells in presence of ascites. NK cells were added to the top of the transwell insert. Ascites samples were added to the bottom of the insert in 1:4 ratio. After 3 hours of SDF-1a, induced migration cells were collected and measured by flow cytometry. **(B and C) Cytotoxicity and tumor cell lysis of stimulated NK-cells directed against A549-cells in presence of ascites.** IL2 activated NK cells were coincubated in 1:1 ratio with A549 lung adenocarcinoma cells with or without Cetuximab (1 μg/ml). 25% ascites supplemented media or media control was added. **(B)** After 6 hours percentage of CD107a-positive NK cells were measured by flow cytometry. Left column shows NK control, middle column shows NC and right column ADCC. **(C)** After 24 hours, the tumor killing was assessed after 7AAD/Annexin-staining in the flow cytometer. Relative percentage of dead tumor cells in absence of Cetuximab (middle column, NC-condition) or presence of Cetuximab (right column, ADCC-condition) and tumor cells only for control (left column) is shown. **(D) Conjugation formation of stimulated NK cells in presence of ascites.** IL2-activated NK cells and IGROV1 cells were mixed in 4:1 effector to target ratio in presence of 1 μg/ml soluble Cetuximab in either normal cell culture media or supplemented with 25% of OC ascites. After 45 minutes of coincubation, percentage of the conjugated NK cells was measured by flow cytometry. Data are presented as individual values with mean value as center of error bar ± standard deviation. For significance testing ordinary one-way ANOVA (S3.A-D) with Dunnet posthoc test was used. ns (non-significant), * ($p < 0.05$), ** ($p < 0.01$), *** ($p < 0.001$).
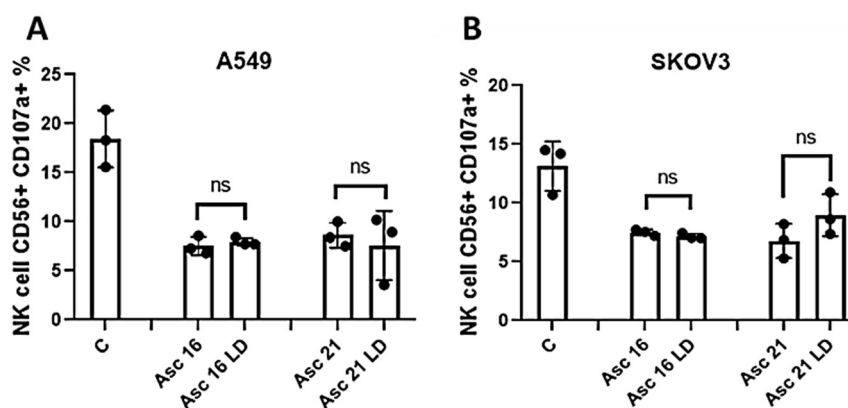
**Supplementary Figure 4. – Activated charcoal delipidation of ascites does not restore cytotoxic NK cell activity.** Ovarian cancer ascites was coincubated with activated charcoal for 1 hour and stirred magnetically, after which charcoal was removed by centrifugation. NK cells were coincubated in 1:1 ratio with EGFR-positive cancer

cells in presence of various ascites samples and ADCC-inducing antibody Cetuximab (1 µg/ml). Percentage of CD107a-positive NK cells was determined after 6 hours by flow cytometry and was normalized to medium control. **(A) and (B)** NK cell mediated ADCC against **(A)** A549 or **(B)** SKOV3 in the presence of medium, untreated ascites and lipid-depleted ascites (LD). Paired t-test was used to assess the significance. ns – no significance.
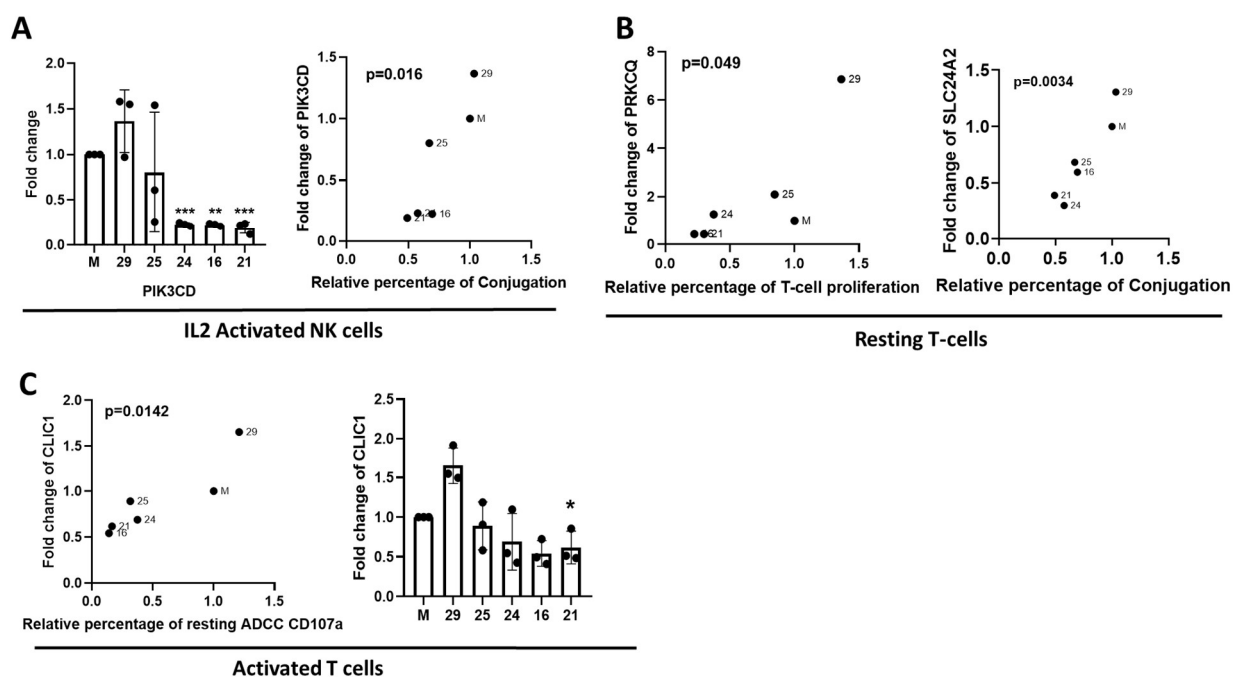
Supplementary Figure 5. – Malignant ascites alters expression of signal transduction molecules and electrolyte channels in immune cells. (A) Effects of ascites on IL2-activated NK cell gene expression. PI3K is significantly downregulated by suppressive malignant ascites (left). Significant Pearson correlation of PI3K to NK-tumor cell conjugation (right). **(B)** Effects of ascites on resting T cell gene expression. Significant Pearson correlation of PRK to T-cell proliferation inhibition (left), and SLC24A2 to NK-Tumor cell conjugation (right). **(C)** Effects of ascites on activated T cell gene expression. Significant Pearson correlation of CLIC1 to ADCC of resting NK cells (left), significant impact of malignant ascites on CLIC1 (right). Data are presented as individual values with mean value as center of error bar ± standard deviation. For significance testing ordinary one-way ANOVA with Dunnet posthoc test (S5.A (left), C right)) and two-tailed Pearson correlation were used (S5.A (left), B, C (right). ** (p<0.01), *** (p<0.001).
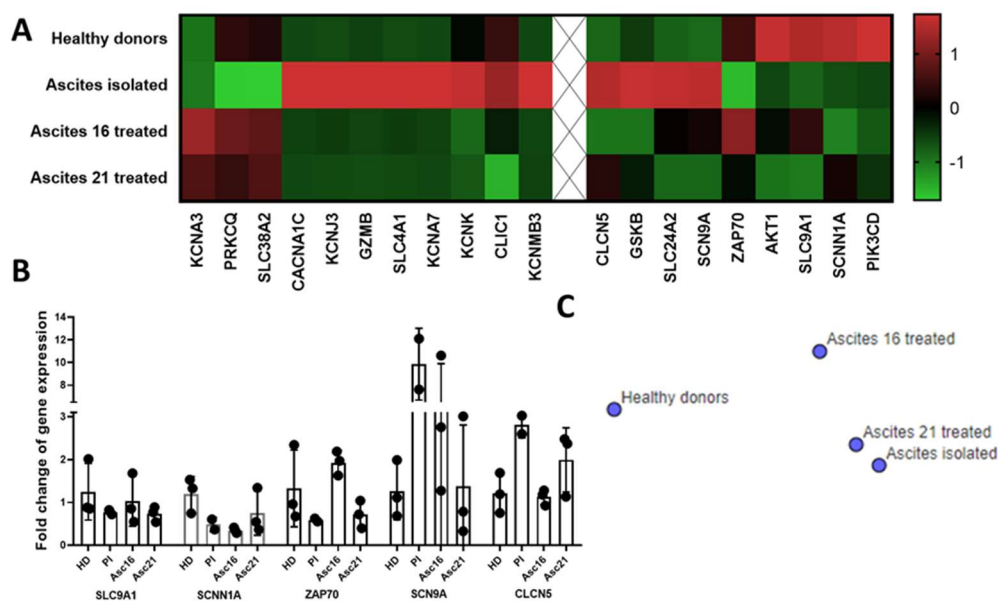
Supplementary Figure 6. – Healthy donor T cells treated with ascites *in vitro* show similar transcriptional profile as patient-isolated T cells from ascites. Resting T cells were exposed either to medium (HD) or 25% ascites supplemented medium (Asc) for 24 hours before proceeding with RNA isolation. RNA Isolation of patient ascites T cells (PI) was performed directly after cell isolation. For calculation of fold-change the gene expression was normalized to housekeeping gene and the mean expression of the indicated genes in the HD group. **(A)** Heatmap overview showing transcript expressions comparison between HD T cells in medium, two ascites-treated healthy donor T cell samples and T cells isolated from patient ascites. **(B)** Bar graph depicting gene transcript expression as determined by RNAseq. **(C)** t-SNE clustering of transcript expressions in healthy donor T cells, T cells from patient ascites and two ascites-treated healthy donor T cells.

Patient No.	FIGO/ UICC	Neoplastic grading	Cancer type	Histology	Time of diagnosis	Survival
1.	----	G3	Ovarian	High-grade serous-papillary	Recurrence	1Y 2M 10D
2.	----	G2	Ovarian	High-grade serous	Recurrence	6Y 2M 12D
3.	----	G2	Ovarian	High-grade serous	Recurrence	2Y 5M 20D
4.	IV	G3	Ovarian	Signet ring cell adenocarcinoma	Initial	13D
5.	----	G3	Ovarian	High-grade serous-papillary	Recurrence	8M 20 D
6.	IIIc	G2	Ovarian	High-grade serous	Initial	Unknown
7.	----	G3	Ovarian	High-grade serous	Recurrence	11M 20 D
8.	IV	G3	Ovarian	High-grade serous-papillary	Initial	1Y 7M 2D
9.	IV	G3	Ovarian	High-grade serous-papillary	Initial	7Y 5M 2D
10.	III	G2	Ovarian	Small cell hypercalcemic carcinoma	Initial	1Y 0M 2D
11.	IV	G3	Ovarian	Invasive mucinous	Initial	3M 8D
12.	IV		B-cell Lymphoma	Diffuse large cell	Initial	Unknown
13.	IV	G3	Ovarian	High-grade serous	Initial	Unknown
16.	IIIc	G3	Ovarian	High-grade serous	Initial	1M 15D
18.	IV	G2	Colon carcinoma	Adenocarcinoma	Initial	2Y 8M 4D
19.	IV	G3	Ovarian	Invasive mucinous	Initial	1Y 0M 6D
20.	IIIc	G3	Ovarian	High-grade serous	Initial	7M 21D
21.	IV	G3	Unknown	Invasive adenocarcinoma	Initial	1Y 10M 23D
22.	IIIc	G3	Ovarian	High-grade serous-papillary	Initial	1Y 5M
24.	IIIc	G2	Ovarian	High-grade serous-papillary	Initial	5D
25.	IIIc	G3	Ovarian	High-grade serous	Initial	Unknown

26.	IV	G2	Ovarian	High-grade serous-papillary	Initial	7M 8D
27.	IIIc	G3	Ovarian	High-grade serous-papillary	Initial	6Y 0M 8D
28.	IIIc	G3	Ovarian	High-grade serous-papillary	Initial	Unknown
29.	----	-----	Congestive heart failure, benign diagnosis		----	Still alive
30.	IIIc	G3	Ovarian	High-grade serous-papillary	Initial	Unknown
32.	IIIc	G3	Ovarian	High-grade serous	Initial	Still alive
33.	----	G3	Ovarian	High-grade serous	Recurrence	Still alive

Supplementary Table 1. – Patient characteristics from ascites donors. Table contains patient cohort information starting from left to right: Patient/Ascites number designation, FIGO/UICC cancer staging, histological grade, cancer tissue and type classification, timepoint and survival time since ascites collection.

Primer pair	Sequence (5´ - 3´)		Amplicon (bp)
hu_CACNA1C_NM_000719	forward	GCAGGAGTACAAGAACTGTGAGC	143
	reverse	CGAAGTAGGTGGAGTTGACCAC	
hu_CLCN5_NM_000084	forward	GTATCTGTAGCCTTTGGAGCACC	105
	reverse	GGCAGCAAAGAATGAACGCCAC	
hu_CLIC1_NM_001288	forward	CCTGCTGTATGGCACTGAAGTG	120
	reverse	GCTGTGTTGGACTCAGGGTTCA	
hu_SCNN1A_NM_001038	forward	GTGCCTACATCTTCTATCCGCG	110
	reverse	GTCTGAGGAGAAGTCAACCTGG	
hu_SLC24A2_NM_020344	forward	CCATCCAGTGATGCTTCAGAACC	141
	reverse	CGTGACTTGCTTGCGGGTTTCA	
hu_SLC4A1_NM_000342	forward	CTGCTGGTGTTTGAGGAAGCCT	102
	reverse	CACCAGCAGGATGAGCCAGAAG	
hu_SCN9A_NM_002977	forward	GTGGAAGGATTGTCAGTTCTGCG	140
	reverse	GCCAACACTAAGGTGAGGTTACC	
hu_SLC9A1 _NM_003047	forward	GAACTGGACCTTCGTCATCAGC	109
	reverse	GGTCAGCTTCACGATACGGAAC	
hu_KCNA3_NM_002232	forward	CGGTGTCTTGACCATCGCATTG	131
	reverse	AAGAGGAGAGGTGCTGGCAACT	

hu_KCNA7_NM_031886	forward	TCGAGACGCTGCCTGACTTCC	152
	reverse	CACCACGAAGAACGGGTCATTG	
hu_KCNMB3_NM_014407	forward	TCAGCCATCCAGGTCAGAAAGC	98
	reverse	TCTATCTTGGTGGCACTTAGGTG	
hu_KCNJ3_NM_002239	forward	GATCTCCATGAGGGACGGAAAAC	131
	reverse	GAAGGAACTCACCCTCAGGTGT	
hu_KCNK3_NM_002246	forward	GGCTCCTTCTACTTCGCCATCA	137
	reverse	CTCTGGAACATGACGAGCGTGA	
hu_ORAI1_NM_032790	forward	AGGTGATGAGCCTCAACGAGCA	151
	reverse	AGTCGTGGTCAGCGTCCAGCT	
hu_ZAP70_NM_207519	forward	CACTACGCCAAGATCAGCGACT	139
	reverse	GGCTGGAGAACTTGCGGAAGTT	
hu_PRKCQ_NM_006257	forward	GCATCCGTTTCTGACGCACATG	133
	reverse	CGCTCTGGAAAGGTCGAACTTG	
hu_PIK3CD_NM_005026	forward	TGCCAAACCACCTCCCATTCCT	160
	reverse	CATCTCGTTGCCGTGGAAAAGC	
hu_GZMB_NM_004131	forward	CGACAGTACCATTGAGTTGTGCG	122
	reverse	TTCGTCCATAGGAGACAATGCCC	
hu_GSK3b_NM_002093	forward	CCGACTAACACCACTGGAAGCT	150
	reverse	AGGATGGTAGCCAGAGGTGGAT	
hu_AKT1_NM_005163	forward	TGGACTACCTGCACTCGGAGAA	154
	reverse	GTGCCGCAAAAGGTCTTCATGG	

Supplementary Table 2. – List of all primers used for qPCR gene expression experiments. Table contains from left to right: primer designation and NCBI Reference Sequence, primer direction and sequence, product (amplicon) length.

	Relative percentage of effector function of NK cells			
	NC CD107a	ADCC CD107a	NC lysis	ADCC lysis
Asc No.	Extremely strong inhibitory ascites (CD107a<25%)			
21	4.9	9.4	44.6	71.2
16	3.7	11.0	25.4	51.7

	Strong inhibitory ascites (50%>CD107a>25%)			
22	12.6	28.7	70.1	94.6
25	7.0	30.7	57.5	75.81992
19	20.8	32.7	52.0	71.0
20	12.7	35.3	66.9	97.3
30	11.7	39.6	75.2	101.5
11	21.7	43.9	63.8	93.8
24	8.0	44.3	40.3	88.5
26	8.7	44.9	59.0	89.2
	Medium inhibitory ascites (75%>CD107a>50%)			
27	14.7	51.7	90.6	105.2
32	19.0	55.6	65.6	93.8
18	21.0	56.6	64.0	96.9
13	14.2	61.6	73.9	102.6
8	20.0	61.8	79.2	104.0
2	7.0	68.3	52.4	88.0
9	9.0	68.3	52.7	83.1
7	18.4	69.5	79.2	104.0
5	17.5	70.3	76.9	102.3
	Weak inhibitory ascites (100%>CD107a>75%)			
3	22.5	79.3	104.3	104.3
1	46.3	80.3	91.3	104.9
10	22.0	81.2	72.1	96.8
4	102.0	83.4	77.3	89.4
	Stimulatory ascites (CD107a>100%)			
29	71.3	116.0	81.4	102.4

Supplementary Table 3. – List of ascites samples ordered according to their inhibitory power. Table contains overview of used patient ascites samples ranked into five different categories depending on its effects on average ADCC NK cell degranulation in coculture system. Listed from left to right: relative percentage of NK cell natural toxicity degranulation and **cetuximab induced ADCC degranulation**, relative percentage of IGROV1 lysis in natural toxicity and ADCC conditions. The average relative percentage of degranulation (CD107a) or lysis was calculated after four independent experiments by normalizing ascites condition samples to appropriate medium controls. Each experiment was performed using NK cells isolated from different healthy donors.

Author contributions

3.2.2. Reactivity of NK Cells Against Ovarian Cancer Cells Is Maintained in the Presence of Calcium Phosphate Nanoparticles.
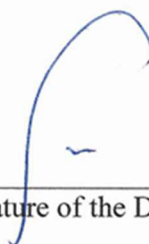
<u>Antonio Hrvat</u>, Mathias Schmidt, Martin Obholzer, Sonja Benders, Sebastian Kollenda, Peter A. Horn, Matthias Epple, Sven Brandau, and Nina Mallmann-Gottschalk

Contributions:

- Conception – 30%

- Conduction of experimental work – 60%: All experiments excluding DLS and SEM nanoparticle characterization, fluorescence microscopy, IFNy ELISA and ELISpot

- Data analysis – 80%: All data analysis in the study except fluorescence microscopy, IFNy ELISA and ELISpot

- Statistical analysis – 100%

- Writing the manuscript – 60%: Contributed to all parts of the manuscript

- Revision of the manuscript – 80%: Revisiting the manuscript, performing additional experiments and responding to reviewer comments

_____
Signature of the Doctoral Candidate

_____
Signature of the Doctoral Supervisor

Reactivity of NK Cells Against Ovarian Cancer Cells Is Maintained in the Presence of Calcium Phosphate Nanoparticles

Antonio Hrvat[1], Mathias Schmidt[1], Martin Obholzer[1†], Sonja Benders[1], Sebastian Kollenda[2], Peter A. Horn[3], Matthias Epple[2], Sven Brandau[1,4*] and Nina Mallmann-Gottschalk[1,5]

[1] Experimental and Translational Research, Department of Otorhinolaryngology, University Hospital Essen, Essen, Germany, [2] Inorganic Chemistry and Center for Nanointegration Duisburg-Essen (CeNIDE), University of Duisburg-Essen, Essen, Germany, [3] Institute for Transfusion Medicine, University Hospital Essen, Essen, Germany, [4] German Cancer Consortium, Partner Site Essen-Düsseldorf, Essen, Germany, [5] Department of Gynecology and Obstetrics, University Hospital Essen, Essen, Germany

Calcium phosphate nanoparticles (CaP-NPs) are biodegradable carriers that can be functionalized with biologically active molecules. As such, they are potential candidates for delivery of therapeutic molecules in cancer therapies. In this context, it is important to explore whether CaP-NPs impair the natural or therapy-induced immune cell activity against cancer cells. Therefore, in this study, we have investigated the effects of different CaP-NPs on the anti-tumor activity of natural killer (NK) cells using different ovarian cancer (OC) cell line models. We explored these interactions in coculture systems consisting of NK cells, OC cells, CaP-NPs, and therapeutic Cetuximab antibodies (anti-EGFR, ADCC-inducing antibody). Our experiments revealed that aggregated CaP-NPs can serve as artificial targets, which activate NK cell degranulation and impair ADCC directed against tumor targets. However, when CaP-NPs were properly dissolved by sonication, they did not cause substantial activation. CaP-NPs with SiO2-SH-shell induced some activation of NK cells that was not observed with polyethyleneimine-coated CaP-NPs. Addition of CaP-NPs to NK killing assays did not impair conjugation of NK with OC and subsequent tumor cytolytic NK degranulation. Therapeutic antibody coupled to functionalized CaP-NPs maintained substantial levels of antibody-dependent cellular cytotoxic activity. Our study provides a cell biological basis for the application of functionalized CaP-NPs in immunologic anti-cancer therapies.

Keywords: NK cells, nanoparticles, ADCC, calcium phosphate, cetuximab, aggregation, ovarian cancer, immunotherapy

INTRODUCTION

Nanomedicine has developed into an emerging field of research originating from applied biomedicine and novel nanotechnology (1). Due to their specific physical and biochemical properties nanoparticles offer new opportunities for diagnostic and therapeutic applications, e.g. in cancer therapy or autoimmune diseases (2, 3).

Besides commonly used inorganic nanoparticles like gold or iron oxide nanoparticles, calcium phosphate nanoparticles (CaP-NP) are also suitable for application in the medical field. As calcium phosphate is an endogenous biomineral with natural presence in human tissue such as bones and teeth, CaP-NPs display high biocompatibility and low intrinsic toxicity (4). CaP-NPs are clinically applied in traumatology, endoprosthetic applications, and tissue engineering: They can support the regeneration of bone defects and mediate bone contact in biomedical implants (4) (5). Ca-NPs have also been incorporated in different polymers to enhance the biomechanical properties of scaffolds for hard tissue regeneration (6). Additionally, they are valuable components in toothpastes supporting tooth repair and remineralization (7).

CaP-NPs show high chemical stability, especially at physiological pH in tissue or blood. Therefore, in the last decades, CaP-NP have been developed to be also utilized as vehicles for different cargo molecules. They served as carriers for antibiotics and have been applied for vaccination and immunization against infectious diseases successfully (8). In contrast to other nanoparticle-preparations, CaP-NP can be loaded with various immune activating components at flexible dosages simultaneously, which optimizes and individualizes the immune response (9). Taken up by dendritic cells CaP-NPs were able to induce a strong immunization in vivo and showed efficiency against experimental retroviral infections (10).

CaP-NPs are also promising tools for gene therapy which predestined them to become part of immunotherapeutic concepts in cancer therapy. To this end, DNA and short interfering RNA (siRNA) have been incorporated in CaP-NP for transfection in eukaryotic cells successfully as nucleic acids are otherwise unable to cross the cell membrane and are rapidly degraded by specific nucleases (11). Compared to other well-established transfection agents such as Lipofectamine CaP-NP displayed comparable transfection efficacy but significantly less cytotoxicity which is beneficial for application in vivo (12). In pancreatic cancer, VEGF-siRNA-loaded CaP-NP induced high gene silencing efficiency without associated toxicity with consecutive reduction of tumor growth (13). PEGylated siRNA-loaded CaP-NP containing also doxorubicin resulted in enhanced cell apoptosis and tumor growth arrest in vivo (14). The inclusion of dyes or imaging components in CaP-NP facilitates the visualization of the tumor tissue. For example, a MRI contrast agent encapsulated into CaP-NP enhanced the sensitivity of detection of primary hepatocellular carcinoma compared to a standard contrast agent (15). Additionally, the covalent binding of specific antibodies on the surface of CaP-NP enables functionalization of the particles and offers the possibility for individualized targeted cancer therapy (8).

For the therapeutic purpose, it is fundamental that nanocarriers in the physiological environment do not impair the activity of immune cells or diminish the efficacy of their incorporated agents. However, the mechanisms of interactions between nanoparticles and physiological components are still poorly understood (16) (17). According to nanotoxicological studies, CaP-NPs unspecifically adsorb proteins to the surface forming "protein-corona" due to the high protein concentration physiological environment in vivo (18). Further studies could show that CaP-NPs may agglomerate depending on size, charge and surface characteristics which resulted in altered biodistribution, cellular uptake, and toxicity of CaP-NPs in blood and tissue (8).

Despite obvious relevance for therapeutic applications, interactions between CaP-NPs and different immune effector cells have not been studied intensively in the past. Many studies focused on interactions between CaP-NPs and macrophages, and little, if any, data are available on the interplay of Ca-P NPs with T cells or NK cells (9). As part of the innate immune system, NK cells are likely to be one of the first cells coming into contact with nanoparticles when those are systemically applied. Physiologically, NK cells exert direct, natural cytotoxicity to target cells that are altered by infection or malignant transformation. Here, loss of MHC class I-molecules or upregulation of stress-induced ligands such as MICA/B (MHC class I polypeptide-related sequence A/B) and UL16 binding proteins 1—6 (ULBP 1—6) on target cells are crucial triggers inducing NK cell-activation and -cytotoxicity. Thereby, NKG2D and DNAM-1 as well as NKp46, NKp44 and NKp30 are central corresponding receptors on NK cells, whereas CD69 reflects their general activity state (19). By recognizing and binding antibody-coated cells via CD16, NK mediate antibody-dependent cellular cytotoxicity (ADCC) and thus achieve the maximum cytotoxic activity. Finally, they lyse target cells via inducing apoptosis or releasing perforin/granzymes as reflected by the expression of the lysosomal-associated membrane protein-1 LAMP-1 or CD107a on the cell surface (20, 21). NK cells support their activity and regulate other immune cell responses by the secretion of various cytokines like IFNγ or TNFα. Because of these comprehensive antitumoral properties, NK cells represent important cellular components in many immunotherapeutic approaches.

In this study, we analyzed whether CaP-NPs affect natural and antibody-dependent cytotoxicity of NK cells against ovarian cancer cells. To this end, we studied the effects of CaP-NP on interactions between NK cells and tumor cells as well as the direct effects on NK and tumor cells. For our experiments, we used previously established protocols for CaP-NP-preparation including triple-shell CaP-NPs as well as silica shell-coated CaP-NPs (22). For visualization, we utilized fluorescent CaP-NPs and tested also functionalized CaP-NPs. These were bound to the antibody Cetuximab which is directed against EGFR (epidermal growth factor receptor), a common target in ovarian cancer cells.

MATERIALS AND METHODS

Synthesis and Functionalization of Calcium Phosphate Nanoparticles

Single-shell CaP-NPs (CaP) were synthesized by precipitation using 0.25 mL of 6.25 mM calcium nitrate solution (Ca(NO3)2·4

Abbreviations: NC, natural cytotoxicity; NK, NK cells; TC, tumor cells; NP, NP induced degranulation; ADCC, antibody dependent cell-mediated cytotoxicity.

H2O) and 0.25 mL of 3.74 mM diammonium hydrogen phosphate ((NH4)2HPO4) solution (both solutions were adjusted to pH 9.0 with NH3) and 0.05 mL of labelled poly (ethyleneimine) solution diluted with non-labelled PEI 1:5 (PEIFITC/Cy5: 2 mg mL-1, MW 25 kDa, branched, Surflay) or 0.05 mL non-labelled poly(ethyleneimine) solution (PEI: 2 mg mL-1, MW 25 kDa; branched, Sigma-Aldrich) (22). For the synthesis of triple-shell particles (CaP-P) the same procedure of calcium phosphate precipitation and PEI coating was repeated with the single-shell particles dispersion. These generated nanoparticles were centrifuged for 15 min at 12,000 g (MiniSpin®, Eppendorf). Then, the particle pellet was redispersed in 1 mL UltraPureTM DNase/RNase-free water in an ultrasonic water bath (Elmasonic S10, Elma) for 10-15 s.

Silica-shell CaP-NPs (CaP-S) were synthesized for a sequential surface functionalization with antibodies. The synthesis was performed according to previously reported procedure (23). Initially, 20 mL of absolute ethanol were mixed with 0.013 mL of a 30% aqueous ammonium solution and 0.025 mL of Tetraethyl orthosilicate (TEOS) and stirred for 10 min. Next, 5 mL of a dispersion of single-shell CaP-NPs (either stabilized with fluorescently labelled or non-labelled PEI) were pipetted into the ethanol mixture and stirred overnight at room temperature. The crude dispersion of silica-shelled CaP-NPs was centrifuged for 30 min at 66,000 g and redispersed in 5 mL UltraPureTM DNase/RNase-free water by ultrasonication for 10-15 s. Then, the redispersed nanoparticles were added to 20 mL of absolute ethanol containing 0.025 mL of 3-mercaptopropyl) trimethoxysilane (MPS), for a subsequent surface functionalization, and stirred for 6 h at room temperature. The thiol-terminated nanoparticles (CaP-S) were centrifuged and redispersed as described previously. For 1 mL of CaP-S dispersion 500 µg of the Cetuximab (Merck) were coupled to the particle surface overnight. Therefore, the antibodies were incubated in 1 mL of PBS containing 0.025 mL of a 20 mM N Succinimidyl-3 (2-pyridyldithio) propionate (SPDP) solution for 1 h. The reaction mixture was desalted using centrifugal filters with a molecular weight cutoff of 100 kDa (Amicon® Ultra – 0.5 mL, Merck). The activated antibodies were pipetted into the dispersion of CaP-S for the conjugation of the thiol-reactive part of SPDP to the thiol groups on the nanoparticles, incubated overnight at room temperature and the next day centrifuged for 10 min at 12,000 g. The supernatant of these nanoparticles (CaP S C) was used to calculate the number of coupled antibodies per particle. For the long-time storage of all synthesized nanoparticles the final dispersions of each species were supplied with 20 mg mL-1 D-(+)-trehalose (Sigma Aldrich), which serves as a cryoprotectant, and aliquoted to 0.1 mL, shock-frozen with liquid nitrogen and freeze dried with an Alpha- 2-4 LSC system (Christ).

Characterization of Calcium Phosphate Nanoparticles

The number of particle-coupled antibodies was determined with a DS 11 FX+ Nanodrop instrument by UV/Vis spectroscopy of the supernatant (uncoupled antibodies in the supernatant were subtracted from the applied mass). The morphology and size of the solid core diameter of the synthesized nanoparticle species were characterized by scanning electron microscopy (ESEM Quanta 400, FEI and Apreo S LoVac, Thermo Fisher Scientific) after palladium-gold sputtering. Their hydrodynamic diameter and zeta potential were determined by dynamic light scattering (Zetasizer Ultra, λ=532 nm backscatter mode, Malvern Panalytical). All displayed particle size data refer to scattering number distributions. To calculate the number of particles per milliliter the calcium concentrations of the nanoparticles were determined by atomic absorption spectroscopy (AAS; M-Series AA spectrometer; Thermo Electron Corporation) after dissolution of the samples in hydrochloric acid. The calculated nanoparticle concentration was combined with the total amount of coupled antibodies, if applicable, and brought into perspective.

Ovarian Cancer Cell Lines and *In Vitro* Cell Culture

SKOV-3 and OVCAR-3 ovarian cancer cell lines were kindly provided by the Department of Obstetrics and Gynecology, University of Bonn, Germany. OVCAR-4 was obtained from Westdeutsches Tumorzentrum, University of Duisburg-Essen, Germany. SKOV3 ovarian cancer cell line was cultured in Roswell Park Memorial Institute (RPMI Gibco). OVCAR4 ovarian cancer cell line was cultured in a mixture of ¾ of RPMI and ¼ of Dulbecco's Modified Eagle Medium (DMEM). Both media were supplemented with 10% (v/v) heat-inactivated fetal calf serum (FCS Gibco), 100 U/mL penicillin, and 100 mg/mL streptomycin (PenStrep, Gibco by Life Technologies) (supplemented complete media). Cells were cultivated in plastic flask (Sarstedt) at 37°C and 5% CO2 and continuously passaged by treatment with Accutase (Gibco) for 5 minutes at 37°C.

NK Isolation From Peripheral Blood

Healthy donor blood collected in trisodium citrate blood collection tubes was diluted with Dulbecco's Phosphate Buffered Saline (DPBS, Gibco, Life Technologies Limited) in 1:1 ratio and overlayed on a 1.077g/mL separation medium (Biocoll, Merck Millipore). Density centrifugation was performed at room temperature (400g for 30min) without acceleration and brake. PBMCs were collected and washed with PBS followed by centrifugation at 300g for 8min at room temperature. Then plastic adherence was performed to deplete monocytes by incubating them in a T175 flask (Sarstedt) at 37°C and 5% CO2 for 1 hour. For NK isolation NK MACS Isolation Kit (Miltenyi Biotec) was used according to the manufacturer's instructions. Purity of isolated NK cells was routinely tested and ranged from 90% to 97%. After isolation 5 U/ml recombinant human IL-15 (50µg, Immuno Tools) was added to NK cells that were used for functional experiments after overnight incubation.

Use of peripheral blood from healthy donors was approved by the institutional review board of the Medical Faculty of the University of Duisburg-Essen (approval number 07-3500 and 08-3590) and each donor signed an informed consent form.

NK Degranulation Assay

NK cells express CD107a during degranulation, which also correlates to NK cell-mediated tumor cell lysis (21). To

evaluate natural and antibody-dependent NK cell cytotoxicity purified NK cells and SKOV-3/OVCAR-4 cells were coincubated (1:1 ratio) in a flat-bottom 96-well plate with or without different nanoparticles. For ADCC-experiments Cetuximab 1 µg/ml (Erbitux, 5mg/mL, Merck (Serono)) or Cetuximab-bound nanoparticles in corresponding concentrations were added. NK cells were labelled with anti-CD107a-FITC (25µg/mL, clone H4A3, Mouse IgG1, k, BD Biosciences). After incubation for 1 hour at 37°C and 5% CO2, the protein Golgistop-Monesin (BD Biosciences) was added (1:600). After further 5 hours incubation NK cells were stained with CD56-BV421 (12µg/mL, NCAM 16.2, IgG2b,k, BD Biosciences) and CD107 expression analyzed by flow cytometry.

NK cell degranulation was calculated by the following formula in case of natural cytotoxicity:

$$NC \text{ (without NPs)} = (NK + TC) - NK$$

$$NC \text{ (with NPs)} = ((NK + TC + NP) - NK) - NP$$

NP or NP induced degranulation was calculated as:

$$NP = (NK + NP) - NK.$$

For antibody-dependent cell-mediated cytotoxicity the following formula was used:

$$ADCC \text{ (without NPs)}$$
$$= (NK + TC + CET) - NK - NC \text{ (without NPs)}$$

$$ADCC \text{ (with NPs)}$$
$$= (NK + TC + CET + NP) - NK - NP - NC \text{ (with NPs)}$$

Nanoparticle Cytotoxicity and Tumor-Killing Assay

NK cells and SKOV-3/OVCAR-4-cells were coincubated (1:1 ratio) with or without Cetuximab (1 µg/ml) and different types of nanoparticles for 24h at 37°C and 5% CO2. Adherent and suspended cells were harvested with Stem Pro Accutase (Gibco by Life Technologies). After washing step cells were stained using PE Annexin V Apoptosis Detection Kit I (BD Biosciences) according to the manufacturer's protocol and analyzed by flow cytometry. Alive cells were defined as Annexin V-/7AAD-. Tumor cell lysis was calculated by the following formula in case of natural cytotoxicity:

$$NC \text{ (without NPs)} = (TC + NK) - TC$$

$$NC \text{ (with NPs)} = (TC + NK + NP) - TC - NP$$

NP or NP induced killing was calculated as:

$$NP = (TC + NP) - TC$$

For antibody-dependent cell-mediated cytotoxicity the following formula was used:

$$ADCC \text{ (without NPs)}$$
$$= (TC + NK + CET) - TC - NC \text{ (without NPs)}$$

$$ADCC \text{ (with NPs)}$$
$$= (TC + NK + CET + NP) - TC - NP - NC \text{ (with NPs)}$$

Flow Cytometric Analysis of NK Cell and Tumor Cell Markers

After six hour coincubation with nanoparticles, the following antibodies for the flow cytometric analysis of the NK cell marker expression were used: CD56-BV421 (12µg/mL, clone NCAM 16.2, mIgG2b,k, BD Biosciences), CD16-BV510 (180µg/ml, clone 3G8, mIgG1, Biolegend), NKp46-PE (CD335, 50µg/ml, clone 9E2, mIgG1, k, Biolegend), DNAM-1-PerCP-Cy5.5 (CD226, 200µg/ml, clone 11A8, mIgG1, k, Biolegend), NKG2D-PE-Cy7 (CD314, 200µg/ml, clone 1D11, mIgG1, k, Biolegend), CD69-FITC (100µg/ml, clone FN50, mIgG1, k, Biolegend), followed by a live/dead staining using the fixable viability dye eFluor 780 (eBioscience/Thermo Fisher Scientific, Darmstadt, Germany). For intracellular staining with anti-IFNγ-APC (7.5µg/ml, clone 45-15, mIgG1, k, Miltenyi), cells were fixed and permeabilized with BD Cytofix/Cytoperm Solution Kit (BD Biosciences). Before NK stimulation, Golgistop-Monesin (BD Biosciences) was added to the cells. Ovarian cancer cell surface marker expression were detected by staining with the following antibodies: MICA-APC (5µg/ml, clone 159227, mIgG2b, k, RD Systems), UBLP-2/5/6-APC (10µg/ml, clone 165903, mIgG2a, k, RD Systems), CD54-PE (100µg/ml, clone HA58, mIgG1, k, Biolegend), and MHCI-PE (25µg/ml, clone W6/32, mIgG2a, k, Biolegend). The same fixable viability dye as for NK markers was used. In all flow cytometry measurements appropriate isotype controls were used: mIgG1-BV510 (100µg/ml, clone MOPC-21, Biolegend), mIgG1-PE (50µg/ml, clone MOPC-21, BD Bioscience), mIgG1-PE-Cy-7 (200µg/ml, MOPC-21, Biolegend), mIgG1-FITC (500µg/ml, clone MOPC-21, Biolegend), mIgG1-PerCP-Cy5.5 (200µg/ml, clone MOPC-21, Biolegend), mIgG1-APC (200µg/ml, clone MOPC-21, Biolegend), mIgG2b-APC (200µg/ml, clone MPC-11, Biolegend), mIgG2a-APC (200µg/ml, clone MOPC-173, Biolegend), mIgG2a-PE (200µg/ml, clone MOPC-173, Biolegend). Stained cells were analyzed with BD FACSCanto II using DIVA 8.01 software (BD Biosciences) or FlowJo10 (LLC, Ashland, Oregon, USA).

Detection of NK IFNγ -Secretion by ELISpot

The ELISpot-technique was applied for sensitive detection of IFNγ-secreting NK cells. First, Multiscreen 96-well filtration plate (Merck Millipore) was activated with 35% ethanol and coated with anti-IFNγ-capture antibody (200µg/ml, clone 1-D1K, mIgG1, k, Mabtech). After incubation at 4°C overnight the plates were blocked with 200µl of supplemented complete RPMI-1640-media for 2h at 37°C. After washing step isolated NK cells were seeded in triplicates and treated with different

nanoparticle types. NK cells treated with PMA (50ng/ml, Sigma-Aldrich) and Ionomycin (1μg/ml, Sigma-Aldrich) were included for positive control. Untreated NK cells were used as negative control. After incubation with 12,5 μl of calcium phosphate nanoparticles for 24 h at 37°C and 5% CO2 plates were washed in the ELISA-Washer (PBS/0,05% Tween-20.) Biotinylated anti-IFNγ-detection antibody (200μg/ml, clone 7-B6-1, mIgG1, k, Mabtech) was added in 2μg/ml PBS and 1% BSA. The plates were incubated for 2 h at 37°C, washed and incubated with 50μl ExtraAvidin alkaline phosphatase (1:1000 diluted in PBS/1% BSA, Sigma-Aldrich) for 2h at the room temperature. After washing steps 75μl of the ELISpot substrate BCIP/NBT (Roche) was added and incubated for 5-10 minutes. Developed cytokine spots were measured using AID Classic ELISpot Reader and the results were analyzed with AID ELISpot 7.0 software.

ELISA Analysis of Tumor Cell-Secreted Cytokines

The supernatant of 50.000 OVCAR4 and SKOV3 cancer cells incubated with 12,5 μl of calcium phosphate nanoparticles for 24 hours was used to quantify secreted IL-6 and IL-8 using ELISA kits (R&D Systems, Wiesbaden, Germany), according to the manufacturer's instructions.

Conjugation Assay

Adapted from existing literature (24), the conjugation rate of NK and tumor cells was analyzed in presence of nanoparticles. NK cells were stained with Cell Tracker Red (Thermo Fisher Scientific) and tumor cells with Cell Tracker Green (Thermo Fisher Scientific) according to the manufacturer's instructions. NKs (50.000 cells) and tumor cells (200.000 cells) were coincubated (1:4 ratio) in presence of 1 μg/ml Cetuximab with or without different types of CaP-NPs in matching concentrations. After centrifugation (20g (570 rpm), 1 min) tubes were placed in a water bath at 37°C for 45 min. Afterward, the samples were retrieved and briefly vortexed. 300 μl of ice-cold 0,5% PFA in PBS was added and samples were analyzed by flow cytometry.

Live-Cell Microscopy of the NK-Tumor Cell-Calcium Phosphate Nanoparticle Interaction

For microscopy, tumor cells, seeded on 4 Chamber slides (LabTek) the day before, were stained with 500 μl of a 250 nM Calcein-AM (BD Pharmingen) solution in PBS 3% HS for 30 min in a darkened incubator. After washing, tumor cells were incubated in medium without phenol red in the dark. NK Cells were added in a 1:1 ratio and treated with 50 μl of fluorescent Cy5-CaP-NPs. For Live cell imaging, the Zeiss AxioObserver.Z1 at the Imaging Center Essen (IMECS) was used. Pictures of the pre-warmed chamber (37°C for 30 min) were taken every 4 minutes up to 4 hours. Representative position of each well and pictures with FITC, Cy5, and transmitted light channels were recorded. Digital processing was performed with ImageJ.

Microscopy of the Calcium Phosphate Uptake by Tumor Cells

SKOV3 and OVCAR4 cells were seeded on coverslips and incubated in media at 37°C and 5% CO2 until confluent, roughly 72 hours. After replacing media 50μl of FITC-labeled CaP-S and CaP-S-C were added and incubated for 6 hours. Cells were washed and resuspended in PBS supplemented with 3% of human serum. Fixation was done in Cytofix/Cytoperm (BD-Bioscience) at room temperature in the dark for 15 min. After washing steps with Permwash (BD-Bioscience) cells were stained with 1:36000 DAPI/Permwash staining solution at room temperature for 10 min in the dark followed by washing with PBS. Stained coverslips were transferred on top of a drop of mounting liquid (VECTA) cells facing down, stored at 4°C in a sealed box overnight and scanned with AxioScan (Zeiss) at 488 nm (FITC) and 405 nm (DAPI).

Flow Cytometry Analysis of Calcium Phosphate Nanoparticle Uptake in Tumor and NK Cells

For analyzing the uptake of nanoparticles in SKOV3/OVCAR4, the tumor cells were seeded the day before and incubated with 8, 12 or 20 μl of FITC labeled CaP-S or CaP-P and Cap-S-C in matched particles number, respectively. Incubation was performed in the dark, at 37°C, 5% CO2 for 6h. For analyzing preferential uptake coculture of SKOV3 and NK cells was incubated with 12,5 μl of different FITC-labeled CaP-NPs (CaP-P, CaP-S and CaP-S-C) for 3h at 37°C and 5%CO2. After washing step adherent cells were harvested using Accutase (Gibco) and resuspended with suspended cells in PBS 3% HS for analysis in the flow cytometer. FITC-positive cells were defined as cells that bind or take up CaP-NPs.
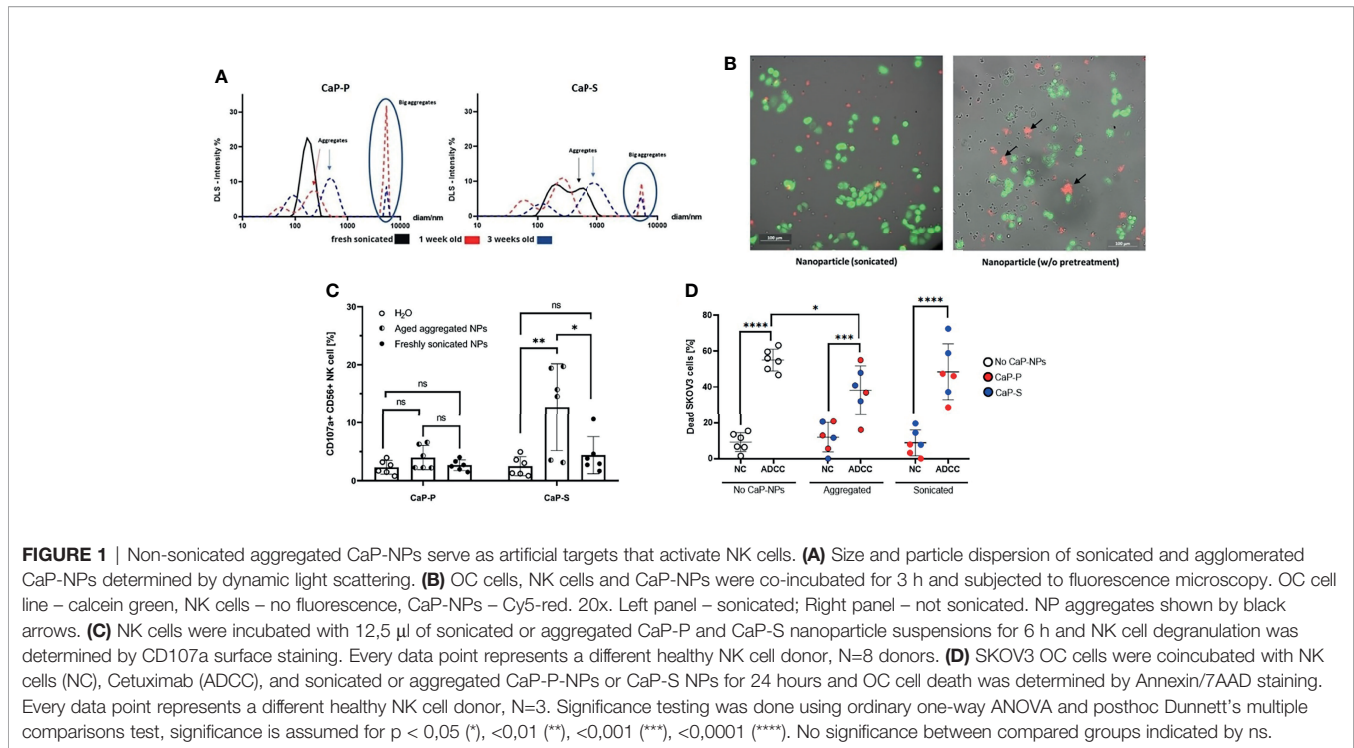
Statistical Analysis

Data are shown as single values, means as center values and error bars for the standard deviation (SD). The ordinary one-way ANOVA test with posthoc Dunnets multiple comparison tests was used to statistically evaluate the difference between the groups (**Figures 1C, D**, **Figures 2A–F**, **Figures 3C, E**, **Figures 4A–G**, **Figures 5A, B**). A two-way ANOVA test with posthoc Sidaks multiple comparison tests were used to statistically evaluate the difference between more than two groups (**Figures 5C, E**). Significance testing was also done using both unpaired t-test with Welch's correction and one-way ANOVA with posthoc Dunnets multiple comparison test (**Figures S3** and **S4**). Calculations were performed using GraphPad Prism 8 software.

RESULTS

Calcium Phosphate Nanoparticles Are Biocompatible State of the Art Produced Nanoparticles

Multi-shell nanoparticles were prepared by precipitation of calcium phosphate (**Figure S1A**). Subsequently, the nanoparticle surface was functionalized with PEI (CaP-P) (**Figure S1B**) and in

FIGURE 1 | Non-sonicated aggregated CaP-NPs serve as artificial targets that activate NK cells. **(A)** Size and particle dispersion of sonicated and agglomerated CaP-NPs determined by dynamic light scattering. **(B)** OC cells, NK cells and CaP-NPs were co-incubated for 3 h and subjected to fluorescence microscopy. OC cell line – calcein green, NK cells – no fluorescence, CaP-NPs – Cy5-red. 20x. Left panel – sonicated; Right panel – not sonicated. NP aggregates shown by black arrows. **(C)** NK cells were incubated with 12,5 μl of sonicated or aggregated CaP-P and CaP-S nanoparticle suspensions for 6 h and NK cell degranulation was determined by CD107a surface staining. Every data point represents a different healthy NK cell donor, N=8 donors. **(D)** SKOV3 OC cells were coincubated with NK cells (NC), Cetuximab (ADCC), and sonicated or aggregated CaP-P-NPs or CaP-S NPs for 24 hours and OC cell death was determined by Annexin/7AAD staining. Every data point represents a different healthy NK cell donor, N=3. Significance testing was done using ordinary one-way ANOVA and posthoc Dunnett's multiple comparisons test, significance is assumed for p < 0,05 (*), <0,01 (**), <0,001 (***), <0,0001 (****). No significance between compared groups indicated by ns.

some cases with silica (CaP-S) (**Figure S1C**). Functionalization with PEI was performed to enable incorporation of nucleic acids and fluorescent molecules. Silica functionalization enabled conjugation of cetuximab anti-EGFR-antibodies onto the nanoparticle surface (CaP-S-C) (**Figure S1D**). Average hydrodynamic particle diameters were determined by dynamic light scattering (DLS) to be 129 ± 32 nm for CaP-P, 309 ± 49 nm for CaP-S and 97 ± 19 nm for CaP-S-C (**Figure S1E**). Use of FITC labeled PEI did not change the hydrodynamic radius (**Table S1**). Zeta potential of CaP-NPs was between +18 and +28 mV due to polycationic PEI and not significantly different between the particle types (**Table S1**). Electron microscopy showed the solid particle core and a spherical particle shape (diameter of 72 ± 5 nm for CaP-P, 64 ± 5 nm for CaP-S and 64 ± 16 nm for CaP-S-C) (**Figure S1F**). Conjugation of nanoparticles with an anti-EGFR-IgG1-antibody, Cetuximab, did not significantly change the diameter of the particles. The difference in average particle diameter obtained between electron microscopy and DLS method is due to some particle aggregation in dispersion. Additionally, all preparations were tested for endotoxin presence which was determined to be below the maximum allowed level (determined <0,1 EU/ml, allowed 0,5 EU/ml) (25).

Unsonicated Aggregated CaP-NPs Serve as Artificial Targets That Activate NK Cells

The aggregation state and colloidal stability are important parameters with respect to the biological applications of nanoparticles, but the effect of aggregated nanoparticles on NK cells has not been explored yet. We hypothesized that larger aggregates of nanoparticles could serve as artificial targets for NK

cells and thus influence NK cell interaction with tumor cells. To test this hypothesis, after synthesis, lyophilized CaP-S and CaP-P NPs were resuspended in sterile distilled water and stored at 4°C for one to three weeks to allow for aggregation. The presence of the aggregates was confirmed by DLS measurement (**Figure 1A**). Thereafter, live cell imaging was performed on cocultures of NK cells, SKOV3 ovarian cancer cells and either freshly resuspended sonicated or long-term stored unsonicated CaP-NPs. From the recorded images (**Figure 1B**) and video (**Video S1A**, https://cloud.uk-essen.de/f/151ced3991ec41039707/?dl=1 and B, https://cloud.uk-essen.de/f/79fd353b893541918139/?dl=1) it can be seen that unsonicated nanoparticles formed aggregates (marked with black arrow; **Figure 1B**, right panel) that were of similar size as tumor cells. Functional NK degranulation assays revealed substantial NK cell degranulation when NK cells were coincubated with aggregated nanoparticles compared to the sonicated ones. (**Figure 1C**). Based on these data we further investigated effects of aggregated NPs in additional presence of ovarian cancer cells (**Figure 1D**). Addition of aggregated CaP-NPs to NK-tumor co-cultures still allowed the induction of substantial antibody-dependent cellular cytotoxicity (ADCC), which, in our experimental system, was induced by anti-EGFR antibody. However, the magnitude of ADCC was significantly reduced compared to control (no CaP-NP added) conditions, an effect that we did not observe for sonicated CaP-NPs. In summary, our data suggest, that aggregated CaP-NPs may cause unspecific and unintentional NK cell activation. This may finally hinder antitumoral NK cell activity against ovarian cancer cells under certain conditions, which could lead to reduced NK cell-mediated tumor cell lysis.
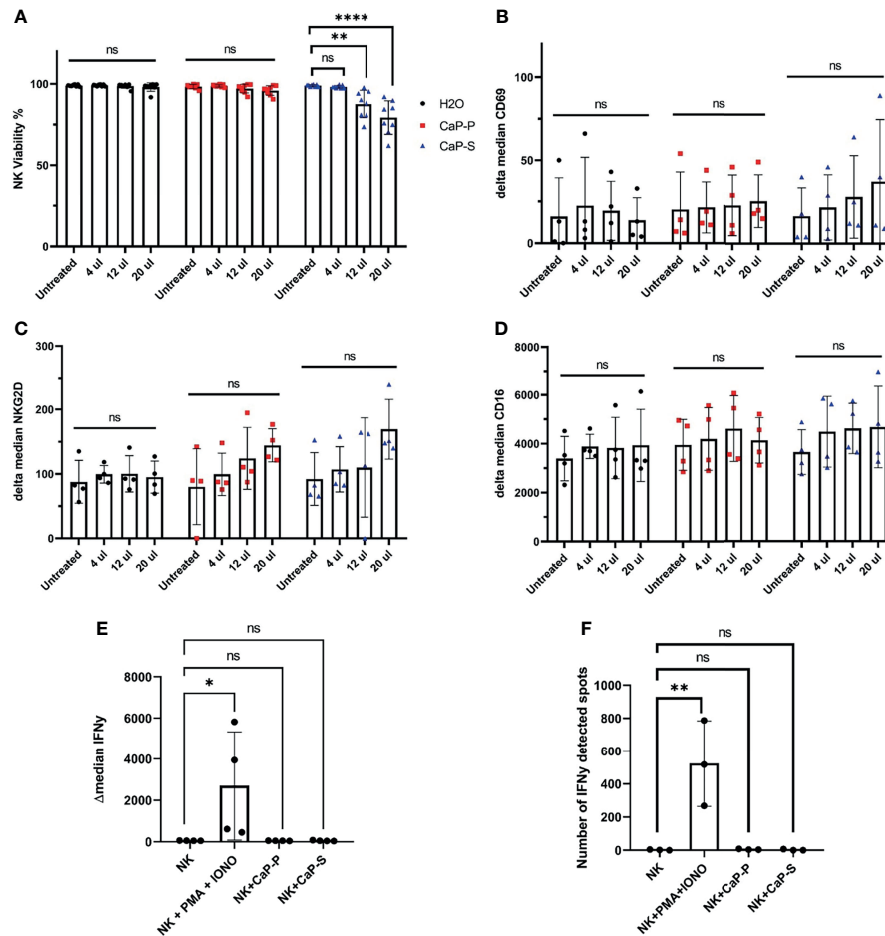
FIGURE 2 | Sonicated and dispersed CaP-NPs do not induce NK cell activation. NK cells were incubated for 6 hours with different volumes of sonicated CaP-NPs or water as vehicle control and **(A)** NK cell viability was determined by Annexin/7AAD staining and flow cytometry. Data points represent four different NK donors and two technical replications, N=8. After 6h stimulation with CaP-NPs changes in expression of NK cells activation marker CD69 **(B)**, NKG2D **(C)**, and Fcγ receptor CD16 **(D)** were determined by surface staining flow cytometry. Data points represent four different NK cell donors, N=4. After stimulating NK cells with 12.5µl CaP-P or CaP-S sonicated nanoparticles for 6 hours **(E)** IFNγ production was determined by intracellular flow cytometry staining. Data points represent 4 different NK cell donors, N=4. **(F)** NK cell secretion of IFNγ after stimulation with 12.5 µl of CaP-NPs for 24 hours as determined by ELISpot. Y-axis indicated the number of cells or spots positive for IFNγ presence. Data points represent 3 different NK cell donors, N=3. As a positive control in both experiments, NK cells treated with PMA (50ng/ml) and Ionomycin (1µg/ml) were included. Significance testing was done using ordinary one-way ANOVA and posthoc Dunnett's multiple comparisons test, significance is assumed for $p < 0{,}05$ (*), $<0{,}01$ (**), $<0{,}0001$ (****). No significance between compared groups indicated by ns.

Fresh and Sonicated Dispersed CaP-NPs Do Not Activate NK Cells

Based on these findings we turned to sonicated dispersed CaP-NPs and assessed the effects on NK viability and various parameters of NK activation. To prevent aggregation, CaP-NPs were sonicated for maximum 30 seconds, before addition to six hour coculture assays with NK cells. Viability assays showed that CaP-P nanoparticles were non-toxic, while CaP-S showed moderate toxicity when applied at higher doses (**Figure 2A**). This cytotoxicity of CaP-S coincided with a slight upregulation of the activation markers CD69 and NKG2D on the NK cell surface (**Figures 2B, C**). Expression of other surface markers such as CD16 (**Figure 2D**), DNAM-1 (data not shown) and NKp46 (data not shown) remained unchanged upon co-incubation with

CaP-NPs. Using flow cytometry, IFNγ-staining (**Figure 2E**) and IFNγ-ELISpot (**Figure 2F**), it was confirmed that dispersed nanoparticles did not cause NK cell activation and any production or secretion of IFNγ compared to unstimulated controls. These results show that sonicated and dispersed CaP-NPs do not induce NK activation, except for minor induction of selected surface molecules in the presence of high NP doses.

CaP-NPs Are Internalized by Ovarian Cancer Cells, Which Causes Cytotoxicity

After having analyzed effects of CaP-NPs on NK cells, we next investigated their interaction with ovarian cancer cells. To this end, we quantified the uptake of CaP-NPs, determined their cytotoxicity on cancer cells and monitored potential cell
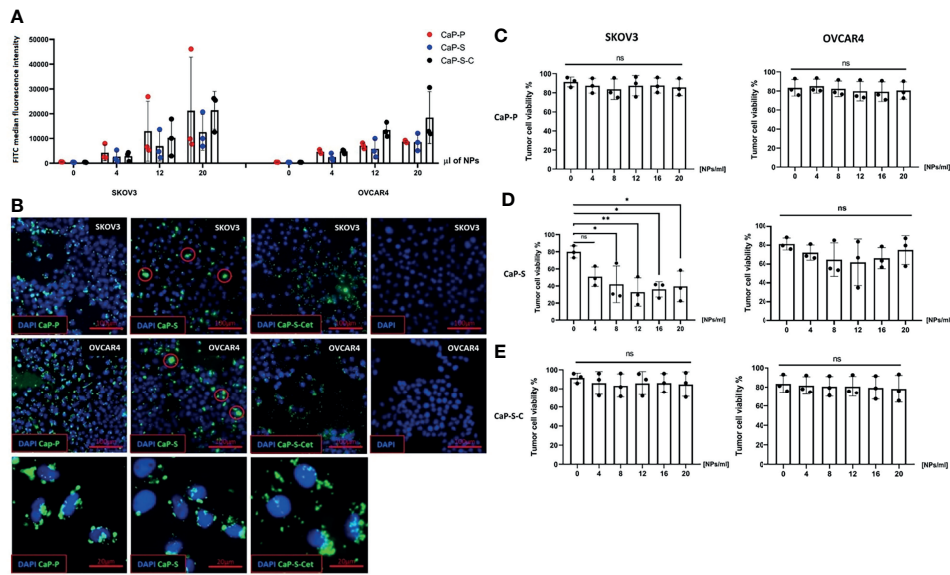
FIGURE 3 | Internalization of CaP-NPs by ovarian cancer cells and cytotoxicity. **(A)** Ovarian cancer cells were exposed to different amounts of FITC labeled CaP-NPs and nanoparticle uptake was measured by flow cytometry after 6 h post addition. Y-axis shows FITC median fluorescence intensity. **(B)** Representative fluorescent microscopy images of different CaP-NP (green FITC label) uptake 3h after addition to ovarian cancer culture (top row - SKOV3, middle row - OVCAR4, bottom row - magnified details from OVCAR4 images. CaP-S aggregates marked with red circle. 40x magnification. Ovarian cancer cell lines (OVCAR4 and SKOV3) were incubated for 24 h with the different volumes of **(C)** CaP-P **(D)** CaP-S and **(E)** CaP-S-C nanoparticles and cell viability was determined by Annexin/7AAD staining. Each data point represents individual experiments, N=3. Statistical analysis was done using ordinary one-way ANOVA and posthoc Dunnett's multiple comparisons test, significance is assumed for $p < 0.05$ (*), <0.01 (**). No significance between compared groups indicated by ns.

biological activation. Tumor cells were coincubated for 6h with nanoparticles before detachment and flow cytometry analysis. Results show that after the treatment the entire tumor cell population internalized CaP-NPs (**Figure S2A**) and fluorescence intensity was increasing with NP dose (**Figure 3A**). Additionally, Cetuximab conjugated silica nanoparticles (CaP-S-C) were taken up faster and stronger compared to CaP-S and CaP-P in OVCAR4 (**Figure 3A**). These results were additionally confirmed by microscopy pictures of coverslides seeded SKOV3 and OVCAR4 cells that were incubated for 3h with the CaP-NPs. There it can be seen that CaP-S-C are more dispersed compared to CaP-S, which appear as extracellular aggregates or on the cell surface (**Figure 3B**, indicated by red circles). Interestingly, CaP-P possess similar distribution as CaP-S-C. Viability of cancer cell lines OVCAR4 and SKOV3 was determined after 24 hour coincubation with various doses of sonicated CaP-P (**Figure 3C**), CaP-S (**Figure 3D**) and CaP-S-C (**Figure 3E**). Similar to **Figure 2** (cytotoxicity towards NK cells), only CaP-S showed toxicity against tumor cells.

Nanomaterials can cause immunomodulatory changes in the tumor microenvironment (TME). We tested whether CaP-NPs induced secretion of immunosuppressive cytokines or disbalance in tumor cell stress ligands, integrins or MHC class I complex, all important for susceptibility towards NK lysis. Supernatant of tumor cells treated with CaP-NPs was collected for measurement by ELISA and cells were analyzed by flow cytometry to determine expression of tumor cell stress ligand MIC-A (**Figure 4A**), ULBP-2,5,6 (**Figure 4B**), MHCI (**Figure 4C**) and CD54 (**Figure 4D**). In all cases, expression of markers

remained unchanged, with a slight tendency of ULBP-2,5,6 downregulation in case of CaP-P addition. The quantification of secreted cytokines in the coculture supernatant after incubation of sonicated CaP-NPs showed a high degree of variability for IL-8 (**Figure 4E**). For both IL-8 and IL-6 (**Figure 4F**), nanoparticle addition did not induce strong or significant secretion changes when compared to vehicle control (H_2O). These findings suggest that CaP-NPs do not significantly affect the expression of cytokines and ligands for NK receptors on ovarian cancer cells.

In order to address potential effects of aggregated nanomaterial on tumor cells we also determined the expression of stress ligands as well as tumor cell viability in the presence of aggregated CaP-NPs. As shown in **Figures S3A, B**, the expression levels of NK-activating ligands on tumor cells were lower in the presence of aggregated as compared to sonicated CaP-P NPs. Regarding tumor cell viability there was no difference of toxicity between aggregated and sonicated CaP-NPs (**Figure S3C**). In summary, our data suggest that in comparison to sonicated nanoparticles the aggregated nanomaterial may cause structural and functional changes on tumor cells but without affecting tumor cell viability.

CaP-NPs Do Not Impair Ovarian Cancer Cell Lysis by NK Cells

In the final part of the study, we performed cocultures of OC and NK cells in the presence of CaP-NPs in order to test how the NPs influence the interaction of NKs with their tumor targets. To this end we analyzed: a) whether the CaP-NPs preferentially associate
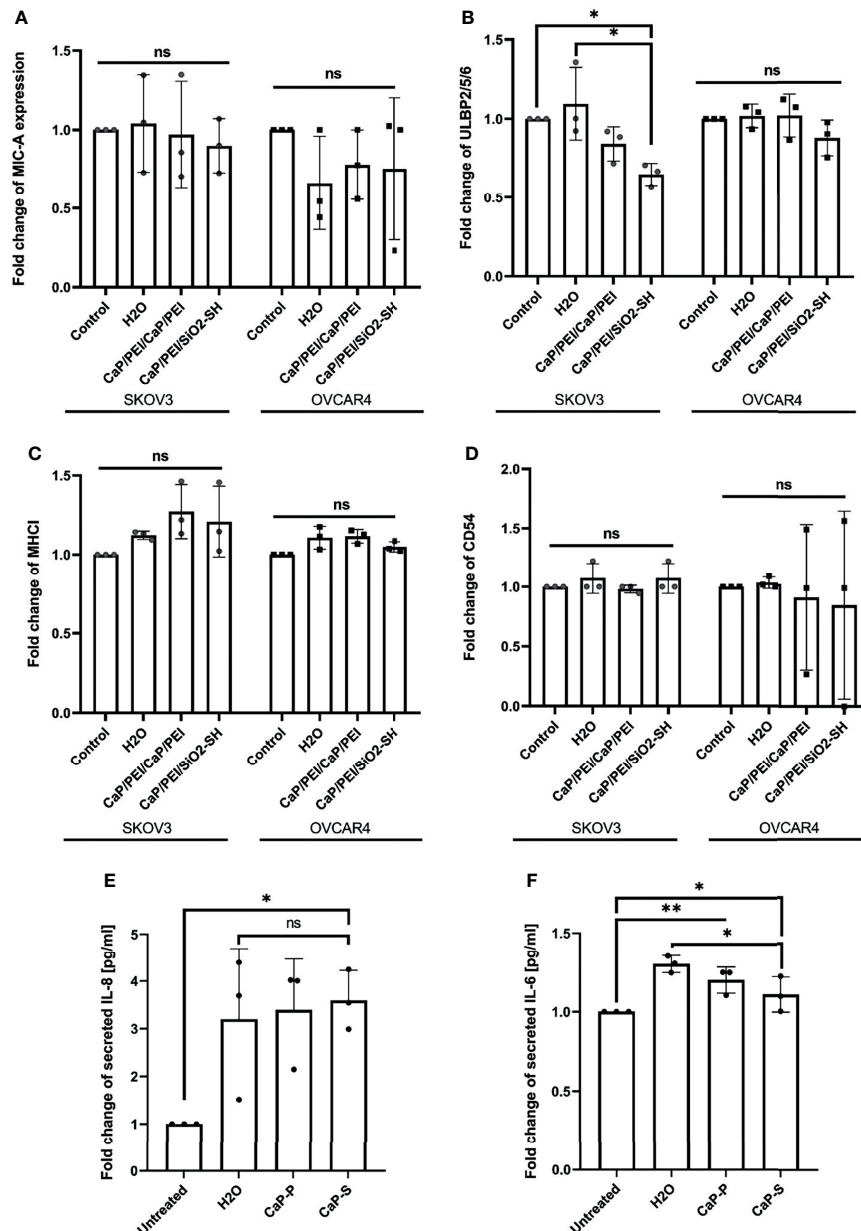
FIGURE 4 | CaP-NPs do not affect ovarian cancer cell stress ligands and immune related markers. Ovarian cancer lines (OVCAR4 and SKOV3) were coincubated with 12.5 µl of sonicated CaP-P or CaP-S suspensions for 24 hours after which cell culture supernatant was collected and expression of stress ligands **(A)** MICA/B, **(B)** ULBP-2,5,6 and expression of **(C)** MHCl and **(D)** CD54 were determined by flow cytometry. Y-axis shows delta median. Each data point represents individual experiments, N=3. The amount of proinflammatory cytokines **(E)** IL-8 and **(F)** IL-6 secreted from SKOV3 (OVCAR4 secretion was below detection) was determined by ELISA. Each data point in the figure represents individual experiments, N=3. Significance testing was done ordinary one-way ANOVA test with posthoc Dunnett's multiple comparison tests, significance is assumed for $p < 0,05$ (*), $<0,01$ (**). No significance between compared groups indicated by ns.

with OC or NK cells in co-cultures, b) whether the CaP-NPs induce changes in expression of functional surface markers on NK cells during the immune reaction, c) whether the CaP-NPs modulate natural and antibody-dependent cellular cytotoxicity (ADCC) of NKs against OC cells, d) whether Cetuximab that was coupled to CaP-NPs (CaP-S-C) retained ADCC-inducing activity. Our binding and uptake experiments show that all

CaP-NP types are primarily taken up by tumor cells and not by the NKs. Only a portion of NK cells takes up or binds CaP-NPs (**Figure S2B**) and in case of CaP-S-C this is stronger than CaP-S or CaP-P (**Figure 5A**). The presence of CaP-NPs did not negatively affect conjugation between NK cells and SKOV3 cells, showing that contact to target cells is preserved (**Figure 5B**). We next analyzed effects of NPs on NK surface molecules under NK-
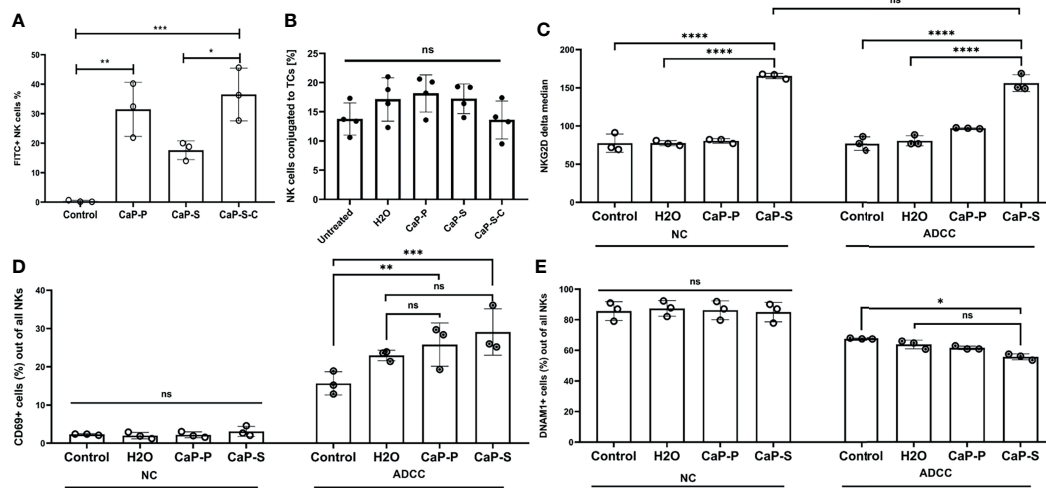
FIGURE 5 | Presence of CaP-NPs does not interfere with the NK-target cell interaction. **(A)** NK-TC 1:1 coculture was coincubated with 12.5 µl of FITC labeled CaP-NPs for 3 h and percentage of NK cells that take up CaP-NPs was determined by flow cytometry. **(B)** NK cells and SKOV3 cells were mixed in a 4:1 effector to target ratio in the presence of 1 µg/ml soluble Cetuximab or a corresponding concentration of antibody that was coupled to NP (CaP-S-C). After 45 minutes of coincubation, the percentage of the conjugated NK cells was measured by flow cytometry. Each data point represents an individual NK cell donor, N=4. Significance testing was done using ordinary one-way ANOVA and posthoc Dunnett's multiple comparisons test, significance is assumed for $p < 0.05$ (*), <0.01 (**), <0.001 (***). NK and TC were co-cultured in 1:1 ratio and stimulated with 12.5 µl of sonicated CaP-NPs for 6h. Expression of NK cell activation markers **(C)** NKG2D, **(D)** CD69, and **(E)** DNAM-1 was assessed by surface staining and flow cytometry. In all experiments, each data point represents NK cells from an individual healthy donor, N=3. Significance testing was done using ordinary two-way ANOVA and posthoc Sidaks multiple comparisons test, significance is assumed for $p < 0.05$ (*), <0.01 (**), <0.001 (***), <0.0001 (****). No significance between compared groups indicated by ns.

tumor co-culture conditions. Especially in the presence of ADCC-inducing Cetuximab antibodies CaP-S modulated expression of NKG2D, CD69 and DNAM-1 (**Figures 5C–E**). No NP-induced changes were found for CD16 (data not shown) and NKp46 (data not shown).

Lastly, we tested whether CaP-NPs would affect NK cell natural cytotoxicity and ADCC response, which is of the highest importance in our study. Since these responses are the main mechanisms by which NK cells exert antitumor activity it was of crucial relevance to investigate whether the CaP-NPs would impair these functions. To fully assess whether CaP-NPs cause any impairment on NK cell functionality we have calculated degranulation and tumor-killing contributions of individual components of the coculture system, using a formula explained in the materials and method section (Cetuximab, different CaP-NP species, NK cells). The detailed description of experimental conditions and calculated contributions is included in the legend to **Figure 6**. A more direct comparison of the calculated NC and ADCC fractions of total degranulation (**Figure S4A**) or tumor lysis (**Figure S4B**) was included in the supplementary data. The addition of dispersed CaP-P (**Figure 6A**) or CaP-S (**Figure 6B**) did not negatively affect NK natural degranulation or degranulation induced by soluble Cetuximab in both cocultures with SKOV3 or OVCAR4 as there was no significant difference in percentage of CD56+ CD107a+ NK cells between CaP-NP and control conditions. Similarly, the overall levels of tumor cell lysis under natural or antibody-mediated (ADCC) conditions were also maintained in the presence of CaP-P (**Figure 6C**). Lastly, it

was tested whether CaP-NP coupled Cetuximab would retain ADCC-inducing functionality. To this end, the activity of CaP-S-C (Cetuximab coupled to CaP-S) was tested against its internal control CaP-S (**Figures 6B, D**). CaP-S-C conjugates retained NK degranulation inducing activity, although it was reduced compared to the soluble unconjugated cetuximab used in control conditions (**Figure 6B**). When total tumor lysis was assessed, it remained largely unchanged in the presence of CaP-S-C when compared to CaP-S (**Figure 6D**). It must be noted here that silica-coated NPs display some inherent toxicity for tumor cells (NP induced toxicity in **Figure 6D**) that seems to overlap with tumor cell killing induced by the Cetuximab antibody.

DISCUSSION

The medical nanotechnology has reached multiple medical fields, since the use of nanoparticles enables new options in diagnostics and offers novel possibilities in medical therapy. Because of their potential use as carriers for drugs and immunomodulators, nanoparticles also represent interesting tools for cancer immunotherapy (2). Among the broad variety of nanoparticles CaP-NPs have become attractive tools because of their biocompatibility, high mechanic stability and standardized producibility (4).

However, the functional activity of CaP-NPs within biological environments has not been explored sufficiently. Particularly, the impact on function of different components of the immune system is almost unknown. Thereby, it is mandatory for their
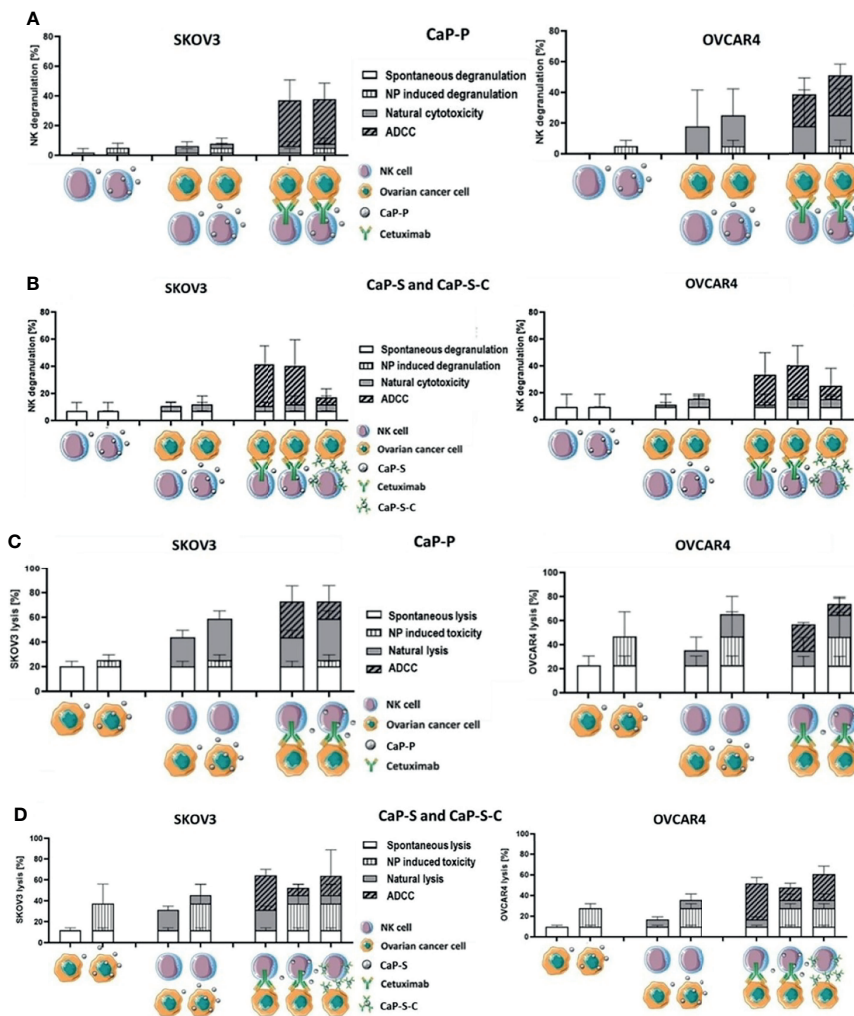
FIGURE 6 | CaP-NPs do not inhibit NK cell reactivity and Cetuximab that is conjugated to NPs retains partial ADCC activity. Ovarian cancer cells, NK cells, Cetuximab and 12.5 µl of CaP-P **(A, C)** or CaP-S and CaP-S-C **(B, D)** were coincubated for 6 h or 24 h. Then **(A, B)** NK cell degranulation (CD107a assay) or **(C, D)** tumor cell lysis (Annexin/7AAD assay) were measured by flow cytometry. Cell schematics illustrate the experimental conditions. For each condition the spontaneous degranulation/lysis (background activity; 1st (starting from left) column), the NP-induced degranulation/toxicity (2nd column), natural cytotoxicity by NKs (3rd column) and ADCC (5th column) were determined and shown. Fourth column depicts natural cytotoxicity in the presence of NP and 6th column shows ADCC in the presence of NPs. The 7th column (only panels **B, D**) shows the degranulation/tumor lysis induced by Cetuximab that was coupled to NPs (CaP-S-C). A more direct comparison of the calculated NC and ADCC fractions of total degranulation (**Figure S4A**) or tumor lysis (**Figure S4B**) was included in the supplementary data. Both experiments were performed using OVCAR4 and SKOV3 cell lines. Three individual NK cell donors were used.

use *in vivo* that nanocarriers do not impair immune cell activity. Single studies on osseous macrophages revealed that CaP-NPs enhanced inflammation by modulating macrophages while osteogenesis was attenuated (26). Other studies could show that CaP-NPs lead to maturation of antigen presenting cells, cytokine secretion and activation of cytotoxic T cells resulting in a strong immune response (9). Natural killer cells (NK cells) are among the first cells to interact with applied nanoparticles as these innate immune cells can act without prior sensitization. Previous studies demonstrated that cationic NPs augmented cytotoxic activity of NK cells while silver NPs enhanced expression of inhibitory receptors and thus reduced NK

effector functions (27, 28). So far, no studies are available investigating the interaction between CaP-NPs and NK cells.

Therefore, in this study we investigated how CaP-NPs affect NK-tumor cell immune interactions. For this, we tested the effects of different preparations of CaP-NPs in an *in vitro* model of ovarian cancer immunotherapy. We cocultured NK cells and ovarian cancer cells in the presence of therapeutic anti-EGFR antibody Cetuximab and added triple-shell nanoparticles (CaP-P NPs), silica-shell nanoparticles (CaP-S NPs) as well as functionalized particles with Cetuximab bound to the surface of silica-shell-particles (CaP-S-C NPs). For visualization and uptake studies we included CaP-NPs with fluorescent dye. In our studies, we examined effects of

nanoparticles on basic cell biological features of ovarian cancer cells. We mainly focused on the impact of CaP-NPs on cytotoxic and secretory functions of NK cells targeted against ovarian cancer cells and defined their role in interaction between NK and tumor cells.

First, we could observe that, over time, CaP-NPs tend to agglomerate in our culture system. It is known for some time that nanoparticles form aggregates when exposed to a biological environment (29). As interactions between CaP-NPs and NK cells have not been studied so far, we could show here for the first time that aggregates themselves may serve as artificial targets for NK cells, which may result in unspecific non-target cell directed cytotoxic NK cell activity. In line with this hypothesis, the magnitude of ADCC by NK in the presence of aggregated NP was reduced when compared to control conditions. In contrast, properly dispersed CaP-NP, which were generated by short sonication, did not lead to significant NK cell activation. These findings were supported by our data from DLS measuring particle size distribution. DLS data showed that sonication could completely prevent aggregation of CaP-P NPs, while some small aggregates (up to 1000 nm) were detected in sonicated CaP-S NPs. Furthermore, direct interaction between NK cells and aggregates could be observed during our live-cell imaging-studies. Here we could see that in coculture of NK and ovarian cancer cells aggregates of CaP-NPs substantially distracted NK cells from their original target. The potential biological relevance of this observation was demonstrated in our direct comparison of sonicated and unsonicated CaP-NPs influencing cytotoxic NK cell activity. Aggregated particles, especially CaP-S NPs, enhanced NK cell degranulation in contrast to sonicated CaP-NPs but in the presence of cocultured ovarian cancer cells the aggregated NPs tend deviate NK killing away from their intended cancer targets. Thus, we could show here, that standardized production and differentiated processing is mandatory before application of CaP-NPs *in vivo* in order to prevent adverse artificial immune cell activation and enable specific cellular modulation.

Further, we could demonstrate that dispersed CaP-NPs only showed slight immunotoxicity towards NK cells. This data is supported by other studies showing that CaP-NPs display low toxicity due to their composition of endogenous biomineral (4). However, certain degree of toxicity was observed in cocultures with CaP-S NPs. Furthermore, toxicity of CaP-S NPs was correlated to enhanced NK cell degranulation and to a tendential upregulation of CD69. The advantage of silica shell-containing CaP-S NPs is the possibility of their functionalization since proteins or antibodies cannot be covalently bound onto the calcium phosphate surface (8). Due to our results, certain components which are prerequisites for functionalization or contribute to the stabilization of particles can lead to a slight increase in toxicity but do not lead to substantial impairment of NK function.

In further studies we wanted to define the role of CaP-NPs during the interaction between NK and ovarian cancer cells. Principally, we could demonstrate that cytotoxic and secretory function of NK cells and NK-mediated tumor cell lysis remained unaffected by different preparations of CaP-NPs. In parallel, we investigated the expression of different NK cell markers. We could observe that natural cytotoxicity as well as antibody-dependent

cellular cytotoxicity (ADCC) were accompanied by an upregulation of NKG2D and CD69 and by downregulation of DNAM-1 which indicates NK cell activation. Interestingly, Cetuximab-functionalized CaP-S-C NPs were still able to induce ADCC and tumor cell lysis. However, the antibody conjugation onto the nanoparticle surface lead to reduced Cetuximab activity (30). One possible explanation could be that conjugation of randomly orientated antibodies leads to geometrical inaccessibility or inactivation of Fc and Fab antibody fragments which could be responsible for reduced ADCC (31). Another possible mechanism could be, that nanoparticle-bound Cetuximab is taken up faster by tumor cells and therefore inaccessible for NK cell interaction in contrast to free Cetuximab. Even though CaP-S-C nanoparticles were noted to induce lower NK degranulation in our study, the degree of tumor lysis is comparable to the ADCC induced by free Cetuximab which could be due to a fundamentally slightly increased cytotoxicity of CaP-S-C. Related to NK tumor cell interaction we also investigated formation of conjugates in presence of different types of CaP-NPs. Most importantly, addition of CaP-NPs did not impair the conjugate formation being mandatory for tumor immune cell interaction. In conclusion, CaP-NPs did not interfere with antitumoral NK activity but rather induced a slight activation.

In further experiments we studied the uptake of CaP-NPs by ovarian cancer cells. We could show that all types of CaP-NPs were taken up by tumor cells in a dose-dependent manner. In detail, microscopic as well as flow cytometry proved that functionalized CaP-S-C NP and to a lesser extent also CaP-P NPs displayed the highest uptake rate. In contrast, CaP-S NPs tend to form bigger aggregates (up to 10 μm diameter) which may explain their lower uptake rate and localization on the surface of the tumor cell. In a coculture of tumor cell and NK cells all types of CaP-NPs were predominantly bound to or taken up by ovarian cancer cells while only a small faction interacted with NK cells. Interestingly, NK cells bind CaP-S-C stronger than CaP-S NPs which could indicate antibody recognition by NK cells. Basically, in biological fluids cellular uptake of CaP-NPs is dependent on size, charge and surface characteristics (8, 32). So, different components like PEI, silica shell or specific antibodies determine state of aggregation, absorption of proteins and cellular uptake (33–35). An alternative explanation could be the targeting-effect by Cetuximab in CaP-S-C NPs, which has been already described in principle (36). In summary, these findings show that CaP-NPs do not impair the tumor cytolytic activity of NK cells and may serve as carriers for therapeutic functional modulation of tumor cell targets.

Interestingly, the intracellular uptake of CaP-NPs in ovarian cancer cells did not lead to altered expression of stress-induced ligands (MIC A and ULBP 2, 5, 6). Additionally, MHC-I and CD54, crucial receptors for NK cell interaction, also remained unaffected. This suggests that recognition by immune cells would be continuously enabled (37). This is consistent with our observation that uptake of CaP-P and CaP-S-C did not cause any direct toxicity. This was not to be expected, especially since the lysosomal escape caused by PEI may lead to necrosis in high particle concentration (38, 39). According to this, we did also not observe any enhanced secretion of tumor cytokines (IL-6 and IL-8)

which can also serve as measure for toxicity of nanoparticles (40). In contrast, CaP-S NPs induced moderate dose-dependent direct toxicity which would argue for a toxic effect of the silica shell. Summarizing our data, with the exception of silica-shell particles, CaP-NPs do not exert direct, unspecific cytotoxicity, which would qualify them for a differentiated immunotherapeutic approach.

In this study we directly added CaP-NPs to tumor-NK cocultures and assessed their direct potential effects on NK and tumor cells as well as on their interaction between tumor and NK cells. In prelimininary work to this project, we also investigated whether a pretreatment of tumor cells with different preparations of CaP-NPs could affect susceptibility of OC cells towards NK cell cytotoxicity. To this end, we pre-incubated tumor cells with the different CaP-NPs and measured natural cytotoxicity and ADCC of added NK cells as well as tumor cell lysis. However, no differences between both settings were observed (data not shown) further supporting the idea that CaP-NPs do not impair antitumor activity of NK cells.

In summary, in this study we could demonstrate that CaP-NPs slightly activate NK cells and do not impair cytotoxic and secretory NK functions. Importantly, aggregated nanoparticles which were not dispersed by sonication may serve as artificial target and deviate NK cells away from their intended targets. Furthermore, Cetuximab-functionalized CaP-NPs preserved ADCC functionality. In conjunction, by confirming CaP-NP biocompatibility, low toxicity and demonstrating efficient uptake in ovarian cancer cells our study offers options for integration of CaP-NPs in prospective immunotherapeutic concepts for cancer therapy.

DATA AVAILABILITY STATEMENT

The original contributions presented in the study are included in the article/**Supplementary Material**. Further inquiries can be directed to the corresponding author.

ETHICS STATEMENT

The studies involving human participants were reviewed and approved by Ethikkommission der Medizinischen Fakultät der Universität Duisburg-Essen. The participants provided their written informed consent to participate in this study.

AUTHOR CONTRIBUTIONS

AH, SBr, MO, and NM-G conceived and planned the experiments. AH, MS, MO, SBe, and SK carried out the experiments. AH, MS, MO, SBe, SBr, and NM-G analyzed and interpreted the data. PAH, SK, and ME provided crucial materials and reagents. AH, NM-G, and SBr wrote the manuscript. MS, ME, and SK edited the manuscript. SBr and NM-G supervised the project. All authors reviewed or contributed to the final manuscript.

FUNDING

ACKNOWLEDGMENTS

SUPPLEMENTARY MATERIAL

The Supplementary Material for this article can be found online at: https://www.frontiersin.org/articles/10.3389/fimmu.2022.830938/full#supplementary-material

REFERENCES

1. Rathor S, Bhatt DC, Aamir S, Singh SK, Kumar VA. A Comprehensive Review on Role of Nanoparticles in Therapeutic Delivery of Medicine. *Pharm Nanotechnol* (2017) 5(4):263–75. doi: 10.2174/2211738505666171113130639
2. Alsaab HO, Al-Hibs AS, Alzhrani R, Alrabighi KK, Alqathama A, Alwithenani A, et al. Nanomaterials for Antiangiogenic Therapies for Cancer: A Promising Tool for Personalized Medicine. *Int J Mol Sci* (2021) 22(4):1631. doi: 10.3390/ijms22041631
3. Ewen ST, Fauzi A, Tang YQ, Chamyuang S, Chia A. A Review on Advances of Treatment Modalities for Alzheimer's Disease. *Life Sci* (2021) 276:119129. doi: 10.1016/j.lfs.2021.119129
4. Epple M. Review of Potential Health Risks Associated With Nanoscopic Calcium Phosphate. *Acta Biomater* (2018) 77:1–14. doi: 10.1016/j.actbio.2018.07.036
5. Tadic D, Epple M. A Thorough Physicochemical Characterisation of 14 Calcium Phosphate-Based Bone Substitution Materials in Comparison to Natural Bone. *Biomaterials* (2004) 25(6):987–94. doi: 10.1016/S0142-9612(03)00621-5
6. Levingstone TJ, Herbaj S, Dunne NJ. Calcium Phosphate Nanoparticles for Therapeutic Applications in Bone Regeneration. *Nanomater (Basel)* (2019) 9(11):1570. doi: 10.3390/nano9111570
7. Enax J, Epple M. Synthetic Hydroxyapatite as a Biomimetic Oral Care Agent. *Oral Health Prev Dent* (2018) 16(1):7–19. doi: 10.3290/j.ohpd.a39690

8. Sokolova V, Epple M. Biological and Medical Applications of Calcium Phosphate Nanoparticles. *Chemistry* (2021) 27:7471–88. doi: 10.1002/chem.202182761

9. Scheffel F, Knuschke T, Otto L, Kollenda S, Sokolova V, Cosmovici C, et al. Effective Activation of Human Antigen-Presenting Cells and Cytotoxic CD8(+) T Cells by a Calcium Phosphate-Based Nanoparticle Vaccine Delivery System. *Vaccines (Basel)* (2020) 8(1):110. doi: 10.3390/vaccines8010110

10. Knuschke T, Rotan O, Bayer W, Kollenda S, Dickow J, Sutter K, et al. Induction of Type I Interferons by Therapeutic Nanoparticle-Based Vaccination Is Indispensable to Reinforce Cytotoxic CD8(+) T Cell Responses During Chronic Retroviral Infection. *Front Immunol* (2018) 9:614. doi: 10.3389/fimmu.2018.00614

11. Tenkumo T, Vanegas Sáenz JR, Takada Y, Takahashi M, Rotan O, Sokolova V, et al. Gene Transfection of Human Mesenchymal Stem Cells With a Nano-Hydroxyapatite-Collagen Scaffold Containing DNA-Functionalized Calcium Phosphate Nanoparticles. *Genes Cells* (2016) 21(7):682–95. doi: 10.1111/gtc.12374

12. Chernousova S, Epple M. Live-Cell Imaging to Compare the Transfection and Gene Silencing Efficiency of Calcium Phosphate Nanoparticles and a Liposomal Transfection Agent. *Gene Ther* (2017) 24(5):282–9. doi: 10.1038/gt.2017.13

13. Pittella F, Miyata K, Maeda Y, Suma T, Watanabe S, Chen Q, et al. Pancreatic Cancer Therapy by Systemic Administration of VEGF siRNA Contained in Calcium Phosphate/Charge-Conversional Polymer Hybrid Nanoparticles. *J Control Release* (2012) 161(3):868–74. doi: 10.1016/j.jconrel.2012.05.005

14. Tobin LA, Xie Y, Tsokos M, Chung SI, Merz AA, Arnold MA, et al. Pegylated siRNA-Loaded Calcium Phosphate Nanoparticle-Driven Amplification of Cancer Cell Internalization In Vivo. *Biomaterials* (2013) 34(12):2980–90. doi: 10.1016/j.biomaterials.2013.01.046

15. Zhang N, Lu C, Shu G, Li J, Chen M, Chen C, et al. Gadolinium-Loaded Calcium Phosphate Nanoparticles for Magnetic Resonance Imaging of Orthotopic Hepatocarcinoma and Primary Hepatocellular Carcinoma. *Biomater Sci* (2020) 8(7):1961–72. doi: 10.1039/C9BM01544B

16. Shetab Boushehri MA, Lamprecht A. Nanoparticles as Drug Carriers: Current Issues With In Vitro Testing. *Nanomed (Lond)* (2015) 10(21):3213–30. doi: 10.2217/nnm.15.154

17. Hannon G, Lysaght J, Liptrott NJ, Prina-Mello A. Immunotoxicity Considerations for Next Generation Cancer Nanomedicines. *Adv Sci (Weinh)* (2019) 6(19):1900133. doi: 10.1002/advs.201900133

18. Caracciolo G, Farokhzad OC, Mahmoudi M. Biological Identity of Nanoparticles In Vivo: Clinical Implications of the Protein Corona. *Trends Biotechnol* (2017) 35(3):257–64. doi: 10.1016/j.tibtech.2016.08.011

19. Moretta L, Pietra G, Montaldo E, Vacca P, Pende D, Falco M, et al. Human NK Cells: From Surface Receptors to the Therapy of Leukemias and Solid Tumors. *Front Immunol* (2014) 5:87. doi: 10.3389/fimmu.2014.00087

20. Screpanti V, Wallin RPA, Grandien A, Ljunggren HG. Impact of FASL-Induced Apoptosis in the Elimination of Tumor Cells by NK Cells. *Mol Immunol* (2005) 42(4):495–9. doi: 10.1016/j.molimm.2004.07.033

21. Alter G, Malenfant JM, Altfeld M. CD107a as a Functional Marker for the Identification of Natural Killer Cell Activity. *J Immunol Methods* (2004) 294 (1-2):15–22. doi: 10.1016/j.jim.2004.08.008

22. Kollenda SA, Klose J, Knuschke T, Sokolova V, Schmitz J, Staniszewska M, et al. In Vivo Biodistribution of Calcium Phosphate Nanoparticles After Intravascular, Intramuscular, Intratumoral, and Soft Tissue Administration in Mice Investigated by Small Animal PET/CT. *Acta Biomater* (2020) 109:244–53. doi: 10.1016/j.actbio.2020.03.031

23. Kozlova D, Chernousova S, Knuschke T, Buer J, Westendorf AM. Cell Targeting by Antibody-Functionalized Calcium Phosphate Nanoparticles. *J Mater Chem* (2012) 22:396–404. doi: 10.1039/C1JM14683A

24. Burshtyn DN, Davidson C. Natural Killer Cell Conjugate Assay Using Two-Color Flow Cytometry. *Methods Mol Biol* (2010) 612:89–96. doi: 10.1007/978-1-60761-362-6_7

25. US Department of Health and Human Services/Public Health Services/Food and Drug Administration. *Guideline on Validation of the Limulus Amebocyte Lysate Test as an End-Product Endotoxin Test for Human and Animal Parental Drugs, Biological Products and Medical Devices* (1987). Available at: http://www.fda.gov/cber/gdlns/lal.pdf.

26. Chen L, Qiao P, Liu H, Shao L. Amorphous Calcium Phosphate NPs Mediate the Macrophage Response and Modulate BMSC Osteogenesis. *Inflammation* (2021) 44(1):278–96. doi: 10.1007/s10753-020-01331-9

27. Kim KS, Han JH, Choi SH, Jung HY, Park JD, An HJ, et al. Cationic Nanoparticle-Mediated Activation of Natural Killer Cells for Effective Cancer Immunotherapy. *ACS Appl Mater Interfaces* (2020) 12(51):56731–40. doi: 10.1021/acsami.0c16357

28. Müller L, Steiner SK, Rodriguez-Lorenzo L, Petri-Fink A, Rothen-Rutishauser B, Latzin P, et al. Exposure to Silver Nanoparticles Affects Viability and Function of Natural Killer Cells, Mostly *via* the Release of Ions. *Cell Biol Toxicol* (2018) 34:167–76. doi: 10.1007/s10565-017-9403-z

29. Rausch K, Reuter A, Fischer K, Schmidt M. Evaluation of Nanoparticle Aggregation in Human Blood Serum. *Biomacromolecules* (2010) 11 (11):2836–9. doi: 10.1021/bm100971q

30. Ahmed M, Pan DW, Davis ME. Lack of In Vivo Antibody Dependent Cellular Cytotoxicity With Antibody Containing Gold Nanoparticles. *Bioconjug Chem* (2015) 26(5):812–6. doi: 10.1021/acs.bioconjchem.5b00139

31. Iijima M, Araki K, Liu Q, Somiya M, Kuroda S. Oriented Immobilization to Nanoparticles Enhanced the Therapeutic Efficacy of Antibody Drugs. *Acta Biomater* (2019) 86:373–80. doi: 10.1016/j.actbio.2019.01.011

32. Walkey CD, Olsen JB, Guo H, Emili A, Chan WC. Nanoparticle Size and Surface Chemistry Determine Serum Protein Adsorption and Macrophage Uptake. *J Am Chem Soc* (2012) 134(4):2139–47. doi: 10.1021/ja2084338

33. Xia T, Kovochich M, Liong M, Meng H, Kabehie S, George S, et al. Polyethyleneimine Coating Enhances the Cellular Uptake of Mesoporous Silica Nanoparticles and Allows Safe Delivery of siRNA and DNA Constructs. *ACS Nano* (2009) 3(10):3273–86. doi: 10.1021/nn900918w

34. Wartlick H, Michaelis K, Balthasar S, Strebhardt K, Kreuter J, Langer K, et al. Highly Specific HER2-Mediated Cellular Uptake of Antibody-Modified Nanoparticles in Tumour Cells. *J Drug Target* (2004) 12(7):461–71. doi: 10.1080/10611860400010697

35. Wen L, Wang Q, Zheng T, Chen J. Effects of Polyethylenimine on the Dispersibility of Hollow Silica Nanoparticles. *Front Chem Eng China* (2007) 1:277–82. doi: 10.1007/s11705-007-0050-4

36. Tseng SH, Chou MY, Chu IM. Cetuximab-Conjugated Iron Oxide Nanoparticles for Cancer Imaging and Therapy. *Int J Nanomed* (2015) 20 (10):3663–85. doi: 10.2147/IJN.S80134

37. Barber DF, Faure M, Long EO. LFA-1 Contributes an Early Signal for NK Cell Cytotoxicity. *J Immunol* (2004) 173(6):3653–9. doi: 10.4049/jimmunol.173.6.3653

38. Akinc A, Thomas M, Klibanov AM, Langer R. Exploring Polyethylenimine-Mediated DNA Transfection and the Proton Sponge Hypothesis. *J Gene Med* (2005) 7:657–63. doi: 10.1002/jgm.696

39. Liu Z, Xiao Y, Chen W, Wang Y, Wang B, Wang G, et al. Calcium Phosphate Nanoparticles Primarily Induce Cell Necrosis Through Lysosomal Rupture: The Origination of Material Cytotoxicity. *J Mater Chem B* (2014) 2(22):3480–9. doi: 10.1039/c4tb00056k

40. Elsabahy M, Wooley KL. Cytokines as Biomarkers of Nanoparticle Immunotoxicity. *Chem Soc Rev* (2013) 42(12):5552–76. doi: 10.1039/c3cs60064e

Supplementary Material

| Nanoparticle type	DLS [nm]	SEM [nm]	PDI	Zeta Potential [mV]	[Ca2+] [µg/mL]	CaP Conc. [µg/mL]	Particles/mL	Antibodies [mg/mL]
CaP-PEI -CaP-PEI CaP-	129 ± 32	57 ± 9	0.343	18.0 ± 1.4	62.50	156.88	$5.12 \cdot 10^{11}$	-
PEI_FITC-CaP-PEI	131 ± 19	72 ± 5	0.262	17.9 ± 0.8	39.70	99.65	$1.61 \cdot 10^{11}$	-
CaP-PEI -SiO$_2$-SH CaP-	309 ± 49	58 ± 7	0.140	22.2 ± 0.4	46.55	116.84	$3.62 \cdot 10^{11}$	-
PEI_FITC-SiO$_2$-SH	122 ± 32	64 ± 5	0.382	28.2 ± 1.2	62.50	156.88	$3.62 \cdot 10^{11}$	-
CaP-PEI -SiO$_2$-S-Cetuximab CaP-	97 ± 19	88 ± 15	0.151	18.8 ± 1.5	9.30	23.34	$2.07 \cdot 10^{10}$	0.058
PEI_FITC-SiO$_2$-S-Cetuximab	123 ± 26	64 ± 16	0.246	23.8 ± 2.7	34.83	87.42	$2.02 \cdot 10^{11}$	0.053

Supplementary Table S1. Representative physicochemical properties of different CaP-NPs. Notice that different NP species have comparatively similar properties such as size, potential, and particle number.
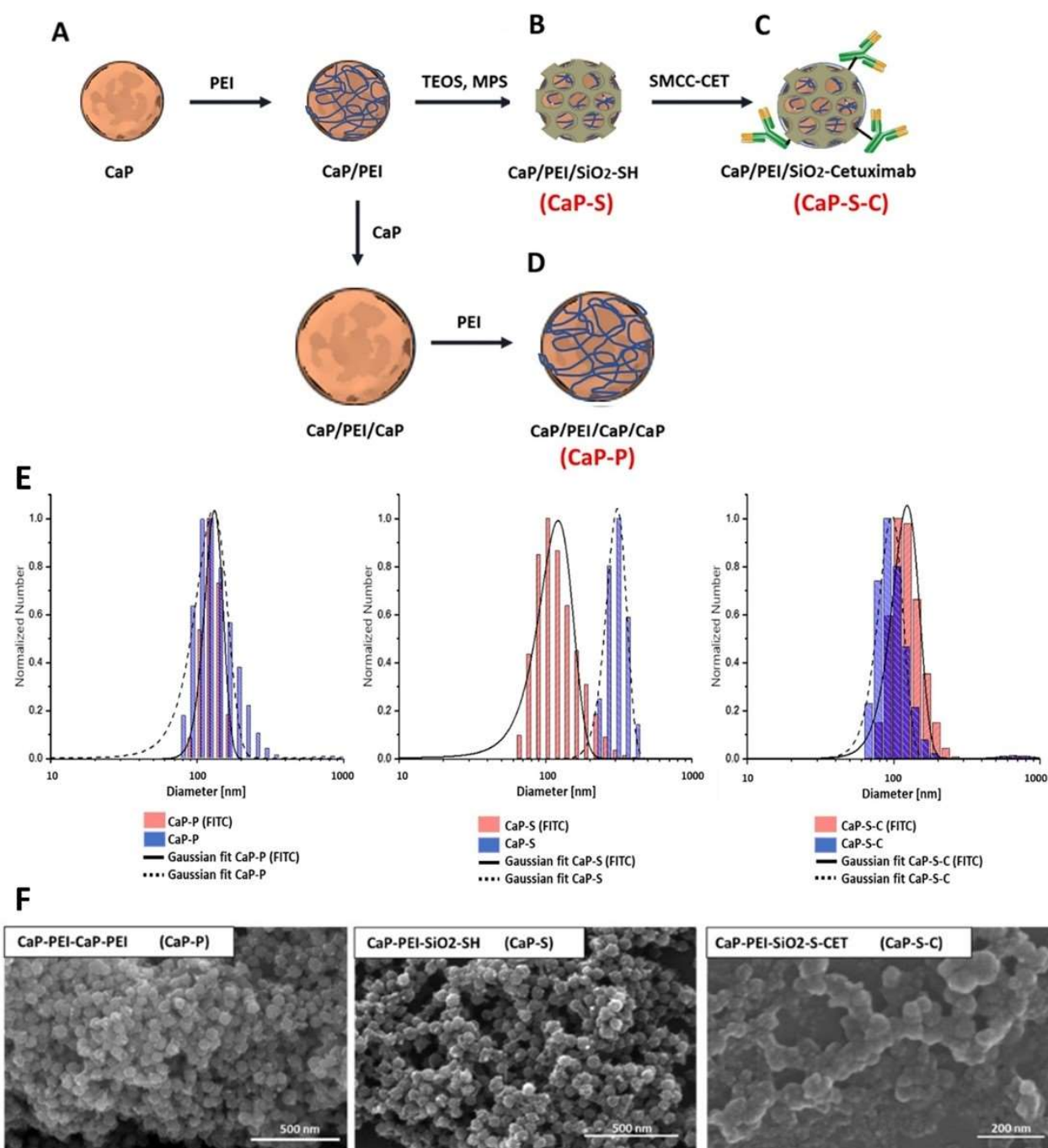
Supplementary Figure S1.: Calcium phosphate nanoparticles are biocompatible state of art produced nanoparticles. (A) Schematic representations of the chemical steps needed for the synthesis of different calcium phosphate nanoparticles. **(B)** CaP/PEI/SiO$_2$-SH – Silica coated CaP-NPs (referred as **CaP-S**), **(C)** CaP/PEI/SiO$_2$-S-CET – Silica coated CaP-NPs functionalized with Cetuximab antibody (referred as **CaP-S-C**), **(D)** CaP/PEI/CaP/PEI – Triple shell CaP-NPs (referred as **CaP-P**).
(E) Representative nanoparticle size and distribution quantified by dynamic light scattering.
(F)
Representative nanoparticle micrographs obtained by scanning electron microscopy.
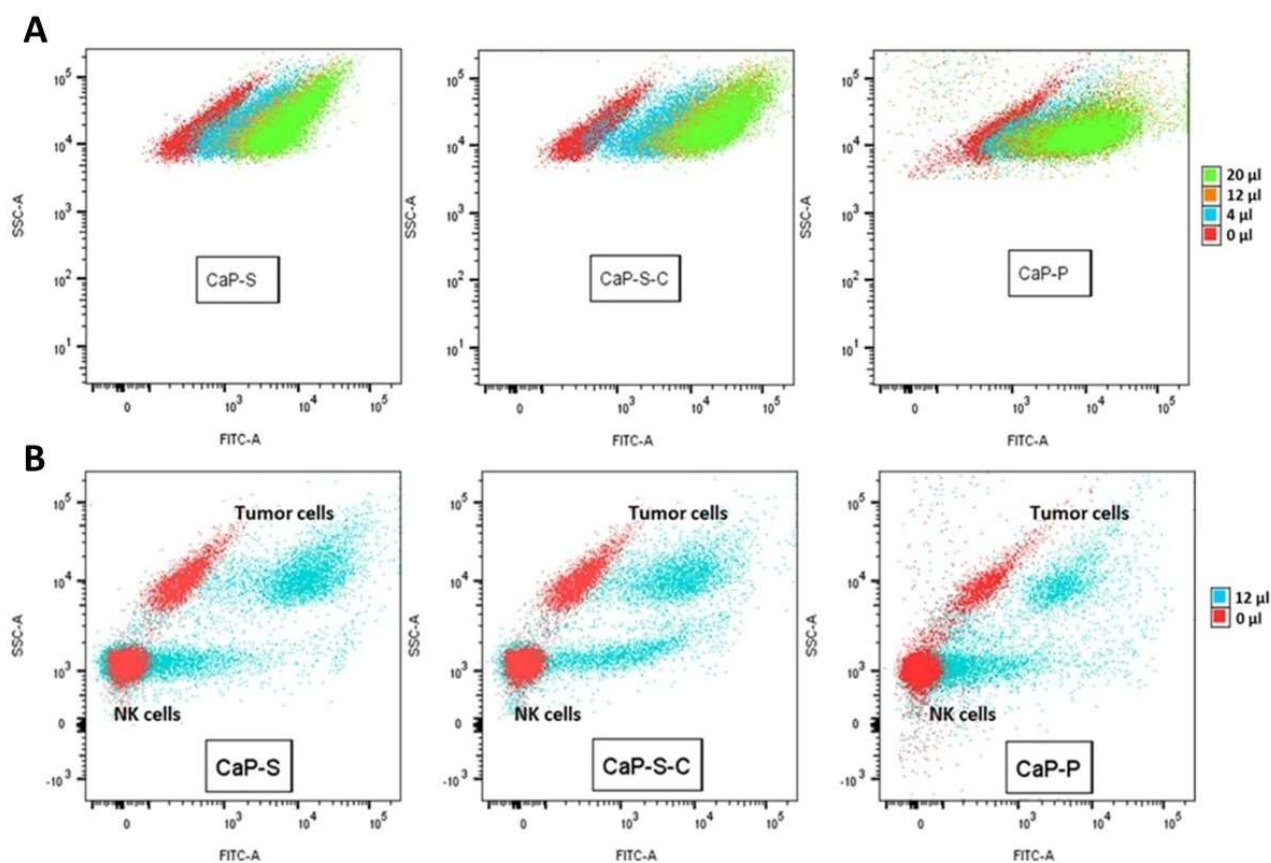
Supplementary Figure S2.: Uptake of CaP-NPs in cancer cell mono-cultures and co-cultures withNK cells. (A) Representative plot showing the uptake of CaP-NPs by SKOV3 cancer cells from Fig.
4.A after 6 hours, analyzed by flow cytometry. **(B)** Representative plot showing the uptake of 12 µl of CaP-NPs in the NK-TC coculture after 3 hours from Fig 6.A, analyzed by flow cytometry.
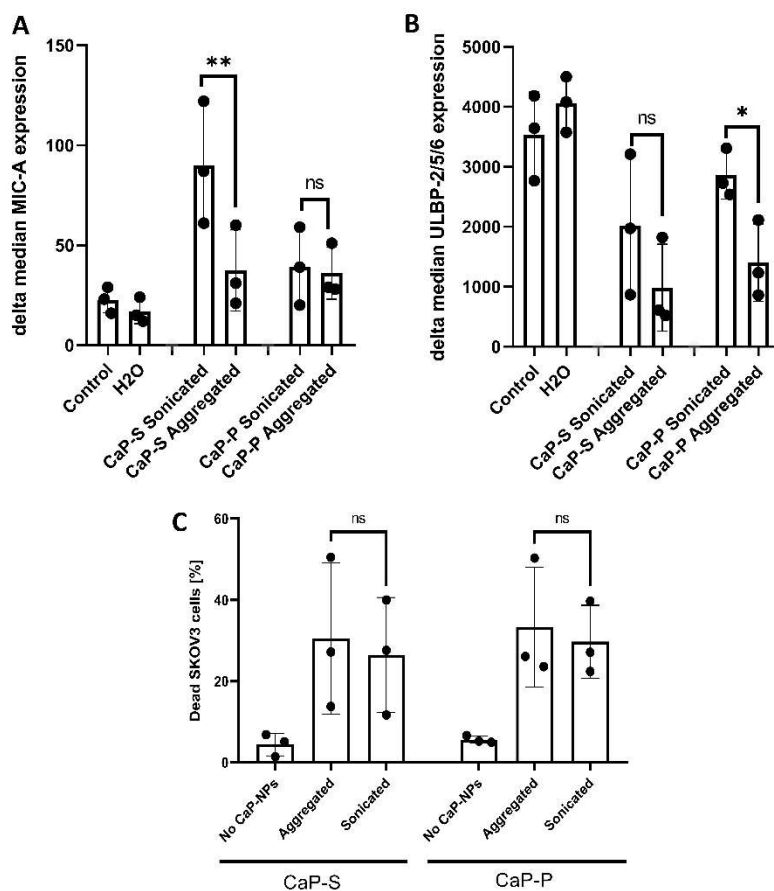
Supplementary Figure S3.: Effect of aggregated and sonicated CaP-NPs on cancer cell stress marker expression and tumor cell viability. SKOV3 OC cells were coincubated with 12,5 µl of sonicated or aggregated CaP-P and CaP-S nanoparticle suspensions for 24 h and expression of MICA

(A) and ULBP-2/5/6 **(B)** was determined by surface staining flow cytometry. **(C)** SKOV3 cell lysis after 24 h coincubation with aggregated or sonicated CaP-NPs was determined by Annexin/7AAD flow cytometry staining. Data points represent three individual experiments. Significance testing was done using paired t-test, significance is assumed for p<0,1 (*), <0,01 (**). No significance between compared groups indicated by ns.
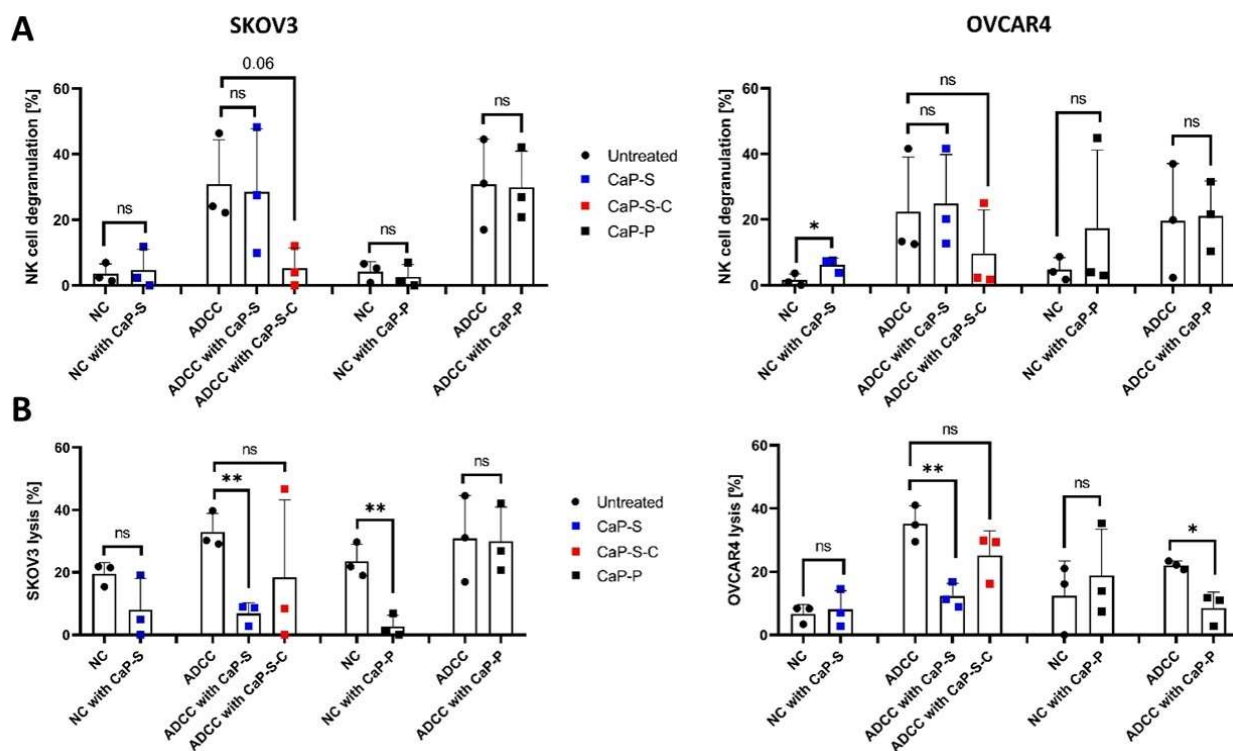
Supplementary Figure S4.: Simplified comparison of the calculated NC and ADCC. NK degranulation **(A)** and tumor lysis **(B)** in control conditions and the presence of CaP-NPs using data shown in the Fig 6. Both experiments were performed using SKOV3 (left panels) and OVCAR4 (right panels) cell lines. Each data point represents an individual NK cell donor, N=3. Significance testing was done using both unpaired t-test with Welch's correction and one-way ANOVA with posthoc Dunnets multiple comparison test, significance is assumed for $p < 0,05$ (*), $<0,01$ (**). No significancebetween compared groups indicated by ns.
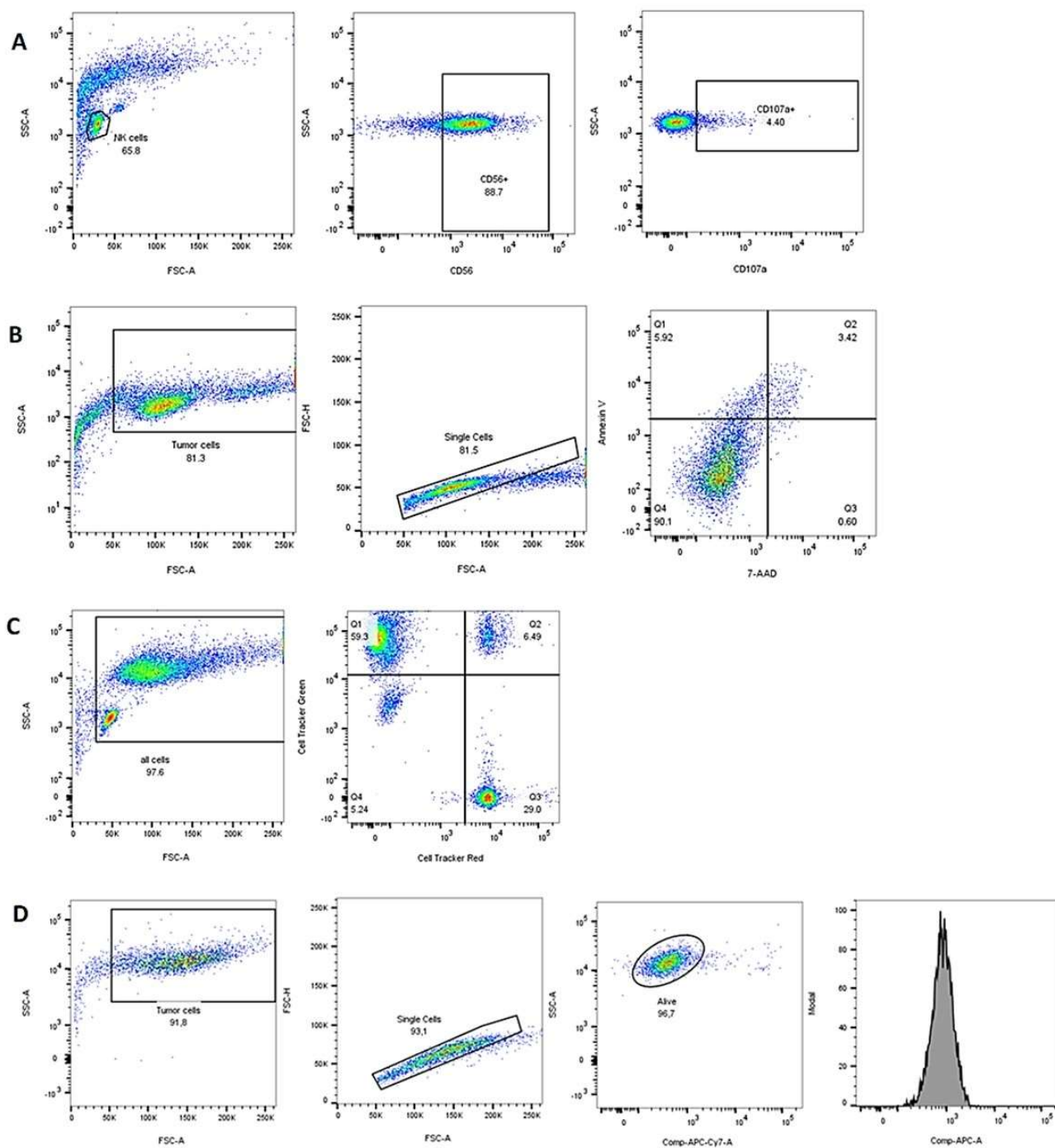
Supplementary Figure S5.: Representative flow cytometry gating strategy for **(A)** NK Degranulation,
(B) Tumor killing, **(C)** NK-Tumor cell conjugate assay and **(D)** Tumor cell stress ligand staining.
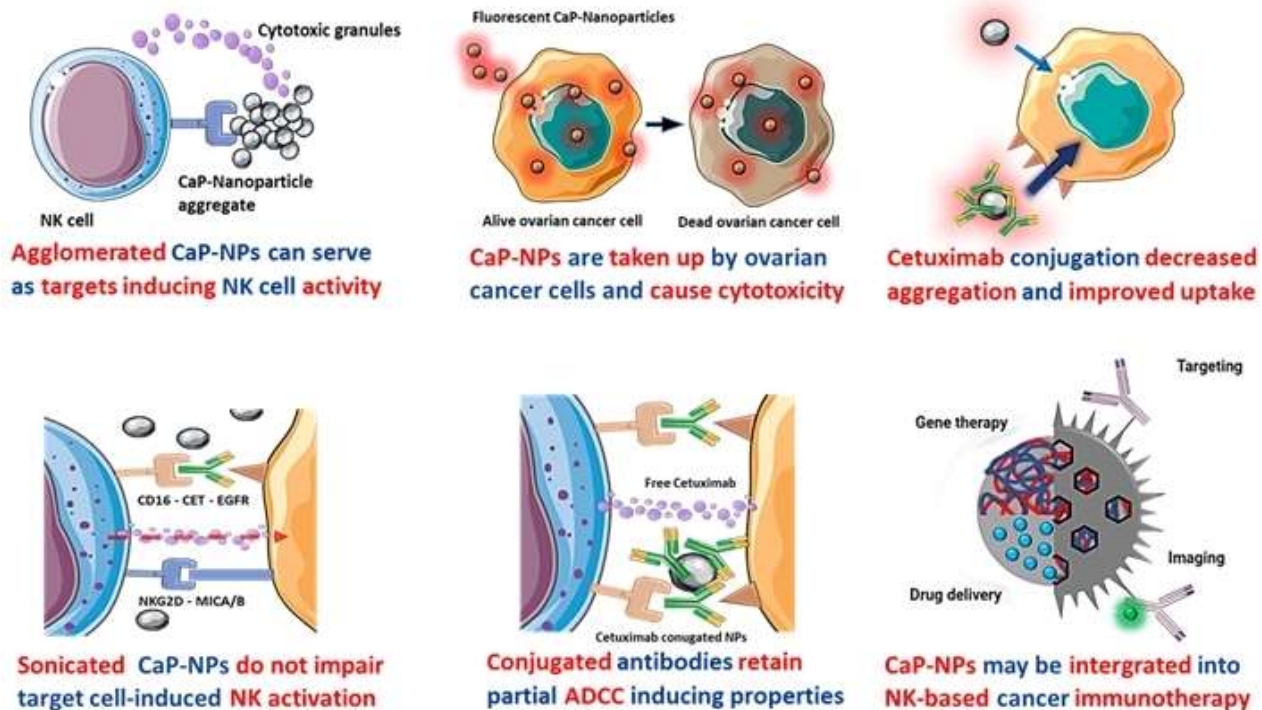
Supplementary Figure S6.: Graphical abstract and summary of the most important findings in the study. Figure was assembled using open-source illustrations provided by Sevier Medical Art (smart.servier.com).

4. Discussion

4.1. What is the origin and role of electrolyte imbalance in the TME?

During potentiometric analysis, we identified electrolyte imbalance (high sodium, low chloride and potassium content) as the likeliest immunosuppressive factor. In the literature, immunomodulatory effects of ionic imbalances are often studied in the context of "high salt" diet, which is defined as sodium above 170 mM. This is often simulated *in vitro* by adding 40 mM of NaCl (Probst et al., 2019). It should be stated that the electrolyte-based immunosuppression we observed is unlike the "high salt" mechanism. The "high salt" is often incorrectly referred to as high sodium condition, while disregarding potential effects of abnormal chloride environment concentration. In our ascites samples we did not have high concentrations of both sodium and chloride ions, rather high sodium and low chloride. It is often reported in high salt studies, that such environment dysregulated T cell proliferation and effector function. For example, in CD8+ T cells it induced immunosuppression and allowed for tumor immune escape (Zielinski, 2021). Furthermore, high salt environment induced transcriptional changes, osmoprotective signaling and altered mitochondrial metabolism, consistent with exhaustion. Mechanistic studies described that high salt led to increase in intracellular sodium, which interfered with electron transport chain and caused FOXP3 downregulation (Hernandez et al., 2015).

Our preliminary metabolic studies on ascites exposed NK and T cells have also shown dysregulated mitochondrial potential (data not shown) and increased intracellular sodium. During our ascites studies we could demonstrate that cytotoxic and secretory NK cell functions were significantly impaired by acellular ascites fluid. This was associated with impaired upregulation of NK cell activation markers CD69, CD107a, and IFNγ secretion. Additionally, the downregulation of DNAM-1 and upregulation of TIGIT were hindered as well, which indicated that immunosuppression is not caused by classic NK cell exhaustion. One *in vivo* NK cell study reports that after 15 days of high salt diet, mouse NK cells demonstrated upregulation of CD107a, downregulation of PD1 and TIGIT (Rizvi et al., 2021). The effects described in most of *in vitro* high salt studies were achieved after 24h to five days of priming cells. In our study, six hours NaCl exposure did not impact NK cell degranulation (data not shown). Furthermore, intracellular calcium flux studies have shown inhibition onset after three to four minutes. NK cell killing and conjugation were also visibly impaired within 15-30 minutes.

These suppressive effects occurred only upon the addition of malignant ascites, but not with benign intraperitoneal fluid samples.

Going further we tried to elucidate the exact immunosuppressive mechanism. Since we hypothesized that sodium imbalance was responsible for immunosuppression, we investigated the effect of sodium channel blockers in sodium-rich ascites coculture. We found that amiloride and lidocaine were most effective in preventing ascites-induced changes of intracellular calcium and sodium in activated T cells. Amiloride and lidocaine pretreatment also significantly reversed ascites-mediated inhibition of NK cell degranulation (six hours) and conjugation (45 minutes). Using a similar approach, we confirmed that sodium-induced aberrant gene expressions of PIK3CD, PRKCQ, AKT1, and GZMB were reversed by direct addition of amiloride. Amiloride was also capable of restoring phosphorylation and membrane recruitment of the signaling protein p85-PI3K in NK cells after short activation and exposure to an ascites environment (five minutes). The lidocaine mode of action relies on blocking the activity of VGSC (X. Yang et al., 2020). On the other hand, amiloride works by directly blocking ENaC and NHE-1 in a reversible manner that prevents transient or induced ion flow (Kleyman & Cragoe, 1988; Qadri et al., 2012). It should be mentioned that ion channels work in unison to maintain electrolyte homeostasis. For example, the sodium influx via VGSC channels stimulates the activity of NHE1 (Brisson et al., 2011), which could explain why blocking any of these channels in our experimental model yields similar restorative effects.

While electrolyte imbalance has been described in certain TMEs, it is not fully understood how this electrolyte imbalance develops. In addition to the peritoneal pressure and vessel permeability affecting the imbalance, it has been suggested that sodium can accumulate in the tissues, where it binds to the negatively charged matrix glycosaminoglycan (Ito et al., 2023). Cytokine signaling, such as EGF has been shown to modulate activity of potassium, chloride and sodium channels, which can contribute to their extracellular increase (Bowlby et al., 1997; S. P. Fraser et al., 2014; Jeulin et al., 2008). Furthermore, the necrosis-released potassium ions can also cause strong T cell suppression by impairing TCR receptor and Akt-mTOR phosphorylation through serine/threonine phosphatase PP2A3 (Eil et al., 2016). All of these factors likely contribute to the development of electrolyte imbalance within malign ascites compared to benign samples we studied.

The exact molecular mechanism of ionic immunosuppression is unclear. A possible explanation for why electrolytes can modulate protein activity is that ions can bind to their protein helices, which changes their conformation and prevents interaction with other ligands (Zhou & Pang, 2018). Disrupting the Na^+, Ca^{2+}, and H^+ homeostasis and respective ion channel activities can activate protein kinases and pathways that affect proliferation, invasion, (Bose et al., 2015; Leslie et al., 2019) and immunomodulation. Some studies have shown that binding of chloride ions to specific residues affected the catalytic activity, stability or function of the protein. For example, chloride binding to catalytic subunit has been found to modulate both the activity and optimal pH range of human pancreatic α-amylase (Maurus et al., 2005). Similarly, chloride binding sites with regulatory function were found to modulate permeability of AE1 ion channel (Jennings, 2005). Furthermore, signaling kinases such as JNK2 and WNK1 have been found to be regulated by intracellular chloride ions. The increase in the intracellular chloride concentration activates JNK2 kinase, which triggers Na^+/K^+ pump in response to hypotonicity (Capasso et al., 2003), while the decrease causes WNK1 activation, which changes permeability of CFTR to surrounding chloride ions (Piala et al., 2014). These studies further highlight the importance of considering other major ions besides the sodium, since their imbalance can also affect important signaling and enzymatic processes. Therefore, our high-sodium, low-chloride and low-potassium ascites cannot be fully equated to high salt (high-sodium and high-chloride) conditions.

Our study investigated mainly ascites effects on healthy donor NK and T cells in coculture system. The electrolyte-based regulatory mechanism we describe is novel and further validation could be done by comparing NK and T cells isolated from ascites to ones from patient and healthy donor blood. In this ex vivo study, cells would be assessed for their degranulation, cytokine secretion and ADCC capabilities. The functional and phenotype changes of NK and T cells would be studied via flow cytometry. qPCR and western blot would be used to assess the changes in activation and metabolic genes.

4.2.   Which other candidates induce immunosuppression in ascites TME?

In our studies we were able to confirm that electrolytes were a major suppressive component, but we also considered the possibility that there are additional factors in the ascites that contribute to its suppressive effects. Besides classical inhibitory molecules (cytokines, tumor cell ligands and metabolites) other important molecules, though not typically inhibitory

themselves, can cause suppression when imbalanced. This category includes endogenous antibodies, various serum proteins, and electrolytes.. Several studies have shown that physiological IgG levels in human serum strongly inhibited NK cell ADCC by competing with therapeutic IgG1 antibodies for binding to ADCC receptor CD16 (Li et al., 2018; Preithner et al., 2006). Therefore, ascites-derived immunoglobulins could also compete with therapeutic antibody and impair ADCC.

Historically, some healthy serum proteins have been described as inhibitory. *In vitro* experiments have demonstrated that activation of lymphocytes was disrupted by serum proteins, such as α-globulin, albumin, and α-1 acid glycoprotein (Elg et al., 1997). It has been proposed that some of these essential proteins have context-dependent immunoregulatory functions. Recently, a study was published showing that abundant serum proteins like albumin and Fab fragment, can also impair ADCC as non-competitive inhibitors (Yanaka et al., 2023). In pathologic conditions, their effects are much stronger because of increase in concentration. The tumor marker CA125 (MUC16, mucin) also belongs to this group, since it was recently shown that at higher concentration it can impair NK cell effector function and prevent conjugation to tumor cells (C. C. Fraser et al., 2022; Kline et al., 2017).

The historical studies which investigated ascites inhibitory mechanisms often contain inconsistent reports about the properties (size, heat and protease sensitivity, etc.) of immunosuppressive factors (Badger et al., 1981; Fumita et al., 1984; Medoff et al., 1986). The failure to fully identify immunosuppressive components in ascites may be due to methodological challenges in separating ascites components while retaining full biological activity of the sample. Often these studies performed chromatographic fractionalization and used precipitation agents or other chemical additives which could lead to the loss of some components.

Since peritoneal ascites can be rich in proteins and antibodies, as was confirmed for our samples using nephelometry, we initially suspected that they are the main inhibitory mediators. The proposed mechanism was that protein excess interfered with the effector to target conjugation and excess of irrelevant IgGs competed with the ADCC-inducing antibody Cetuximab. To further explore the contribution of antibodies and proteins, we performed dialysis. Electrolyte concentrations were normalized to culture medium levels, in which dialysis was performed. Additionally, no substantial loss of proteins or IgG antibodies happened during the dialysis. When dialyzed samples were used in degranulation assay,

restorative effect could be seen, but still a degree of inhibition persisted. Furthermore, in ascites samples without electrolyte imbalance, dialysis did nothing to revert suppression. When the suppression degree of dialyzed samples was correlated to the ascites components, we only found significant correlation to IgG antibody concentration. Similarly, the correlation between NK cell degranulation and IgG antibody concentration in ascites samples with low sodium (<145 mM) was significant as well. The addition of healthy donor serum had the same inhibitory effect, but serum permeate did not impair NK activity (data not shown). Therefore, these data imply that besides electrolytes other components, specifically the IgG antibodies, cause suppression as well. In subsequent studies we plan to isolate ascites antibodies to prove mechanistically their suppressive effects.

We also used fluid composition data to adjust the protein and antibody concentration in our coculture system by supplementing the medium with different concentrations of serum proteins (albumin) and irrelevant antibodies (Rituximab). When we tested these components using our coculture system, we saw a dose-dependent inhibition on NK cell degranulation and conjugation when Rituximab or albumin were added (data not shown).

In the end, we plan to further examine our published and preliminary findings using an *in vivo* mouse model. Currently, there are no *in vivo* studies regarding ascites immunosuppressive mechanisms on immune or NK cells in particular. Likewise, there are no studies that explicitly address intrinsic NK cell resistance in ovarian carcinoma and investigate therapeutic solutions. Since ascites is a complex environment, such investigation can only be performed using animal experiments. We plan to perform the experiments in NOD-SCID-gamma (NSG) mice, which is a well-characterized immunosuppressed mouse strain. Mice will be injected intraperitoneally with luciferin-transfected human ovarian cancer cell line SKOV3 and human NK92 leukemia cell line. This will enable us to study the efficacy of NK cell adoptive therapy and interactions between NK cells and tumor entity. *In vivo* investigation of fluid microenvironment effects will be achieved through intraperitoneal injection of patient or donor derived fluids (peritoneal ascites and healthy serum) or several possible suppressive candidates (salt solutions, albumin, IgG antibodies and lipids). Given that antibodies and serum proteins can be dysregulated in other conditions and fluid compartments, this investigation could provide valuable insights into novel immunoregulators and possible treatments. Ion channel blockers and siRNA molecules offer potential for normalizing the peritoneal environment and augmenting NK and T cell functions. However, given their toxic off-target effects and vulnerability to enzymatic

degradation, it is necessary to encapsulate them in functionalized nanoparticles for *in vivo* therapy.

4.3. Therapeutic application of nanoparticles *in vivo*: prerequisites and pre-therapeutic considerations

While *in vivo* application of therapeutic nanoparticles holds promise, caution is warranted, as not much is known on how these novel and foreign nanomaterials can interact with the human body. The persistent accumulation of such materials can cause severe side-effects such as chronic inflammation, blood coagulation and even strong immune response (Zolnik et al., 2010). This is often accompanied by secretion of signaling molecules, which can impair and polarize immune cells. Because of this, it is important that any application should be preceded with thorough nanotoxicological studies which consider particle size distribution, surface area, charge and aggregation (Zielińska et al., 2020). When we assessed our nanoparticles, we were able to demonstrate that sonicated CaP-NPs did not impair cytotoxic or secretory NK functions. Nor did they induce the proinflammatory cytokines connected to nanoparticle exposure as described in literature. For example, intraperitoneal application of titanium oxide particles increased TNF-α, IL-1β and IL-8 in mouse pleural fluid (Moon et al., 2010). The addition of CaP-NP presence to the coculture system caused only low unspecific toxicity to both tumor and NK cells. However, it should be kept in mind when NPs are incubated in biological fluids for longer time, their behavior is altered to the point that they act as haptens and bind surrounding proteins (B.-X. Chen et al., 1998; Lee et al., 2004). The new aggregated particles with adsorbed proteins could trigger immune response which original sonicated material would not trigger. Therefore, the only way to anticipate the *in vivo* effects is to also perform *in vitro* experiments with unsonicated aggregated particles.

The behavior of nanoparticles in biological colloids and their cellular interactions are strongly influenced by particle surface charge, which modulates particle aggregation (Villanueva-Flores et al., 2020). For example, when particles are in electrolyte imbalanced solutions, their electrostatic repulsion becomes weaker and causes fast homo-aggregation. This can lead to easier cell adherence and activation of immune cells (Barbero et al., 2022; Zhao et al., 2021). As interactions between CaP-NPs and NK cells have not been studied so far, we performed coculture studies to assess their effects on degranulation, tumor cell killing and conjugation.

Our study shows for the first time that nanoparticle aggregates may serve as artificial targets for NK cells. Direct interaction between NK cells and aggregates could be observed during our live-cell imaging studies. Aggregated particles, especially CaP-S NPs, enhanced NK cell unspecific degranulation in contrast to sonicated CaP-NPs, but when cocultured with ovarian cancer cells the aggregated NPs tend to deviate NK killing away from their intended targets. This further highlights the importance of proper study and surface modifications before safe *in vivo* application of CaP-NPs is possible.

In order to prevent adverse immune cell activation and aggregation, NPs are often stabilized by conjugating long chained hydrophilic polymers such as PEG (Suk et al., 2016). Particles can be further functionalized by covalent binding of specific antibodies on the CaP-NP surface, which offers the possibility for individualized targeted cancer therapy. Cetuximab-functionalized CaP-NPs preserved ADCC functionality of the antibody. When compared to free Cetuximab, the degree of induced degranulation was lower, which could imply that conjugation decreased antibody efficiency. This likely happens due to random orientation of IgGs, which could also conjugate in a manner to make Fc fragment inaccessible to CD16 (Welch et al., 2017). While this might impair therapeutic effect, the targeting effect of antibodies was strong enough to improve CaP-NP uptake. Different technologies could be used to ensure that there is no loss of therapeutic antibody efficiency. Studies show that difference of *in vivo* therapeutic effect depends on the degree of IgG fucosylation and other glyco-modification (Braster et al., 2021). Another approach would be using specific coupling methods and reagents that could ensure that Fc fraction is neither blocked nor rendered inert. One group developed such a method based on specific adaptor proteins, which can be used to tune the amount of functional Fc or Fab antibody fragments (Tholen et al., 2023).

Existing studies have shown that CaP-NPs are promising tools for gene and immunotherapy. Both DNA and siRNA have been used as nanoparticle payload for eukaryotic cell transfection (Kovtun et al., 2009). CaP-NPs also display comparable transfection efficacy while being less toxic than the more often used Lipofectamine (Chernousova & Epple, 2017). Due to these properties, CaP-NPs have been applied for *in vivo* imaging, gene therapy and vaccination. For example, CaP-NPs containing MRI contrast agent have been used for targeted and improved detection sensitivity (N. Zhang et al., 2020). Furthermore, encapsulation of therapeutic molecules such as doxorubicin and siRNA loaded PEGylated CaP-NP have shown *in vivo*

tumor growth arrest (Tobin et al., 2013). In our further studies we wish to capitalize on the versatility of this nanomaterial and its interesting properties.

So far, there are only few *in vivo* studies on the therapeutic use of calcium phosphate nanoparticles in ovarian cancer (X. Cheng & Kuhn, 2007; Zhao et al., 2020). We plan to use CaP-NPs in a previously described NSG mouse model. These CaP-NPs would encapsulate siRNA to transiently downregulate either suppressive tumor cell surface markers (MHCI, PD-1, CD112 and CD155) or NK cell sodium electrolyte channels (VGSC, NHE-1 and ENaC). To assist with targeting tumor or NK cell, the CaP-NP surface could be functionalized with Cetuximab or anti-NKp46/anti-NKG2D antibodies, respectively. A similar approach was used to treat autoimmunity in a study utilizing liposomes loaded with siRNA against potassium ion channels (Hajdu et al., 2013). In one study authors were able to revert immunosuppression caused by extracellular potassium by overexpressing potassium channel Kv1.3, which reduced its intracellular concentration and rescued *in vitro* and *in vivo* effector function of T cells (Eil et al., 2016). These studies and our proposed approach combine adoptive immunotherapy with targeted gene therapy, promising improved treatment and better patient outcomes.

5.   Conclusion and future perspectives

In the first part of our study, through correlations, descriptive and mechanistic experiments, we demonstrated that a major inhibitory factor in malignant ascites was the imbalance of electrolytes, particularly high sodium. Strong *in vitro* NK suppression as well as low chloride concentrations in ascites correlated with poor patient outcomes, suggesting clinical relevance of our findings. In future studies we wish to explore therapeutic interventions that are based on our findings and investigate other mechanisms of immunosuppression that operate in parallel to the mechanisms discovered in our study. Specifically, we wish to:

I) Develop peritoneal xenograft mouse model in which we can investigate the interaction between NK cells, ovarian cancer cells and ascites in clinically relevant environment. We would then asses the feasibility of ion channel inhibitors as therapeutics.

II) Investigate what are the effects of malignant ascites and electrolyte imbalance on NK and T cell metabolic functions and how it relates to their activation

III)   Evaluate the inhibitory potential of other potential immunosuppressive molecules contained in ascites, such as metabolites, proteins and antibodies

In the second part of our study, we revealed that CaP-NPs only slightly activate NK cells and do not impair NK effector functions. Cetuximab retained its ADCC functionality even when conjugated onto the surface of CaP-NPs. These properties indicate that our nanoparticle preparation is safe for biomedical application. Considering the biocompatibility, ease of uptake and low toxicity of CaP-NPs, which are desired nanomedical properties, we plan to:

I) Prepare CaP-NPs loaded with siRNA molecules of prospective targets expressed upon ovarian cancer cell (MHC-I, TIGIT ligands, etc.) or NK cell (NHE-1, VGSC or other ion channels).

II) Administer prepared CaP-NPs as siRNA delivery system which would downregulate the therapeutic target and possibly leads to the enhancement of NK effector function

6. List of figures

7.   Acknowledgments

Želio bih zahvaliti svojoj najvećoj podršci kroz cijeli život, svojoj majci, Danijeli Hrvat. Ona je probudila I podržavala znatiželju u meni od malena. Uvijek mi je pomogla dok sam bio u nedoumici ili kada mi je bilo teško. Puno želim zahvaliti svome ocu, Marku Hrvatu, koji je uvijek bio tu za mene i bio moj zaštitnik.

Također, duboko sam zahvalan svojoj baki, Ziti Pranjić koja je oduvijek bila nježna, brižna i puna ljubavi prema meni. Želim zahvaliti i svome djedu Mili Pranjiću koji me uvijek znao oraspoložiti nekom dogodovštinom. Uvijek ću imati lijepe uspomene iz djetinjstva sa vama u svom srcu.

Bez vaše podrške, razumijevanja i ljubavi od prvih dana ne bih uspio postići svoje uspjehe i ne bi postao čovjek koji jesam. Za to sam vam zauvijek dužan i zahvalan. Volim vas najviše na svijetu !

Posebno moram zahvaliti svome Kumu I najboljem prijatelju, Bruni Vučkoviću. Razgovori s njime su me uvijek nasmijali i oraspoložili za daljnje borbe. Zahvalan sam i Matiji Vučkoviću, Pauli Žejavac, Nikoli Marini, Juri Kešini, Tinu Kremiću I Ivanu Stjepiću za dobro provedeno vrijeme kad se vidimo doma.

(Translated from Croatian):

(I would like to thank my greatest support throughout my life, my mother, Danijela Hrvat. She awakened and supported curiosity in me from a young age. She always helped me when I was in doubt or when I was having a hard time. I want to thank my father, Marko Hrvat, who was always there for me and was my protector.

Also, I am deeply grateful to my grandmother, Zita Pranjić, who has always been gentle, caring and full of love for me. I also want to thank my grandfather Mili Pranjić, who always knew how to cheer me up with a story. I will always have beautiful childhood memories with you in my heart.

Without your support, understanding and love from the first days, I wouldn't have been able to achieve my successes and I wouldn't have become the man I am. For that I am forever indebted and grateful to you. I love you the most in the world!

I must especially thank my best friend, Bruno Vučković. Conversations with him always made me laugh and cheer me up for further fights. I am also grateful to Matija Vučković, Paula Žejavac, Nikola Marina, Jure Kešina, Tin Kremić and Ivan Stjepić for the time well spent when we see each other at home.)

Finally, I would like to thank the light of my life and my fiancé, Jana Riedesel. She supported me, comforted me and made me happy throughout my PhD journey. I never thought I would meet someone as amazing as her. I would like to thank the fate for bringing us together. Without her I can sincerely say I would not manage to finish these studies in one piece.

8. References

Alfarouk, K. O., Ahmed, S. B. M., Ahmed, A., Elliott, R. L., Ibrahim, M. E., Ali, H. S., Wales, C. C., Nourwali, I., Aljarbou, A. N., Bashir, A. H. H., Alhoufie, S. T. S., Alqahtani, S. S., Cardone, R. A., Fais, S., Harguindey, S., & Reshkin, S. J. (2020). The interplay of dysregulated ph and electrolyte imbalance in cancer. In *Cancers* (Vol. 12, Issue 4). MDPI AG. https://doi.org/10.3390/cancers12040898

Allard, D., Turcotte, M., & Stagg, J. (2017). Targeting A2 adenosine receptors in cancer. *Immunology & Cell Biology*, *95*(4), 333–339. https://doi.org/10.1038/icb.2017.8

Allen, C., Zeidan, A. M., & Bewersdorf, J. P. (2021). BiTEs, DARTS, BiKEs and TriKEs—Are Antibody Based Therapies Changing the Future Treatment of AML? *Life*, *11*(6), 465. https://doi.org/10.3390/life11060465

Apiz Saab, J. J., Dzierozynski, L. N., Jonker, P. B., AminiTabrizi, R., Shah, H., Menjivar, R. E., Scott, A. J., Nwosu, Z. C., Zhu, Z., Chen, R. N., Oh, M., Sheehan, C., Wahl, D. R., Pasca di Magliano, M., Lyssiotis, C. A., Macleod, K. F., Weber, C. R., & Muir, A. (2023). Pancreatic tumors exhibit myeloid-driven amino acid stress and upregulate arginine biosynthesis. *ELife*, *12*. https://doi.org/10.7554/eLife.81289

Asem, M., Young, A., Oyama, C., ClaureDeLaZerda, A., Liu, Y., Ravosa, Matthew. J., Gupta, V., Jewell, A., Khabele, D., & Stack, M. S. (2020). Ascites-induced compression alters the peritoneal microenvironment and promotes metastatic success in ovarian cancer. *Scientific Reports*, *10*(1), 11913. https://doi.org/10.1038/s41598-020-68639-2

Atallah-Yunes, S. A., & Robertson, M. J. (2022). Cytokine Based Immunotherapy for Cancer and Lymphoma: Biology, Challenges and Future Perspectives. *Frontiers in Immunology*, *13*. https://doi.org/10.3389/fimmu.2022.872010

Badger, A. M., Oh, S. K., & Moolten, F. R. (1981). Differential Effects of an Immunosuppressive Fraction from Ascites Fluid of Patients with Ovarian Cancer on Spontaneous and Antibody-dependent Cytotoxicity1. In *CANCER RESEARCH* (Vol. 41).

Barbero, F., Michelini, S., Moriones, O. H., Patarroyo, J., Rosell, J., F. Gusta, M., Vitali, M., Martín, L., Canals, F., Duschl, A., Horejs-Hoeck, J., Mondragón, L., Bastús, N. G., & Puntes, V. (2022). Role of Common Cell Culture Media Supplements on Citrate-Stabilized Gold Nanoparticle Protein Corona Formation, Aggregation State, and the Consequent Impact on Cellular Uptake. *Bioconjugate Chemistry*, *33*(8), 1505–1514. https://doi.org/10.1021/acs.bioconjchem.2c00232

Barrow, A. D., Martin, C. J., & Colonna, M. (2019). The Natural Cytotoxicity Receptors in Health and Disease. *Frontiers in Immunology*, *10*. https://doi.org/10.3389/fimmu.2019.00909

Borrelli, S., De Nicola, L., De Gregorio, I., Polese, L., Pennino, L., Elefante, C., Carbone, A., Rappa, T., Minutolo, R., & Garofalo, C. (2021). Volume-Independent Sodium Toxicity in Peritoneal Dialysis: New Insights from Bench to Bed. *International Journal of Molecular Sciences*, *22*(23), 12804. https://doi.org/10.3390/ijms222312804

Bose, T., Cieślar-Pobuda, A., & Wiechec, E. (2015). Role of ion channels in regulating Ca2+ homeostasis during the interplay between immune and cancer cells. *Cell Death & Disease*, *6*(2), e1648–e1648. https://doi.org/10.1038/cddis.2015.23

Bowlby, M. R., Fadool, D. A., Holmes, T. C., & Levitan, I. B. (1997). Modulation of the Kv1.3 Potassium Channel by Receptor Tyrosine Kinases. *The Journal of General Physiology*, *110*(5), 601–610. https://doi.org/10.1085/jgp.110.5.601

Braster, R., Bögels, M., Benonisson, H., Wuhrer, M., Plomp, R., Bentlage, A. E. H., Korthouwer, R., Visser, R., Verbeek, J. S., van Egmond, M., & Vidarsson, G. (2021). Afucosylated IgG Targets FcγRIV for Enhanced Tumor Therapy in Mice. *Cancers*, *13*(10), 2372. https://doi.org/10.3390/cancers13102372

Brisson, L., Gillet, L., Calaghan, S., Besson, P., Le Guennec, J.-Y., Roger, S., & Gore, J. (2011). NaV1.5 enhances breast cancer cell invasiveness by increasing NHE1-dependent H+ efflux in caveolae. *Oncogene*, *30*(17), 2070–2076. https://doi.org/10.1038/onc.2010.574

Burt, R., Warcel, D., & Fielding, A. K. (2019). Blinatumomab, a bispecific B-cell and T-cell engaging antibody, in the treatment of B-cell malignancies. *Human Vaccines & Immunotherapeutics*, *15*(3), 594–602. https://doi.org/10.1080/21645515.2018.1540828

Capasso, J. M., Rivard, C. J., Enomoto, L. M., & Berl, T. (2003). Chloride, not sodium, stimulates expression of the γ subunit of Na/K-ATPase and activates JNK in response to hypertonicity in mouse IMCD3 cells. *Proceedings of the National Academy of Sciences*, *100*(11), 6428–6433. https://doi.org/10.1073/pnas.1130871100

Catar, R., Witowski, J., Zhu, N., Lücht, C., Derrac Soria, A., Uceda Fernandez, J., Chen, L., Jones, S. A., Fielding, C. A., Rudolf, A., Topley, N., Dragun, D., & Jörres, A. (2017). IL-6 Trans–Signaling Links

Inflammation with Angiogenesis in the Peritoneal Membrane. *Journal of the American Society of Nephrology*, 28(4), 1188–1199. https://doi.org/10.1681/ASN.2015101169

Chan, J. M., Valencia, P. M., Zhang, L., Langer, R., & Farokhzad, O. C. (2010). *Polymeric Nanoparticles for Drug Delivery* (pp. 163–175). https://doi.org/10.1007/978-1-60761-609-2_11

Chaplin, D. D. (2010). Overview of the immune response. *Journal of Allergy and Clinical Immunology*, 125(2), S3–S23. https://doi.org/10.1016/j.jaci.2009.12.980

Chen, B.-X., Wilson, S. R., Das, M., Coughlin, D. J., & Erlanger, B. F. (1998). Antigenicity of fullerenes: Antibodies specific for fullerenes and their characteristics. *Proceedings of the National Academy of Sciences*, 95(18), 10809–10813. https://doi.org/10.1073/pnas.95.18.10809

Chen, L., & Flies, D. B. (2013). Molecular mechanisms of T cell co-stimulation and co-inhibition. *Nature Reviews Immunology*, 13(4), 227–242. https://doi.org/10.1038/nri3405

Chen, X., Gao, W., Gambotto, A., & Finn, O. J. (2009). Lentiviral vectors encoding human MUC1-specific, MHC-unrestricted single-chain TCR and a fusion suicide gene: potential for universal and safe cancer immunotherapy. *Cancer Immunology, Immunotherapy*, 58(6), 977–987. https://doi.org/10.1007/s00262-008-0624-0

Cheng, M., Chen, Y., Xiao, W., Sun, R., & Tian, Z. (2013). NK cell-based immunotherapy for malignant diseases. *Cellular & Molecular Immunology*, 10(3), 230–252. https://doi.org/10.1038/cmi.2013.10

Cheng, X., & Kuhn, L. (2007). Chemotherapy drug delivery from calcium phosphate nanoparticles. *International Journal of Nanomedicine*, 2(4), 667–674.

Chernousova, S., & Epple, M. (2017). Live-cell imaging to compare the transfection and gene silencing efficiency of calcium phosphate nanoparticles and a liposomal transfection agent. *Gene Therapy*, 24(5), 282–289. https://doi.org/10.1038/gt.2017.13

Chiesa, M. Della, Carlomagno, S., Frumento, G., Balsamo, M., Cantoni, C., Conte, R., Moretta, L., Moretta, A., & Vitale, M. (2006). The tryptophan catabolite l-kynurenine inhibits the surface expression of NKp46- and NKG2D-activating receptors and regulates NK-cell function. *Blood*, 108(13), 4118–4125. https://doi.org/10.1182/blood-2006-03-006700

Chung, C., & Iwakiri, Y. (2013). The lymphatic vascular system in liver diseases: its role in ascites formation. *Clinical and Molecular Hepatology*, 19(2), 99. https://doi.org/10.3350/cmh.2013.19.2.99

Cohnen, A., Chiang, S. C., Stojanovic, A., Schmidt, H., Claus, M., Saftig, P., Janßen, O., Cerwenka, A., Bryceson, Y. T., & Watzl, C. (2013). Surface CD107a/LAMP-1 protects natural killer cells from degranulation-associated damage. *Blood*, 122(8), 1411–1418. https://doi.org/10.1182/blood-2012-07-441832

Coiffier, B., Altman, A., Pui, C.-H., Younes, A., & Cairo, M. S. (2008). Guidelines for the Management of Pediatric and Adult Tumor Lysis Syndrome: An Evidence-Based Review. *Journal of Clinical Oncology*, 26(16), 2767–2778. https://doi.org/10.1200/JCO.2007.15.0177

Coussens, L. M., & Werb, Z. (2002). Inflammation and cancer. *Nature*, 420(6917), 860–867. https://doi.org/10.1038/nature01322

Dahmani, A., & Delisle, J.-S. (2018). TGF-β in T Cell Biology: Implications for Cancer Immunotherapy. *Cancers*, 10(6), 194. https://doi.org/10.3390/cancers10060194

Dasari, S., & Bernard Tchounwou, P. (2014). Cisplatin in cancer therapy: Molecular mechanisms of action. *European Journal of Pharmacology*, 740, 364–378. https://doi.org/10.1016/j.ejphar.2014.07.025

Degli Esposti, L., Carella, F., Adamiano, A., Tampieri, A., & Iafisco, M. (2018). Calcium phosphate-based nanosystems for advanced targeted nanomedicine. *Drug Development and Industrial Pharmacy*, 44(8), 1223–1238. https://doi.org/10.1080/03639045.2018.1451879

Dilley, J., Burnell, M., Gentry-Maharaj, A., Ryan, A., Neophytou, C., Apostolidou, S., Karpinskyj, C., Kalsi, J., Mould, T., Woolas, R., Singh, N., Widschwendter, M., Fallowfield, L., Campbell, S., Skates, S. J., McGuire, A., Parmar, M., Jacobs, I., & Menon, U. (2020). Ovarian cancer symptoms, routes to diagnosis and survival – Population cohort study in the 'no screen' arm of the UK Collaborative Trial of Ovarian Cancer Screening (UKCTOCS). *Gynecologic Oncology*, 158(2), 316–322. https://doi.org/10.1016/j.ygyno.2020.05.002

Dristant, U., Mukherjee, K., Saha, S., & Maity, D. (2023). An Overview of Polymeric Nanoparticles-Based Drug Delivery System in Cancer Treatment. *Technology in Cancer Research & Treatment*, 22, 153303382311520. https://doi.org/10.1177/15330338231152083

Dustin, M. L., & Long, E. O. (2010). Cytotoxic immunological synapses. *Immunological Reviews*, 235(1), 24–34. https://doi.org/10.1111/j.0105-2896.2010.00904.x

Eil, R., Vodnala, S. K., Clever, D., Klebanoff, C. A., Sukumar, M., Pan, J. H., Palmer, D. C., Gros, A., Yamamoto, T. N., Patel, S. J., Guittard, G. C., Yu, Z., Carbonaro, V., Okkenhaug, K., Schrump, D. S., Linehan, W. M., Roychoudhuri, R., & Restifo, N. P. (2016). Ionic immune suppression within the tumour

microenvironment limits T cell effector function. *Nature*, *537*(7621), 539–543. https://doi.org/10.1038/nature19364

Eleftheriadis, T., Pissas, G., Antoniadi, G., Liakopoulos, V., & Stefanidis, I. (2015). Indoleamine 2,3-dioxygenase depletes tryptophan, activates general control non-derepressible 2 kinase and down-regulates key enzymes involved in fatty acid synthesis in primary human CD4 $^+$ T cells. *Immunology*, *146*(2), 292–300. https://doi.org/10.1111/imm.12502

Elg, S. A., Mayer, A. R., Carson, L. F., Twiggs, L. B., Hill, R. B., & Ramakrishnan, S. (1997). ?-1 acid glycoprotein is an immunosuppressive factor found in ascites from ovarian carcinoma. *Cancer*, *80*(8), 1448–1456. https://doi.org/10.1002/(SICI)1097-0142(19971015)80:8<1448::AID-CNCR12>3.0.CO;2-5

Ford, C. E., Werner, B., Hacker, N. F., & Warton, K. (2020). The untapped potential of ascites in ovarian cancer research and treatment. *British Journal of Cancer*, *123*(1), 9–16. https://doi.org/10.1038/s41416-020-0875-x

Fraser, C. C., Jia, B., Hu, G., Al Johani, L. I., Fritz-Klaus, R., Ham, J. D., Fichorova, R. N., Elias, K. M., Cramer, D. W., Patankar, M. S., & Chen, J. (2022). Ovarian Cancer Ascites Inhibits Transcriptional Activation of NK Cells Partly through CA125. *The Journal of Immunology*, ji2001095. https://doi.org/10.4049/jimmunol.2001095

Fraser, S. P., Ozerlat-Gunduz, I., Brackenbury, W. J., Fitzgerald, E. M., Campbell, T. M., Coombes, R. C., & Djamgoz, M. B. A. (2014). Regulation of voltage-gated sodium channel expression in cancer: hormones, growth factors and auto-regulation. *Philosophical Transactions of the Royal Society B: Biological Sciences*, *369*(1638), 20130105. https://doi.org/10.1098/rstb.2013.0105

Fumita, Y., Tanaka, F., Saji, F., & Nakamuro, K. (1984). Immunosuppressive Factors in Ascites Fluids From Ovarian Cancer Patients. *American Journal of Reproductive Immunology*, *6*(4), 175–178. https://doi.org/10.1111/j.1600-0897.1984.tb00133.x

Gortzak-Uzan, L., Ignatchenko, A., Evangelou, A. I., Agochiya, M., Brown, K. A., St.Onge, P., Kireeva, I., Schmitt-Ulms, G., Brown, T. J., Murphy, J., Rosen, B., Shaw, P., Jurisica, I., & Kislinger, T. (2008). A proteome resource of ovarian cancer ascites: Integrated proteomic and bioinformatic analyses to identify putative biomarkers. *Journal of Proteome Research*, *7*(1), 339–351. https://doi.org/10.1021/pr0703223

Gottschalk, N., Kimmig, R., Lang, S., Singh, M., & Brandau, S. (2012). Anti-Epidermal Growth Factor Receptor (EGFR) Antibodies Overcome Resistance of Ovarian Cancer Cells to Targeted Therapy and Natural Cytotoxicity. *International Journal of Molecular Sciences*, *13*(12), 12000–12016. https://doi.org/10.3390/ijms130912000

Gupta, S. L., Basu, S., Soni, V., & Jaiswal, R. K. (2022). Immunotherapy: an alternative promising therapeutic approach against cancers. *Molecular Biology Reports*, *49*(10), 9903–9913. https://doi.org/10.1007/s11033-022-07525-8

Hajdu, P., Chimote, A. A., Thompson, T. H., Koo, Y., Yun, Y., & Conforti, L. (2013). Functionalized liposomes loaded with siRNAs targeting ion channels in effector memory T cells as a potential therapy for autoimmunity. *Biomaterials*, *34*(38), 10249–10257. https://doi.org/10.1016/j.biomaterials.2013.09.019

Harley, J. C., Suchowerska, N., & McKenzie, D. R. (2020). Cancer treatment with gas plasma and with gas plasma–activated liquid: positives, potentials and problems of clinical translation. *Biophysical Reviews*, *12*(4), 989–1006. https://doi.org/10.1007/s12551-020-00743-z

Hernandez, A. L., Kitz, A., Wu, C., Lowther, D. E., Rodriguez, D. M., Vudattu, N., Deng, S., Herold, K. C., Kuchroo, V. K., Kleinewietfeld, M., & Hafler, D. A. (2015). Sodium chloride inhibits the suppressive function of FOXP3+ regulatory T cells. *Journal of Clinical Investigation*, *125*(11), 4212–4222. https://doi.org/10.1172/JCI81151

Hilger, I. (2013). In vivo applications of magnetic nanoparticle hyperthermia. *International Journal of Hyperthermia*, *29*(8), 828–834. https://doi.org/10.3109/02656736.2013.832815

Hu, D., Sheng, Z., Zhu, M., Wang, X., Yan, F., Liu, C., Song, L., Qian, M., Liu, X., & Zheng, H. (2018). Förster Resonance Energy Transfer-Based Dual-Modal Theranostic Nanoprobe for *In Situ* Visualization of Cancer Photothermal Therapy. *Theranostics*, *8*(2), 410–422. https://doi.org/10.7150/thno.22226

Irani, S., Mirfakhraie, R., & Jalili, A. (2016). Combination of cold atmospheric plasma and iron nanoparticles in breast cancer: gene expression and apoptosis study. *OncoTargets and Therapy*, *Volume 9*, 5911–5917. https://doi.org/10.2147/OTT.S95644

Ito, Y., Sun, T., Tanaka, H., Yamaguchi, M., Kinashi, H., Sakata, F., Kunoki, S., Sakai, Y., & Ishimoto, T. (2023). Tissue Sodium Accumulation Induces Organ Inflammation and Injury in Chronic Kidney Disease. *International Journal of Molecular Sciences*, *24*(9), 8329. https://doi.org/10.3390/ijms24098329

Jeevanandam, J., Barhoum, A., Chan, Y. S., Dufresne, A., & Danquah, M. K. (2018). Review on nanoparticles and nanostructured materials: history, sources, toxicity and regulations. *Beilstein Journal of Nanotechnology*, *9*, 1050–1074. https://doi.org/10.3762/bjnano.9.98

Jennings, M. L. (2005). Evidence for a Second Binding/Transport Site for Chloride in Erythrocyte Anion Transporter AE1 Modified at Glutamate 681. *Biophysical Journal*, *88*(4), 2681–2691. https://doi.org/10.1529/biophysj.104.056812

Jeong, J., Kim, J. H., Shim, J. H., Hwang, N. S., & Heo, C. Y. (2019). Bioactive calcium phosphate materials and applications in bone regeneration. *Biomaterials Research*, *23*(1), 4. https://doi.org/10.1186/s40824-018-0149-3

Jeulin, C., Seltzer, V., Bailbé, D., Andreau, K., & Marano, F. (2008). EGF mediates calcium-activated chloride channel activation in the human bronchial epithelial cell line 16HBE14o⁻: involvement of tyrosine kinase p60 [c-src]. *American Journal of Physiology-Lung Cellular and Molecular Physiology*, *295*(3), L489–L496. https://doi.org/10.1152/ajplung.90282.2008

Jokerst, J. V, Lobovkina, T., Zare, R. N., & Gambhir, S. S. (2011). Nanoparticle PEGylation for imaging and therapy. *Nanomedicine*, *6*(4), 715–728. https://doi.org/10.2217/nnm.11.19

Kelly, M. G., Winkler, S. S., Lentz, S. S., Berliner, S. H., Swain, M. F., Skinner, H. G., & Schwartz, G. G. (2015). Serum Calcium and Serum Albumin Are Biomarkers That Can Discriminate Malignant from Benign Pelvic Masses. *Cancer Epidemiology, Biomarkers & Prevention*, *24*(10), 1593–1598. https://doi.org/10.1158/1055-9965.EPI-15-0443

Khalifehzadeh, R., & Arami, H. (2020). Biodegradable calcium phosphate nanoparticles for cancer therapy. *Advances in Colloid and Interface Science*, *279*, 102157. https://doi.org/10.1016/j.cis.2020.102157

Khan, I., Saeed, K., & Khan, I. (2019). Nanoparticles: Properties, applications and toxicities. *Arabian Journal of Chemistry*, *12*(7), 908–931. https://doi.org/10.1016/j.arabjc.2017.05.011

Kleyman, T. R., & Cragoe, E. J. (1988). Amiloride and its analogs as tools in the study of ion transport. *The Journal of Membrane Biology*, *105*(1), 1–21. https://doi.org/10.1007/BF01871102

Kline, J. B., Kennedy, R. P., Albone, E., Chao, Q., Fernando, S., Mcdonough, J. M., Rybinski, K., Wang, W., Somers, E. B., Schweizer, C., Grasso, L., & Nicolaides, N. C. (2017). Tumor antigen CA125 suppresses antibody-dependent cellular cytotoxicity (ADCC) via direct antibody binding and suppressed Fc-γ receptor engagement. In *Oncotarget* (Vol. 8, Issue 32). www.impactjournals.com/oncotarget/

Kovtun, A., Heumann, R., & Epple, M. (2009). Calcium phosphate nanoparticles for the transfection of cells. *Bio-Medical Materials and Engineering*, *19*(2–3), 241–247. https://doi.org/10.3233/BME-2009-0586

Kuk, C., Kulasingam, V., Gunawardana, C. G., Smith, C. R., Batruch, I., & Diamandis, E. P. (2009). Mining the ovarian cancer ascites proteome for potential ovarian cancer biomarkers. *Molecular and Cellular Proteomics*, *8*(4), 661–669. https://doi.org/10.1074/mcp.M800313-MCP200

Kurkjian, C., & Kim, E. S. (2012). Risks and benefits with bevacizumab: evidence and clinical implications. *Therapeutic Advances in Drug Safety*, *3*(2), 59–69. https://doi.org/10.1177/2042098611430109

Labani-Motlagh, A., Ashja-Mahdavi, M., & Loskog, A. (2020). The Tumor Microenvironment: A Milieu Hindering and Obstructing Antitumor Immune Responses. *Frontiers in Immunology*, *11*. https://doi.org/10.3389/fimmu.2020.00940

Landskron, J., Helland, Ø., Torgersen, K. M., Aandahl, E. M., Gjertsen, B. T., Bjørge, L., & Taskén, K. (2015). Activated regulatory and memory T-cells accumulate in malignant ascites from ovarian carcinoma patients. *Cancer Immunology, Immunotherapy*, *64*(3), 337–347. https://doi.org/10.1007/s00262-014-1636-6

Lee, S. C., Parthasarathy, R., Botwin, K., Kunneman, D., Rowold, E., Lange, G., Klover, J., Abegg, A., Zobel, J., Beck, T., Miller, T., Hood, W., Monahan, J., McKearn, J. P., Jansson, R., & Voliva, C. F. (2004). Biochemical and Immunological Properties of Cytokines Conjugated to Dendritic Polymers. *Biomedical Microdevices*, *6*(3), 191–202. https://doi.org/10.1023/B:BMMD.0000042048.18186.ff

Leslie, T. K., James, A. D., Zaccagna, F., Grist, J. T., Deen, S., Kennerley, A., Riemer, F., Kaggie, J. D., Gallagher, F. A., Gilbert, F. J., & Brackenbury, W. J. (2019). Sodium homeostasis in the tumour microenvironment. *Biochimica et Biophysica Acta (BBA) - Reviews on Cancer*, *1872*(2), 188304. https://doi.org/10.1016/j.bbcan.2019.07.001

Li, Y., Huang, K., Liu, L., Qu, Y., Huang, Y., Wu, Y., & Wei, J. (2018). Effects of complement and serum IgG on rituximab-dependent natural killer cell-mediated cytotoxicity against Raji cells. *Oncology Letters*. https://doi.org/10.3892/ol.2018.9630

Liang, R., Wei, M., Evans, D. G., & Duan, X. (2014). Inorganic nanomaterials for bioimaging, targeted drug delivery and therapeutics. *Chem. Commun.*, *50*(91), 14071–14081. https://doi.org/10.1039/C4CC03118K

Lord, S. J., Rajotte, R. V., Korbutt, G. S., & Bleackley, R. C. (2003). Granzyme B: a natural born killer. *Immunological Reviews*, *193*(1), 31–38. https://doi.org/10.1034/j.1600-065X.2003.00044.x

Lugano, R., Ramachandran, M., & Dimberg, A. (2020). Tumor angiogenesis: causes, consequences, challenges and opportunities. *Cellular and Molecular Life Sciences*, *77*(9), 1745–1770. https://doi.org/10.1007/s00018-019-03351-7

Maas, R. J., Hoogstad-van Evert, J. S., Van der Meer, J. M., Mekers, V., Rezaeifard, S., Korman, A. J., de Jonge, P. K., Cany, J., Woestenenk, R., Schaap, N. P., Massuger, L. F., Jansen, J. H., Hobo, W., & Dolstra, H. (2020). TIGIT blockade enhances functionality of peritoneal NK cells with altered expression of DNAM-1/TIGIT/CD96 checkpoint molecules in ovarian cancer. *OncoImmunology*, *9*(1). https://doi.org/10.1080/2162402X.2020.1843247

MacLeod, D. T., Antony, J., Martin, A. J., Moser, R. J., Hekele, A., Wetzel, K. J., Brown, A. E., Triggiano, M. A., Hux, J. A., Pham, C. D., Bartsevich, V. V., Turner, C. A., Lape, J., Kirkland, S., Beard, C. W., Smith, J., Hirsch, M. L., Nicholson, M. G., Jantz, D., & McCreedy, B. (2017). Integration of a CD19 CAR into the TCR Alpha Chain Locus Streamlines Production of Allogeneic Gene-Edited CAR T Cells. *Molecular Therapy*, *25*(4), 949–961. https://doi.org/10.1016/j.ymthe.2017.02.005

Mantovani, A., Allavena, P., Sessa, C., Bolis, G., & Mangioni, C. (1980). Natural killer activity of lymphoid cells isolated from human ascitic ovarian tumors. *International Journal of Cancer*, *25*(5), 573–582. https://doi.org/10.1002/ijc.2910250505

Maurus, R., Begum, A., Kuo, H., Racaza, A., Numao, S., Andersen, C., Tams, J. W., Vind, J., Overall, C. M., Withers, S. G., & Brayer, G. D. (2005). Structural and mechanistic studies of chloride induced activation of human pancreatic α-amylase. *Protein Science*, *14*(3), 743–755. https://doi.org/10.1110/ps.041079305

Medoff, J. R., Clack, V. D., & Roche, J. K. (1986). Characterization of an immunosuppressive factor from malignant ascites that resembles a factor-induced in vitro by carcinoembryonic antigen. *J Immunol* , *137*(6), 2057–2064. http://www.jimmunol.org/content/137/6/2057

Mehner, C., Oberg, A. L., Goergen, K. M., Kalli, K. R., Maurer, M. J., Nassar, A., Goode, E. L., Keeney, G. L., Jatoi, A., Radisky, D. C., & Radisky, E. S. (2017). EGFR as a prognostic biomarker and therapeutic target in ovarian cancer: evaluation of patient cohort and literature review. *Genes & Cancer*, *8*(5–6), 589–599. https://doi.org/10.18632/genesandcancer.142

Mendelsohn, J., & Baselga, J. (2003). Status of Epidermal Growth Factor Receptor Antagonists in the Biology and Treatment of Cancer. *Journal of Clinical Oncology*, *21*(14), 2787–2799. https://doi.org/10.1200/JCO.2003.01.504

Moon, C., Park, H.-J., Choi, Y.-H., Park, E.-M., Castranova, V., & Kang, J. L. (2010). Pulmonary Inflammation After Intraperitoneal Administration of Ultrafine Titanium Dioxide (TiO $_2$) At Rest or in Lungs Primed with Lipopolysaccharide. *Journal of Toxicology and Environmental Health, Part A*, *73*(5–6), 396–409. https://doi.org/10.1080/15287390903486543

Moretta, L., & Moretta, A. (2004). Unravelling natural killer cell function: triggering and inhibitory human NK receptors. *The EMBO Journal*, *23*(2), 255–259. https://doi.org/10.1038/sj.emboj.7600019

Narendra Kumar, & Sunita Kumbhat. (2016). Carbon-Based Nanomaterials. In *Essentials in Nanoscience and Nanotechnology* (pp. 189–236). Wiley. https://doi.org/10.1002/9781119096122.ch5

Ngoenkam, J., Schamel, W. W., & Pongcharoen, S. (2018). Selected signalling proteins recruited to the T-cell receptor–CD3 complex. *Immunology*, *153*(1), 42–50. https://doi.org/10.1111/imm.12809

Nomura, H., Iwasa, N., Yoshihama, T., Nanki, Y., & Aoki, D. (2017). *Epidemiology and Etiology of Ovarian Cancer* (pp. 1–13). https://doi.org/10.1007/978-981-10-4160-0_1

Orme, J. J., Jazieh, K. A., Xie, T., Harrington, S., Liu, X., Ball, M., Madden, B., Charlesworth, M. C., Azam, T. U., Lucien, F., Wootla, B., Li, Y., Villasboas, J. C., Mansfield, A. S., Dronca, R. S., & Dong, H. (2020). ADAM10 and ADAM17 cleave PD-L1 to mediate PD-(L)1 inhibitor resistance. *OncoImmunology*, *9*(1). https://doi.org/10.1080/2162402X.2020.1744980

Papadouli, I., Mueller-Berghaus, J., Beuneu, C., Ali, S., Hofner, B., Petavy, F., Tzogani, K., Miermont, A., Norga, K., Kholmanskikh, O., Leest, T., Schuessler-Lenz, M., Salmonson, T., Gisselbrecht, C., Garcia, J. L., & Pignatti, F. (2020). EMA Review of Axicabtagene Ciloleucel (Yescarta) for the Treatment of Diffuse Large B-Cell Lymphoma. *The Oncologist*, *25*(10), 894–902. https://doi.org/10.1634/theoncologist.2019-0646

Park, G. M., Lee, S., Park, B., Kim, E., Shin, J., Cho, K., & Ahn, K. (2004). Soluble HLA-G generated by proteolytic shedding inhibits NK-mediated cell lysis. *Biochemical and Biophysical Research Communications*, *313*(3), 606–611. https://doi.org/10.1016/j.bbrc.2003.11.153

Paul, S., & Lal, G. (2017). The Molecular Mechanism of Natural Killer Cells Function and Its Importance in Cancer Immunotherapy. *Frontiers in Immunology*, *8*. https://doi.org/10.3389/fimmu.2017.01124

Pende, D., Bottino, C., Castriconi, R., Cantoni, C., Marcenaro, S., Rivera, P., Spaggiari, G. M., Dondero, A., Carnemolla, B., Reymond, N., Mingari, M. C., Lopez, M., Moretta, L., & Moretta, A. (2005). PVR (CD155) and Nectin-2 (CD112) as ligands of the human DNAM-1 (CD226) activating receptor: involvement in tumor cell lysis. *Molecular Immunology*, *42*(4), 463–469. https://doi.org/10.1016/j.molimm.2004.07.028

Piala, A. T., Moon, T. M., Akella, R., He, H., Cobb, M. H., & Goldsmith, E. J. (2014). Chloride Sensing by

WNK1 Involves Inhibition of Autophosphorylation. *Science Signaling*, *7*(324). https://doi.org/10.1126/scisignal.2005050

Preithner, S., Elm, S., Lippold, S., Locher, M., Wolf, A., Silva, A. J. da, Baeuerle, P. A., & Prang, N. S. (2006). High concentrations of therapeutic IgG1 antibodies are needed to compensate for inhibition of antibody-dependent cellular cytotoxicity by excess endogenous immunoglobulin G. *Molecular Immunology*, *43*(8), 1183–1193. https://doi.org/10.1016/j.molimm.2005.07.010

Probst, Y., Mowbray, E., Svensen, E., & Thompson, K. (2019). A Systematic Review of the Impact of Dietary Sodium on Autoimmunity and Inflammation Related to Multiple Sclerosis. *Advances in Nutrition*, *10*(5), 902–910. https://doi.org/10.1093/advances/nmz032

Qadri, Y. J., Rooj, A. K., & Fuller, C. M. (2012). ENaCs and ASICs as therapeutic targets. *American Journal of Physiology-Cell Physiology*, *302*(7), C943–C965. https://doi.org/10.1152/ajpcell.00019.2012

Raffaghello, L., Prigione, I., Airoldi, I., Camoriano, M., Levreri, I., Gambini, C., Pende, D., Steinle, A., Ferrone, S., & Pistoia, V. (2004). Downregulation and/or Release of NKG2D Ligands as Immune Evasion Strategy of Human Neuroblastoma. *Neoplasia*, *6*(5), 558–568. https://doi.org/10.1593/neo.04316

Randall, K. L. (2016). Rituximab in autoimmune diseases. *Australian Prescriber*, *39*(4), 131–134. https://doi.org/10.18773/austprescr.2016.053

Rawat, R. S. (2015). Dense Plasma Focus - From Alternative Fusion Source to Versatile High Energy Density Plasma Source for Plasma Nanotechnology. *Journal of Physics: Conference Series*, *591*(1). https://doi.org/10.1088/1742-6596/591/1/012021

REIN, D. T., VOLKMER, A. K., VOLKMER, J., BEYER, I. M., JANNI, W., FLEISCH, M. C., WELTER, A. K., BAUERSCHLAG, D., SCHÖNDORF, T., & BREIDENBACH, M. (2012). Systemic administration of bevacizumab prolongs survival in an in vivo model of platinum pre-treated ovarian cancer. *Oncology Letters*, *3*(3), 530–534. https://doi.org/10.3892/ol.2012.553

Rizvi, Z. A., Dalal, R., Sadhu, S., Kumar, Y., Kumar, S., Gupta, S. K., Tripathy, M. R., Rathore, D. K., & Awasthi, A. (2021). High-salt diet mediates interplay between NK cells and gut microbiota to induce potent tumor immunity. *Science Advances*, *7*(37). https://doi.org/10.1126/sciadv.abg5016

Roda, J. M., Joshi, T., Butchar, J. P., McAlees, J. W., Lehman, A., Tridandapani, S., & Carson, W. E. (2007). The activation of natural killer cell effector functions by cetuximab-coated, epidermal growth factor receptor - Positive tumor cells is enhanced by cytokines. *Clinical Cancer Research*, *13*(21), 6419–6428. https://doi.org/10.1158/1078-0432.CCR-07-0865

Sanchez-Correa, B., Valhondo, I., Hassouneh, F., Lopez-Sejas, N., Pera, A., Bergua, J. M., Arcos, M. J., Bañas, H., Casas-Avilés, I., Durán, E., Alonso, C., Solana, R., & Tarazona, R. (2019). DNAM-1 and the TIGIT/PVRIG/TACTILE Axis: Novel Immune Checkpoints for Natural Killer Cell-Based Cancer Immunotherapy. *Cancers*, *11*(6), 877. https://doi.org/10.3390/cancers11060877

Sen, K., & Mandal, M. (2013). Second generation liposomal cancer therapeutics: Transition from laboratory to clinic. *International Journal of Pharmaceutics*, *448*(1), 28–43. https://doi.org/10.1016/j.ijpharm.2013.03.006

Seo, Y., Ishii, Y., Ochiai, H., Fukuda, K., Akimoto, S., Hayashida, T., Okabayashi, K., Tsuruta, M., Hasegawa, H., & Kitagawa, Y. (2014). Cetuximab-mediated ADCC activity is correlated with the cell surface expression level of EGFR but not with the KRAS/BRAF mutational status in colorectal cancer. *Oncology Reports*, *31*(5), 2115–2122. https://doi.org/10.3892/or.2014.3077

Shender, V. O., Pavlyukov, M. S., Ziganshin, R. H., Arapidi, G. P., Kovalchuk, S. I., Anikanov, N. A., Altukhov, I. A., Alexeev, D. G., Butenko, I. O., Shavarda, A. L., Khomyakova, E. B., Evtushenko, E., Ashrafyan, L. A., Antonova, I. B., Kuznetcov, I. N., Gorbachev, A. Yu., Shakhparonov, M. I., & Govorun, V. M. (2014). Proteome–Metabolome Profiling of Ovarian Cancer Ascites Reveals Novel Components Involved in Intercellular Communication. *Molecular & Cellular Proteomics*, *13*(12), 3558–3571. https://doi.org/10.1074/mcp.M114.041194

Sokolova, V., & Epple, M. (2021). Biological and Medical Applications of Calcium Phosphate Nanoparticles. *Chemistry – A European Journal*, *27*(27), 7471–7488. https://doi.org/10.1002/chem.202005257

Song, H., Cicek, M. S., Dicks, E., Harrington, P., Ramus, S. J., Cunningham, J. M., Fridley, B. L., Tyrer, J. P., Alsop, J., Jimenez-Linan, M., Gayther, S. A., Goode, E. L., & Pharoah, P. D. P. (2014). The contribution of deleterious germline mutations in BRCA1, BRCA2 and the mismatch repair genes to ovarian cancer in the population. *Human Molecular Genetics*, *23*(17), 4703–4709. https://doi.org/10.1093/hmg/ddu172

Sperling, R. A., & Parak, W. J. (2010). Surface modification, functionalization and bioconjugation of colloidal inorganic nanoparticles. *Philosophical Transactions of the Royal Society A: Mathematical, Physical and Engineering Sciences*, *368*(1915), 1333–1383. https://doi.org/10.1098/rsta.2009.0273

Suk, J. S., Xu, Q., Kim, N., Hanes, J., & Ensign, L. M. (2016). PEGylation as a strategy for improving

nanoparticle-based drug and gene delivery. *Advanced Drug Delivery Reviews*, *99*, 28–51. https://doi.org/10.1016/j.addr.2015.09.012

Terkelsen, T., Pernemalm, M., Gromov, P., Børresen-Dale, A., Krogh, A., Haakensen, V. D., Lethiö, J., Papaleo, E., & Gromova, I. (2021). High-throughput proteomics of breast cancer interstitial fluid: identification of tumor subtype-specific serologically relevant biomarkers. *Molecular Oncology*, *15*(2), 429–461. https://doi.org/10.1002/1878-0261.12850

Tholen, M. M. E., Rosier, B. J. H. M., Vermathen, R. T., Sewnath, C. A. N., Storm, C., Woythe, L., Izquierdo-Lozano, C., Riera, R., van Egmond, M., Merkx, M., & Albertazzi, L. (2023). Mapping Antibody Domain Exposure on Nanoparticle Surfaces Using DNA-PAINT. *ACS Nano*, *17*(12), 11665–11678. https://doi.org/10.1021/acsnano.3c02195

Thomsen, T. W., Shaffer, R. W., White, B., & Setnik, G. S. (2006). Paracentesis. *New England Journal of Medicine*, *355*(19), e21. https://doi.org/10.1056/NEJMvcm062234

Tobin, L. A., Xie, Y., Tsokos, M., Chung, S. I., Merz, A. A., Arnold, M. A., Li, G., Malech, H. L., & Kwong, K. F. (2013). Pegylated siRNA-loaded calcium phosphate nanoparticle-driven amplification of cancer cell internalization in vivo. *Biomaterials*, *34*(12), 2980–2990. https://doi.org/10.1016/j.biomaterials.2013.01.046

Tummers, B., & Green, D. R. (2017). Caspase-8: regulating life and death. *Immunological Reviews*, *277*(1), 76–89. https://doi.org/10.1111/imr.12541

Vecchio, E., Caiazza, C., Mimmi, S., Avagliano, A., Iaccino, E., Brusco, T., Nisticò, N., Maisano, D., Aloisio, A., Quinto, I., Renna, M., Divisato, G., Romano, S., Tufano, M., D'Agostino, M., Vigliar, E., Iaccarino, A., Mignogna, C., Andreozzi, F., … Fiume, G. (2021). Metabolites Profiling of Melanoma Interstitial Fluids Reveals Uridine Diphosphate as Potent Immune Modulator Capable of Limiting Tumor Growth. *Frontiers in Cell and Developmental Biology*, *9*. https://doi.org/10.3389/fcell.2021.730726

Vermeulen, L. M. P., De Smedt, S. C., Remaut, K., & Braeckmans, K. (2018). The proton sponge hypothesis: Fable or fact? *European Journal of Pharmaceutics and Biopharmaceutics*, *129*, 184–190. https://doi.org/10.1016/j.ejpb.2018.05.034

Villanueva-Flores, F., Castro-Lugo, A., Ramírez, O. T., & Palomares, L. A. (2020). Understanding cellular interactions with nanomaterials: towards a rational design of medical nanodevices. *Nanotechnology*, *31*(13), 132002. https://doi.org/10.1088/1361-6528/ab5bc8

Wachsmann, T. L. A., Meeuwsen, M. H., Remst, D. F. G., Buchner, K., Wouters, A. K., Hagedoorn, R. S., Falkenburg, J. H. F., & Heemskerk, M. H. M. (2023). Combining BCMA-targeting CAR T cells with TCR-engineered T-cell therapy to prevent immune escape of multiple myeloma. *Blood Advances*, *7*(20), 6178–6183. https://doi.org/10.1182/bloodadvances.2023010410

Wan, Y. Y. (2010). Multi-tasking of helper T cells. *Immunology*, *130*(2), 166–171. https://doi.org/10.1111/j.1365-2567.2010.03289.x

Wang, W. (2015). NK cell-mediated antibody-dependent cellular cytotoxicity in cancer immunotherapy. *Frontiers in Immunology*, *6*. https://doi.org/10.3389/fimmu.2015.00368

Welch, N. G., Scoble, J. A., Muir, B. W., & Pigram, P. J. (2017). Orientation and characterization of immobilized antibodies for improved immunoassays (Review). *Biointerphases*, *12*(2). https://doi.org/10.1116/1.4978435

White, M. C., Holman, D. M., Boehm, J. E., Peipins, L. A., Grossman, M., & Jane Henley, S. (2014). Age and Cancer Risk. *American Journal of Preventive Medicine*, *46*(3), S7–S15. https://doi.org/10.1016/j.amepre.2013.10.029

Wiemer, A. J., Hegde, S., Gumperz, J. E., & Huttenlocher, A. (2011). A Live Imaging Cell Motility Screen Identifies Prostaglandin E2 as a T Cell Stop Signal Antagonist. *The Journal of Immunology*, *187*(7), 3663–3670. https://doi.org/10.4049/jimmunol.1100103

Wu, J., Gao, F., Wang, C., Qin, M., Han, F., Xu, T., Hu, Z., Long, Y., He, X., Deng, X., Ren, D., & Dai, T. (2019). IL-6 and IL-8 secreted by tumour cells impair the function of NK cells via the STAT3 pathway in oesophageal squamous cell carcinoma. *Journal of Experimental & Clinical Cancer Research*, *38*(1), 321. https://doi.org/10.1186/s13046-019-1310-0

Xu, N., Zhang, X., Qi, T., Wu, Y., Xie, X., Chen, F., Shao, D., & Liao, J. (2022). Biomedical applications and prospects of temperature-orchestrated photothermal therapy. *MedComm – Biomaterials and Applications*, *1*(2). https://doi.org/10.1002/mba2.25

Yanaka, S., Yogo, R., Yagi, H., Onitsuka, M., Wakaizumi, N., Yamaguchi, Y., Uchiyama, S., & Kato, K. (2023). Negative interference with antibody-dependent cellular cytotoxicity mediated by rituximab from its interactions with human serum proteins. *Frontiers in Immunology*, *14*. https://doi.org/10.3389/fimmu.2023.1090898

Yang, X., Wei, X., Mu, Y., Li, Q., & Liu, J. (2020). A review of the mechanism of the central analgesic effect of lidocaine. *Medicine*, *99*(17), e19898. https://doi.org/10.1097/MD.0000000000019898

Yang, Z., Sun, Z., Ren, Y., Chen, X., Zhang, W., Zhu, X., Mao, Z., Shen, J., & Nie, S. (2019). Advances in nanomaterials for use in photothermal and photodynamic therapeutics (Review). *Molecular Medicine Reports*. https://doi.org/10.3892/mmr.2019.10218

Zhang, L., Conejo-Garcia, J. R., Katsaros, D., Gimotty, P. A., Massobrio, M., Regnani, G., Makrigiannakis, A., Gray, H., Schlienger, K., Liebman, M. N., Rubin, S. C., & Coukos, G. (2003). Intratumoral T Cells, Recurrence, and Survival in Epithelial Ovarian Cancer. *New England Journal of Medicine*, *348*(3), 203–213. https://doi.org/10.1056/NEJMoa020177

Zhang, N., Lu, C., Shu, G., Li, J., Chen, M., Chen, C., Lv, X., Xu, X., Weng, W., Weng, Q., Tang, B., Du, Y.-Z., & Ji, J. (2020). Gadolinium-loaded calcium phosphate nanoparticles for magnetic resonance imaging of orthotopic hepatocarcinoma and primary hepatocellular carcinoma. *Biomaterials Science*, *8*(7), 1961–1972. https://doi.org/10.1039/C9BM01544B

Zhang, Y., Luo, F., & Dong, K. (2023). Soluble NKG2D ligands impair CD8 $^+$ T cell antitumor function dependent of NKG2D downregulation in neuroblastoma. *Oncology Letters*, *26*(1), 297. https://doi.org/10.3892/ol.2023.13883

Zhao, J., Chen, G., Pang, X., Zhang, P., Hou, X., Chen, P., Xie, Y.-W., He, C.-Y., Wang, Z., & Chen, Z.-Y. (2020). Calcium phosphate nanoneedle based gene delivery system for cancer genetic immunotherapy. *Biomaterials*, *250*, 120072. https://doi.org/10.1016/j.biomaterials.2020.120072

Zhao, J., Li, Y., Wang, X., Xia, X., Shang, E., & Ali, J. (2021). Ionic-strength-dependent effect of suspended sediment on the aggregation, dissolution and settling of silver nanoparticles. *Environmental Pollution*, *279*, 116926. https://doi.org/10.1016/j.envpol.2021.116926

Zhou, H.-X., & Pang, X. (2018). Electrostatic Interactions in Protein Structure, Folding, Binding, and Condensation. *Chemical Reviews*, *118*(4), 1691–1741. https://doi.org/10.1021/acs.chemrev.7b00305

Zielińska, A., Costa, B., Ferreira, M. V., Miguéis, D., Louros, J. M. S., Durazzo, A., Lucarini, M., Eder, P., V. Chaud, M., Morsink, M., Willemen, N., Severino, P., Santini, A., & Souto, E. B. (2020). Nanotoxicology and Nanosafety: Safety-by-Design and Testing at a Glance. *International Journal of Environmental Research and Public Health*, *17*(13), 4657. https://doi.org/10.3390/ijerph17134657

Zielinski, C. E. (2021). Regulation of T Cell Responses by Ionic Salt Signals. *Cells*, *10*(9), 2365. https://doi.org/10.3390/cells10092365

Zingoni, A., Molfetta, R., Fionda, C., Soriani, A., Paolini, R., Cippitelli, M., Cerboni, C., & Santoni, A. (2018). NKG2D and Its Ligands: "One for All, All for One." *Frontiers in Immunology*, *9*. https://doi.org/10.3389/fimmu.2018.00476

Zolnik, B. S., González-Fernández, A., Sadrieh, N., & Dobrovolskaia, M. A. (2010). Minireview: Nanoparticles and the Immune System. *Endocrinology*, *151*(2), 458–465. https://doi.org/10.1210/en.2009-1082

9. Curriculum vitae

95

The curriculum vitae is not included in the online version for data protection reasons.

10. Declarations

Declarations required for the submission of the thesis

Declaration:

In accordance with § 6 (para. 2, clause g) of the Regulations Governing the Doctoral Proceedings of the Faculty of Biology for awarding the doctoral degree Dr. rer. nat., I hereby declare that I represent the field to which the topic *"Molecular mechanisms of malignant ascites-induced immunosuppression and options for nanoparticle-based therapeutic interventions"* is assigned in research and teaching and that I support the application of Antonio Hrvat.

Essen, date _20.11.23_ _S. BRANDAU_ _____

Name of the scientific
supervisor/member of the
University of Duisburg-Essen

Signature of the supervisor/
member of the University of Duisburg-Essen

Declaration:

In accordance with § 7 (para. 2, clause d and f) of the Regulations Governing the Doctoral Proceedings of the Faculty of Biology for awarding the doctoral degree Dr. rer. nat., I hereby declare that I have written the herewith submitted dissertation independently using only the materials listed, and have cited all sources taken over verbatim or in content as such.

Essen, date _20.11.23_ _____

Signature of the doctoral candidate

Declaration:

In accordance with § 7 (para. 2, clause e and g) of the Regulations Governing the Doctoral Proceedings of the Faculty of Biology for awarding the doctoral degree Dr. rer. nat., I hereby declare that I have undertaken no previous attempts to attain a doctoral degree, that the current work has not been rejected by any other faculty, and that I am submitting the dissertation only in this procedure.

Essen, date _20.11.23_ _____

Signature of the doctoral candidate